STUDY OF PROCESS VARIABLES ON THE DEVELOPMENT OF CUBE TEXTURE IN COPPER BEARING SOFT MAGNETIC Fe-Ni ALLOYS

A Thesis Submitted
in Partial Fulfilment of the Requirements
for the Degree of

MASTER OF TECHNOLOGY

By

VIDYA SAGAR VERMA

DEPARTMENT OF METALLURGICAL ENGINEERING

INDIAN INSTITUTE OF TECHNOLOGY KANPUR

AUGUST, 1981

CERTIFICATE

This is to certify that the work on 'STUDY OF PROCESS VARIABLES ON THE DEVELOPMENT OF CUBE TEXTURE IN COPPER BEARING SOFT MAGNETIC Fe-Ni ALLOYS' has been carried out by VIDYA SAGAR VERMA under my supervision and it has not been submitted elsewhere for a degree.

(K.P. Gupta)
Professor
Department of Metallurgical Engineering
Indian Institute of Technology, Kanpur.

ACKNOWLEDGEMENTS

I wish to express my sincere thanks to Professor K.P. Gupta for his valuable suggestions, guidance and encouragement at every stage of this work without which this work could not have been completed.

I am also grateful to Dr. D.C. Khan for his help during the magnetic measurements, an essential part of the work. I must thank Mr. A. Agnihotri for his kind cooperation throughout the magnetic measurements.

I wish to offer a lot of thanks to Mr. V.P. Gupta for materialisation of the different schemes into actual experimental apparatus. I am also thankful to Mr. M.L. Pandey, Mr. K.P. Mukherjee, Mr. D.K. Biswas and Mr. S.R. Chaurasia for their kind help throughout the work.

Lot of thanks are due to my friends Messrs S. Laha, E.M.T. Velu, A.K. Shah, Vikas Kumar, A. Bharti, S. Roy, D.M.A. Khan, S. Pandian and K.R. Chowdhary for their constant help in various ways and for their entertaining company.

I must acknowledge the financial support of Department of Science and Technology, New Delhi which made this work possible for investigation.

I must thank Mr. B. Bhoumik for helping in mechanical tests and Mr. S. Jha for helping in permeameter measurements.

I express my heartfelt indebtedness to my parents for their inspiring encouragement for completing this work.

At last but not the least, I must thank Mr. M.R. Nathwani for painstakingly typing the almost illegible manuscript.

August, 1981 VIDYA SAGAR VERMA

TABLE OF CONTENTS

Contents

Contents

Contents

LIST OF TABLES

LIST OF FIGURES

SYNOPSIS

Soft magnetic alloys are used for making cores for high frequency transformers ($\gg$ 60 Hz). It is well known that the magnetic properties of permalloys can be improved through the development of perfect cube texture and through suitable heat treatments. Alloys chosen for the study contain 75 pct. Ni-Fe with 5 pct. Cu or 14 pct. Cu and with small additions (upto 2 pct.) of Ti and Cr. Development of cube texture in these alloys depends on various process variables. The process variables chosen for the study are pct. cold reduction (96-98 pct.), annealing time (1-6 hrs.) and atmosphere of annealing (argon and hydrogen). The alloys are annealed at fixed temperature of 1050°C. Addition of Ti and Cr to Cu bearing permalloys has increased pct. elongation, electrical resistivity and has lowered the curie temperature. Cu bearing permalloys containing Ti and Cr can be cold rolled easily to very small thickness of 0.0035". Alloy containing 75 Ni, 5Cu, 1Ti, 1Cr, 0.5 Mn, bal. Fe appears to develop the best texture. Hydrogen annealing of alloys appears to show a promise of good texture. Magnetic cooling appears to improve the magnetic properties slightly.

CHAPTER I

INTRODUCTION AND LITERATURE REVIEW

CHAPTER I
INTRODUCTION AND LITERATURE REVIEW

I.1 Introduction

Ferromagnetic materials are used in electric machines, communication systems and various control devices. The important common elements which show ferromagnetism are iron, cobalt and nickel. These elements together with their various alloys provide magnetic materials having wide range of properties. For engineering applications two types of ferromagnetic materials are employed. One variety, called the hard magnetic materials, require large amount of energy to be expended to magnetise the material but once magnetised they retain their magnetised state. The other variety, called the soft magnetic materials, can be magnetised easily but they do not retain the magnetised state once the external influence causing magnetisation is removed.

Soft magnetic alloys are used for making transformer cores. There are two types of transformers - (i) low frequency (50-60 Hz) transformers and (ii) high frequency ($\gg$ 60 Hz) transformers. Low frequency transformer cores are made of bcc Fe-Si alloys while high frequency transformer cores are made of fcc Fe-Ni base alloys. We are concerned here with the Fe-Ni base soft magnetic materials, simple Fe-Ni alloys are called permalloys. They are named according to their Ni content

e.g. 65 permalloy contains 65 wt. pct. Ni and rest iron. Fe-Ni alloys are also used along with other alloying element additions and they are usually named differently. For example a Fe-Ni alloy with addition of copper is called μ-metal, another Fe-Ni alloy with addition of Cu and Mo is called 1040 alloy, Fe-Ni alloys with different additions of Mo are called Mo-permalloy and supermalloys. For soft magnetic materials the important magnetic characteristics are 1) high saturation induction (B_s), 2) high permeability (μ), 3) small magnetising force to cause saturation, 4) small remanence (B_r), 5) low coerecivity (H_c), and 6) small power loss i.e. small hysteresis and eddy current losses. A good soft magnetic material should possess most of these characteristics. Fe-Ni alloys satisfy these conditions rather well. Some properties of common commercial permalloys are mentioned in Table I.

Although in India, these alloys are in use they are all imported from other countries. So far very little work has been done in India to produce these materials, possibly because not much details of their manufacture is available in published literature. The magnetic properties of these matrials, besides being dependent on alloy composition, depend mainly on processing parameters which produce preferred grain orientation (texture) in the material. Since magnetic properties are anisotropic, materials texture and its perfection

affects magnetic properties. Since the conditions under which the required texture and its perfection is produced are not available in literature, it was therefore decided to determine the optimum process parameters for development of desired texture in various permalloys. The work on permalloys was divided into two parts - one dealing with simple permalloys and the other with permalloys having addition of different alloying elements. The present study involves the second group of permalloys. Since the processing parameters are similar for the two groups of alloys and that lot more data is available for the first group of alloys to understand the effects of process variables, first a brief review of Fe-Ni permalloys is presented and then the second group of alloys relevant to the present study are reviewed in the following sections.

I.2 Permalloys

I.2.1 Non-textured Permalloys

The phase diagram of Fe-Ni system is shown in Fig. 1. A continuous series of solid solution of Fe in Ni occurs at higher temperatures but at room temperature it is stable above 40 pct. Ni. Atomic ordering in Fe-Ni system[2] has been observed at about 500°C for the stoichiometric composition of Ni_3Fe. Order-disorder transformation has been found to be

sluggish[3], taking about one week at 450°C for complete ordering. The critical temperature for ordering decreases on either side of the Ni_3Fe stoichiometry. The fcc Fe-Ni alloys are ferromagnetic and the curie temperature goes through a maximum ($\sim$612°C) near about 65 pct. Ni composition.

Magnetic properties of permalloys are dependent on the composition of alloys and on the various process parameters. Electrical resistivity of Fe-Ni alloys increases with increase in Fe content. Rate of cooling has an effect on the electrical resistivity of Fe-Ni alloys. Higher the cooling rate, more is the resistivity. Saturation induction of Fe-Ni alloys increases with decrease in Ni content. On the other hand increase in Ni content increases μ_o and μ_m each of which reaches maximum at $\simeq$ 78 pct. Ni if permalloy treatment is given (Fig. 2). Coercive force is also minimum for double treated 78 permalloys. The high Ni permalloys, 60 to 78 wt. pct. Ni, show an even greater increase in permeability if subjected to magnetic annealing at 500°C or cooled in a small magnetic field of 10 Oe[4]. All these effects reveal that a critical degree of order is required to get optimum magnetic properties.

I.2.2 Textured Permalloys

Ferromagnetic materials show magnetic anisotropy. For example, in single crystal of Ni (fcc) the magnetization as a function of applied field for three crystallographic directions is as shown in Fig. 3. All the permalloys of our interest has fcc structure and are expected to show magnetic anisotropy. Thus, a polycrystalline material, in which all the grains are oriented in either [111] or [100] direction, shows better magnetic properties compared to a material having randomly oriented grains. Desired orientation of grains can be achieved through proper choice of mechanical and thermal treatments.

Cold rolling of materials produces preferred orientation of grains such that a crystallographic direction tends to become parallel to the rolling direction and a crystallographic plane tends to become parallel to the rolling plane. Texture produced due to cold rolling of Ni and permalloys can be described approximately as (110)[112] and more precisely as (123)[412] or (123)[412] (major) + (145)[211] (minor)[6] (Fig. 4). When the cold rolled material is annealed, the cold rolled texture changes to an annealing texture which may vary quite considerably depending upon the choice of the process variables. Under a very specific set of conditions,

some fcc materials are known to produce {100}<001> texture, called 'CUBE TEXTURE'[7] in which <001> direction becomes parallel to rolling direction and {100} plane becomes parallel to the rolling plane (Fig. 5).

I.2.2.1 Development of Cube Texture in Permalloys

The studies of fcc metals and alloys indicate that development of cube texture in these materials requires fulfilment of several conditions. These conditions may be summarized as[8].

1. The cold rolled texture must be basically copper type (Fig. 4).
2. Very high deformation by cold working prior to annealing.
3. Employment of high annealing temperature.
4. Employment of high annealing time and
5. Small penultimate grains size (PGS).

Benford[9] has found that the sharpness of cube texture in 50 permalloy depends on PGS or rolled grain thickness (RGT). RGT is a function of PGS and pct. cold reduction (Fig. 6). It was found that RGT of 0.004'' to 0.006''produced sharp cube texture. A decrease in hysteresis loop occurs due to decrease of RGT[10]. Littman et al[11] observed that the grain structure in 48 permalloy should be homogeneous and should consist of either very small (100)[001] primary grains or large (120)[001] secondary grains free from annealing twins.

FIGURE CAPTION

Figure 1 : Fe-Ni binary diagram[1].

Figure 2(a) : Effect of heat treatment on initial permeability of Fe-Ni alloys[4].

(b) : Maximum permeability of Fe-Ni alloys due to different heat treatments[4].

Figure 3 : (B-H) vs. H curves for Ni single crystal measured along different crystallographic directions[5].

Figure 4(a) : (111) pole figure for 96.6 pct. CR copper[7].

(b) : (200) pole figure for 96.6 pct. CR copper[7].

Figure 5(a) : (111) pole figure for annealed copper with cube texture[6].

(b) : (200) pole figure for annealed copper with cube texture[6].

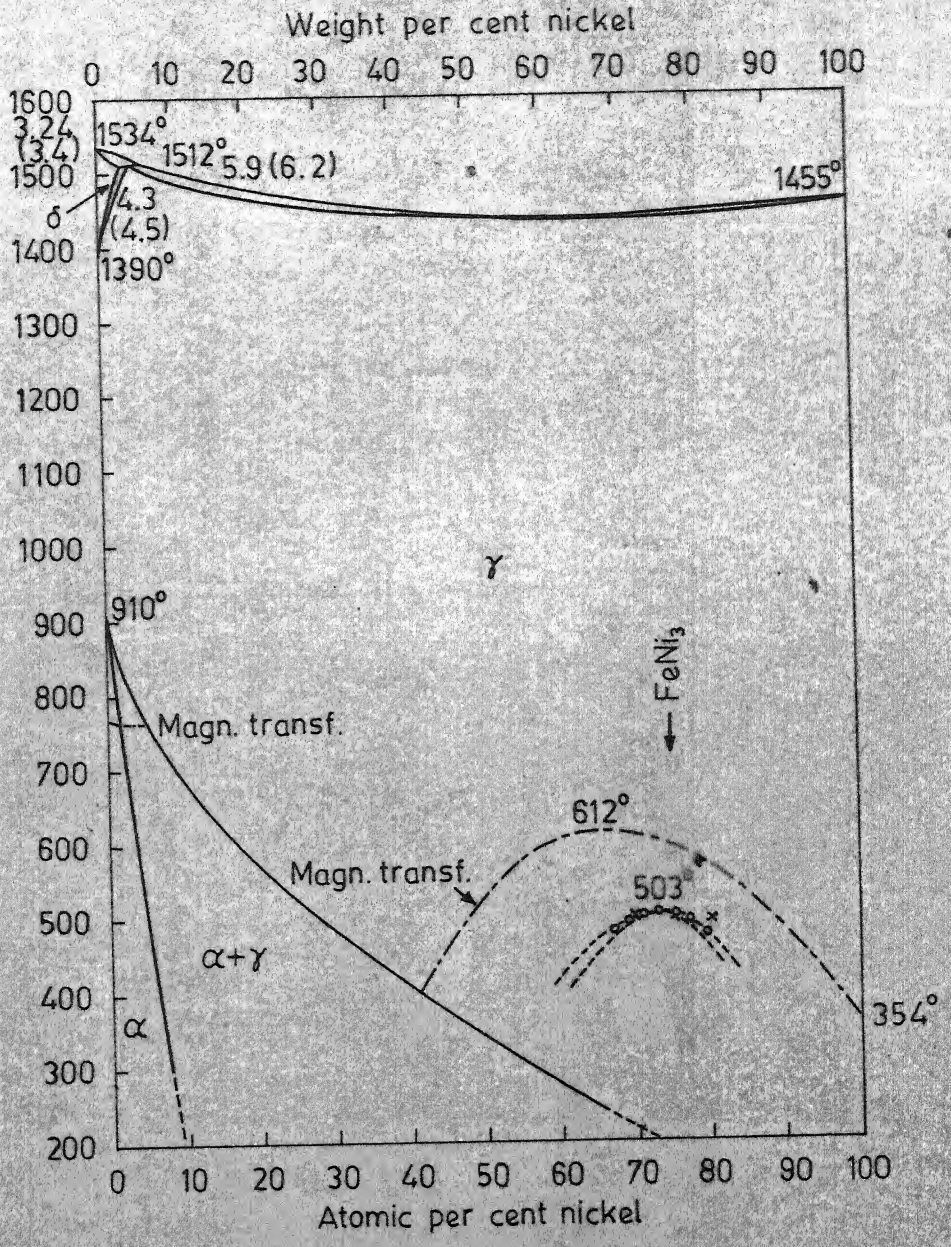
Weight per cent nickel
0 10 20 30 40 50 60 70 80 90 100
1600
1500
1400
1300
1200
1100
1000
900
800
700
600
500
400
300
200
3.24
(3.4)
1534°
1512°
5.9 (6.2)
1455°
δ
4.3
(4.5)
1390°
γ
910°
FeNi3
Magn. transf.
612°
Magn. transf.
503°
α+γ
α
354°
0 10 20 30 40 50 60 70 80 90 100
Atomic per cent nickel

Fig. 1

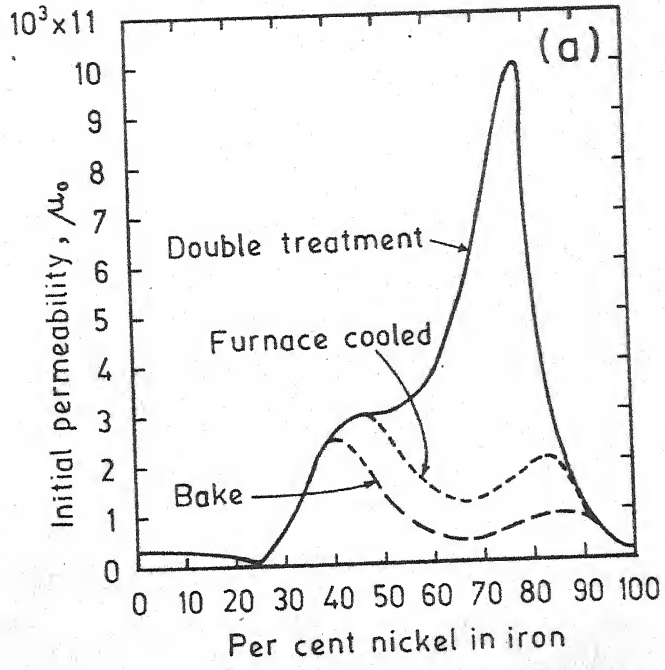
10^3x11
(a)
Initial permeability, μ_0
Double treatment
Furnace cooled
Bake
0 1 2 3 4 5 6 7 8 9 10
0 10 20 30 40 50 60 70 80 90 100
Per cent nickel in iron

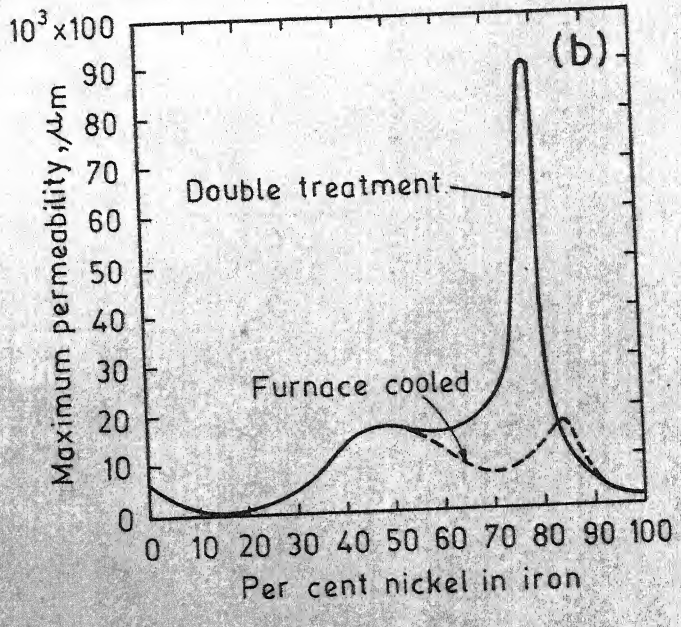
10^3x100
(b)
Maximum permeability, μ_m
Double treatment
Furnace cooled
0 10 20 30 40 50 60 70 80 90 100
0 10 20 30 40 50 60 70 80 90 100
Per cent nickel in iron

Fig. 2

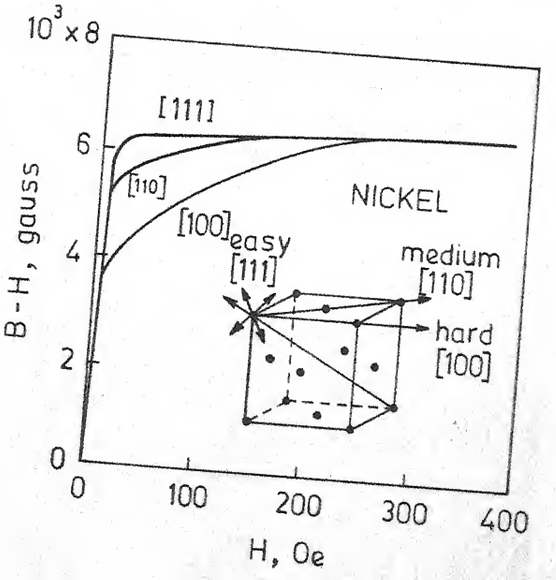
$10^3 \times 8$
[111]
6
[110]
NICKEL
[100]
easy
[111]
medium
[110]
hard
[100]
4
B-H, gauss
2
0
0
100
200
300
400
H, Oe

Fig. 3

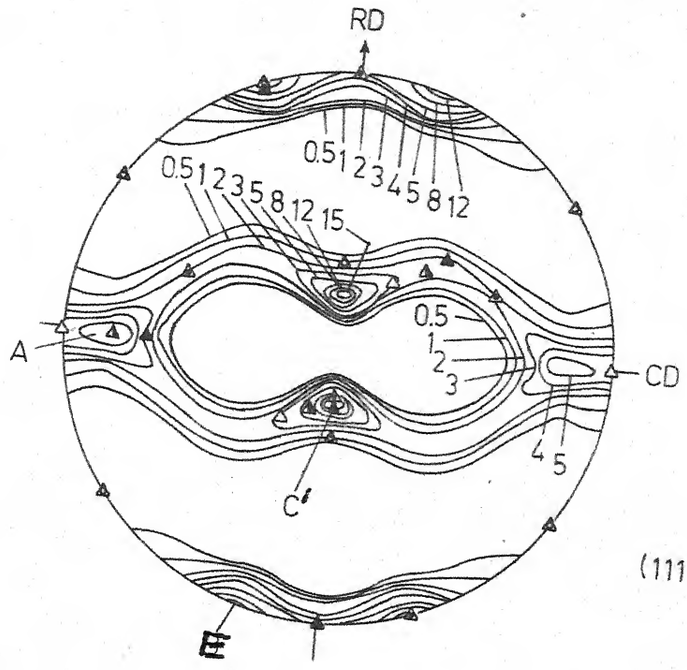

(a)
(111) pole figure

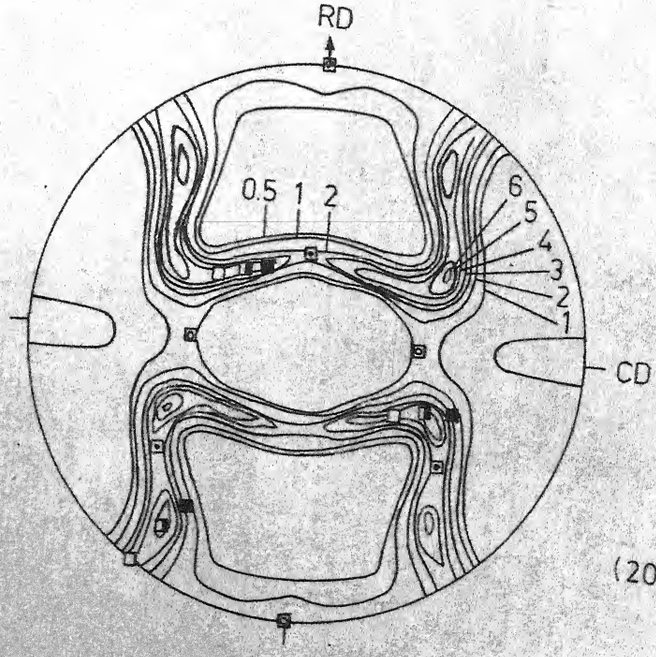

(b)
(200) pole figure

Fig. 4

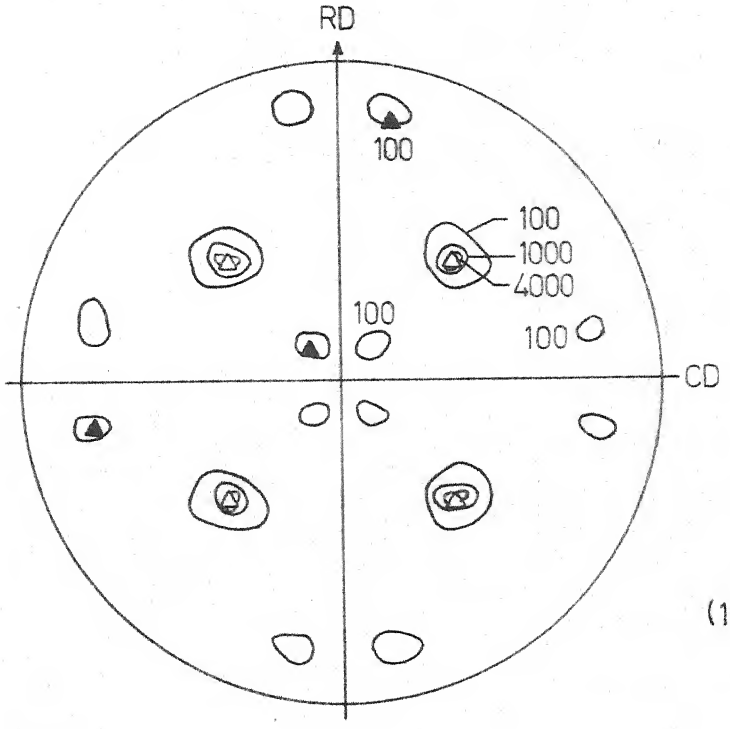

(a)
(111) pole fig

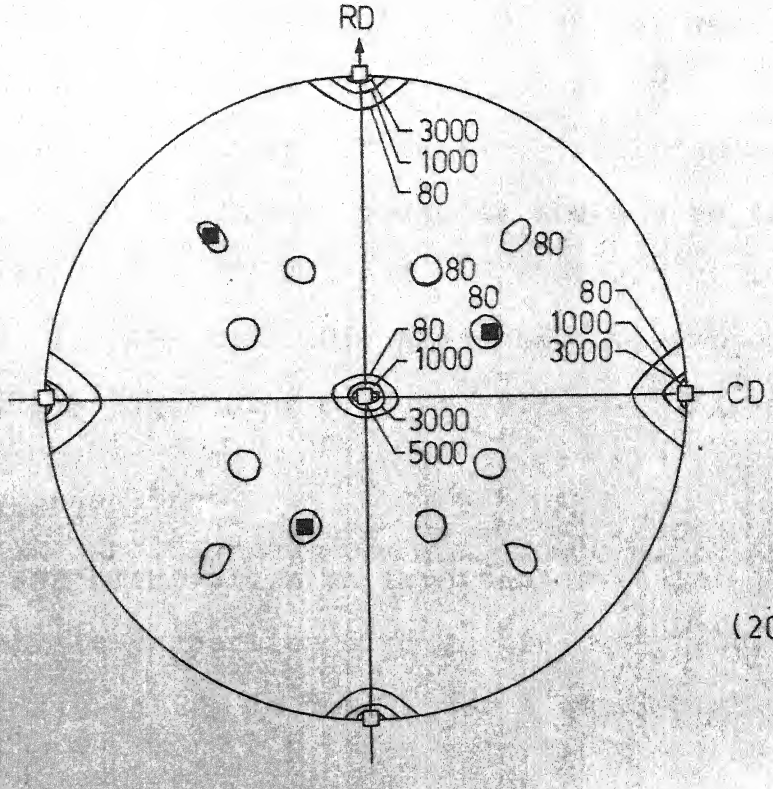

(b)
(200) pole fi

Fig. 5

I.2.2.2 Effect of impurities on texture of permalloys

Savitski[12] studied the effect of impurities, like S (0.025 pct.), oxygen (0.015 pct.) Si (0.025 pct.) and Mn (0.5 pct. and 1 pct.) in 50 permalloy on the annealing temperature range in which good magnetic properties (good loop squareness, low H_c, high incremental permeability and high saturation induction) could be achieved. This study reveals that only Mn addition is beneficial and gives wide range of permissible annealing temperature while Si or oxygen additions tends to narrow the annealing temperature range.

Colling and Aspden[13] found that high permeability in 49 permalloy could be achieved only if S content was kept below 12 ppm. Study on the effect of Si on the sharpness of cube texture produced[9] revealed that the rolled sheet thickness between 0.004" to 0.006" produced sharp cube texture in permalloys containing 0.028 wt. pct. Si whereas still smaller thickness of 0.002 to 0.003" produced similar sharpness in an alloy containing 0.67 wt. pct. Si (Fig. 6).

I.2.2.3 Magnetic Annealing

Magnetic annealing plays an important role in improving the magnetic properties of magnetic materials. In this treatment, annealing is done under a small magnetic

field at a temperature little higher than or just below the curie temperature of the material. This treatment was first employed by Kelsall[14] for 78.5 permalloys. In Fe-Ni alloys, [100] oriented material shows good response to this treatment whereas [111] oriented material does not appear to respond to this treatment[15]. Therefore this treatment is expected to improve the magnetic properties of cube textured Fe-Ni alloys. Magnetic annealing has been carried out mostly on Fe-Ni alloys. Maximum permeability of a 65 permalloy has been found to increase from 10000 to 250000 by heating to 700°C and cooling slowly in a field of 15 Θ_e[16]. Martin and Kang[15] employed this treatment for 53-58 permalloys (Figs. 7-9) and found that permeability increased and magnetostriction decreased due to magnetic annealing. This has been attributed to short range ordering of atom pairs in Fe-Ni alloys. In Fig. 9 initial permeability of 58 permalloy has a peak at 470°C and shows a decreased B-H loop squareness with increasing magnetic annealing temperature.

I.3 Cu-bearing Permalloys

Phase diagram of Fe-Ni-Cu alloys near room temperature is indicated in Fig. 10. Single phase γ-region extends from 35 to 100 pct. Ni on the Fe-Ni side whereas it exists in the whole region on Ni-Cu side. In the central portion of the diagram, the solid solution alloys break up into two

FIGURE CAPTION

Figure 6 : Quality of cube texture produced in 50 permalloy as a function of rolled grain thickness. (A) Fe-Ni alloy with 0.028 pct. Si, (B) Fe-Ni alloy with 0.67 pct. Si[9].

Figure 7 : Permeability vs. flux density curves for 58 permalloys: (A) After primary heat treatment at 1200°C, (B) After subsequent magnetic annealing at 470°C and (C) a conventional 50 permalloy[15].

Figure 8 : Magnetostriction vs flux density curves for 53 permalloy: (A) After magnetic annealing at 450°C and (B) before magnetic annealing (after primary annealing at 1200°C)[15].

Figure 9 : Initial permeability and squareness vs. temperature of magnetic annealing for 58 permalloys[15].

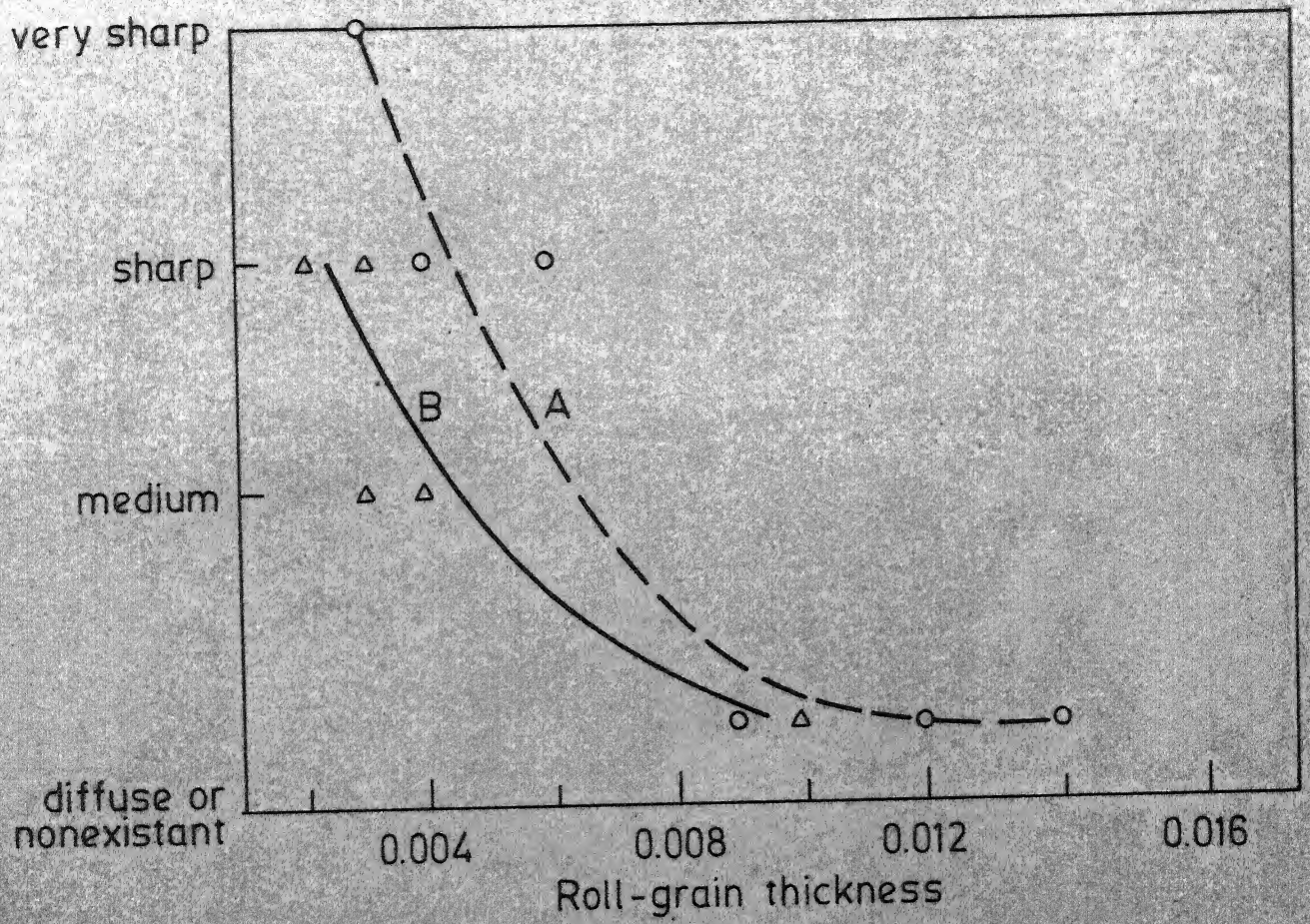
very sharp
sharp
medium
diffuse or
nonexistant
B
A
0.004
0.008
0.012
0.016
Roll-grain thickness

Fig. 6

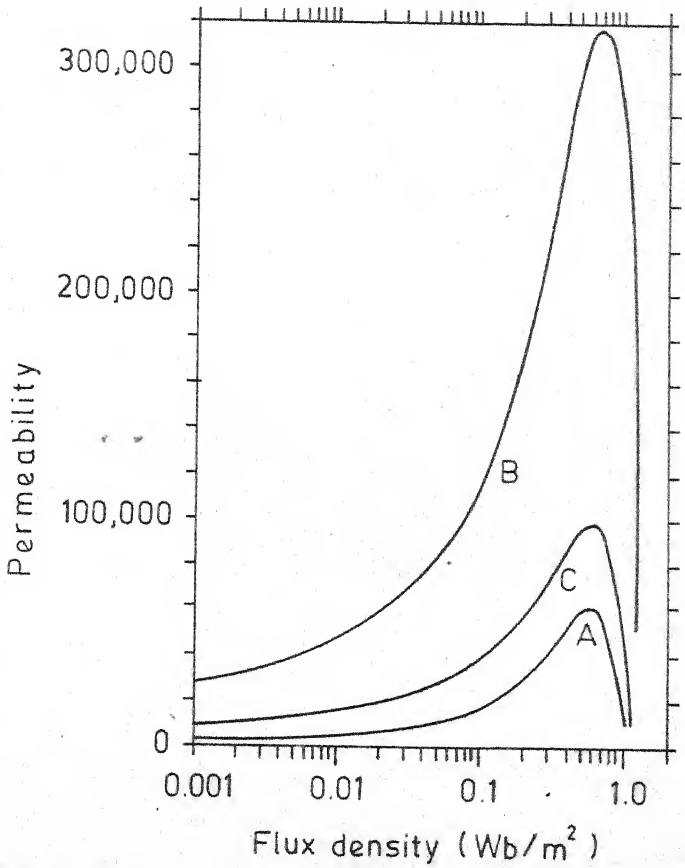

Fig. 7

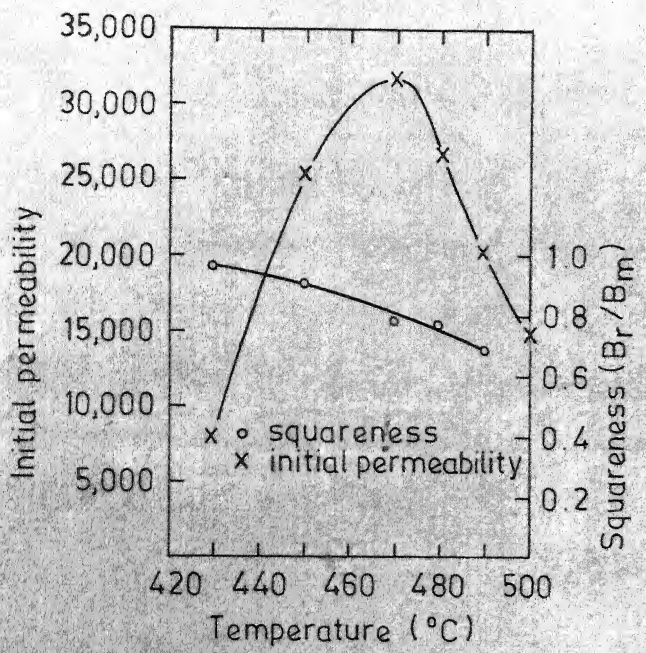

Fig. 9

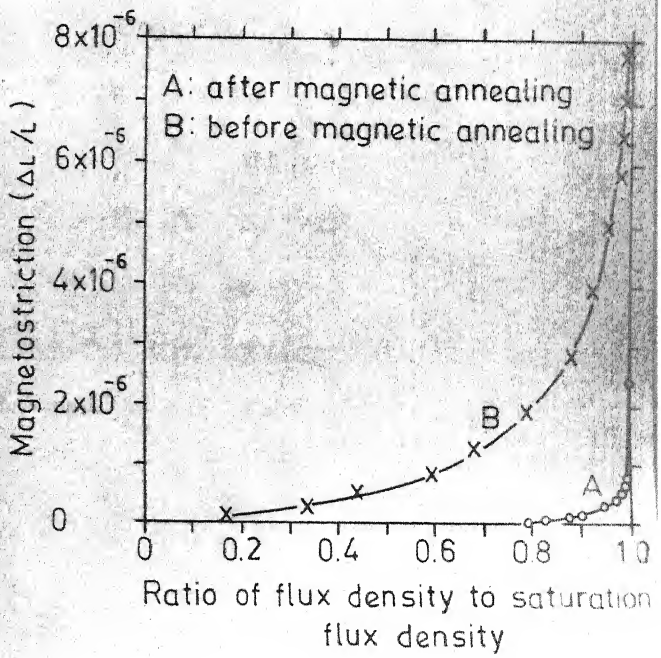

Fig. 8

-phases, one phase rich in Cu content whereas the other phase is rich in Fe and Ni. This decomposition can be supressed to some extent by quenching the alloy from high temperature. Curie temperature and saturation induction of permalloys decrease with increase in copper content. The curie points for various quenched alloys are indicated in Fig. 10. Addition of Cu to Fe-Ni alloys increases the electrical resistivity only to a small extent. Muller[19] indicates that the Fe-Ni Cu alloys can be given mechanical and thermal treatments to develop cube texture over wide range of composition (Fig. 12).

I.3.1 μ-metal

Mumetal is an alloy in the series of Fe-Ni-Cu alloys which is most widely used. Original μ-metal contains 5 wt. pct. Cu, 75 wt. pct. Ni and rest Fe whereas some commercial μ-metals contain upto about 2 pct. Cr and ~ 1 wt. pct. Mn along with 5 wt. pct. Cu and 75 wt. pct. Ni. Permeability of copper containing permalloys increases with increase in Cu content and has the highest permeability with Cu content of 10 to 18 wt. pct. (Fig. 13). H_c for the quenched alloy containing 27 wt. pct. Cu, 60 wt. pct. Ni and rest Fe was found to be 0.025 Oe[21].

Some work has been done in I.I.T. Kanpur on Cu-bearing permalloys containing 5 pct. and 14 pct. Cu. This study has revealed that on air cooling after hot rolling the alloys containing Mn (usually added for imparting ductility to the Fe-Ni alloys) in excess of 0.5 pct. causes brittleness especially for the higher Cu containing alloys. On reheating the hot rolled strips to 800°C and quenching it in water the alloys were found to become more ductile. This indicates that addition of Cu and Mn possibly cause enhancement of ordering reaction that exists in the Fe-Ni system. Svestka and Tischer[22] also found the optimum Mn content in the range of 0.3 - 0.5 pct. at baking temperature of 500-550°C for ensuring good hot workability of μ-metal containing 76 wt pct. Ni - 2 wt. pct. Cr - 5 wt. pct. Cu - rest Fe (Fig. 11). D.J. Snee[23] studied the effect of cooling rate and composition on the initial permeability (μ_o) of μ-metal containing 1-3 pct. Cr, 5 pct. Cu, 74-77 pct. Ni and rest Fe (Fig. 14). Cooling rate of 92°C/hour was found to be optimum for alloys containing 75.5-76.5 pct. Ni, 2-2.9 pct. Cr, 5 pct. Cu and rest Fe. For fixed Ni content, optimum cooling rate increases with decreasing Cr content whereas for given Cr content, cooling rate increases with increase in Ni content.

In the Fe-Cu-Ni alloy series, Isoperm is another alloy in which Ni content varies from 40 to 50 wt. pct. and Cu

content varies from few percent to a maximum of about 15 wt. pct. Cu. At Fe:Ni = 1:1, the H_c is low and remains more or less the same upto about 18 pct. Cu and then increases rapidally with increase in copper content (Fig. 15). Copper bearing permalloys appear to respond to the permalloy treatment, high μ_o is obtained by permalloy treatment at lower copper contents than when furnace cooled (Fig. 16).

I.3.2 Fe-Ni-Cu-Mo alloys

Fe-Ni-Cu-Mo phase diagram is not available but the magnetic characteristics of some of these alloys are available. Fig. 17 summarizes[25] the composition dependence of the magnetocrystalline anisotropy constant K_1 and of the saturation magnetostriction constant λ. Copper may be substituted for Fe without significant alteration of the $K_1 = 0$ line. Away from this line, however, the absolute value of K_1 decreases with Cu and Mo additions. Addition of Cu and Mo reduces the saturation magnetization and Curie temperature. Increasing Mo lowers the cooling rate necessary to obtain $K_1 = 0$ (Fig. 17). The $K_1 = 0$ line is highly sensitive to cooling rate or isothermal annealing, in the region of 300 to 600°C. The $\lambda = 0$ lines are essentially independent of Ni content but highly dependent on Cu. The single crystal $\lambda_{100} = 0$ and $\lambda_{111} = 0$ lines differ by about 2 pct. Ni and are not as much

FIGURE CAPTION

Figure 10 : Fe-Ni-Cu ternary diagram showing curie points[17,18].

Figure 11 : Permeability (μ_4) dependence on Mn content of 76 pct. Ni, 2 pct. Cr, 5 pct. Cu, 17 pct. Fe alloy at various baking temperatures[19].

Figure 12 : Recrystallization textures in Fe-Ni-Cu alloys[20].

Figure 13 : Initial permeability curves in Fe-Ni-Cu ternary diagram[22].

Figure 14 : Effect of cooling rate and composition of 76 pct. Ni, 2.6 pct. Cr, 5 pct. Cu, 16.4 pct. Fe alloys on initial permeability[23].

Figure 15 : Increase of coerecive force with pct. Cu in Fe-Ni alloy (annealed at 900°C)[24].

Figure 16 : Highest initial permeabilities of Fe-Ni-Cu alloys at given Cu contents[20].

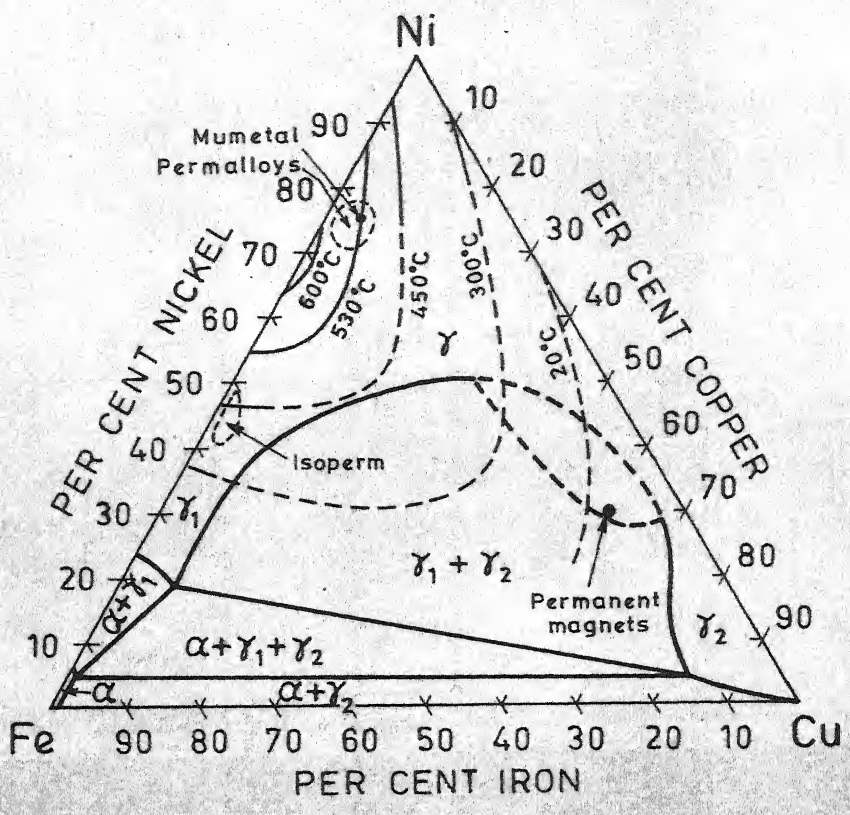
Ni
Mumetal
Permalloys
PER CENT NICKEL
PER CENT COPPER
PER CENT IRON
Fe
Cu
Isoperm
Permanent magnets
600°C
530°C
450°C
300°C
200°C
γ
γ1
γ2
γ1 + γ2
α+γ1
α+γ1+γ2
α+γ2
α

Fig. 10

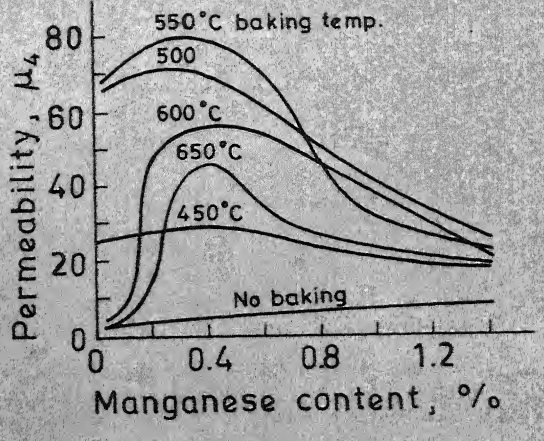
550°C baking temp.
500
600°C
650°C
450°C
No baking
Permeability, μ4
Manganese content, %

Fig. 11

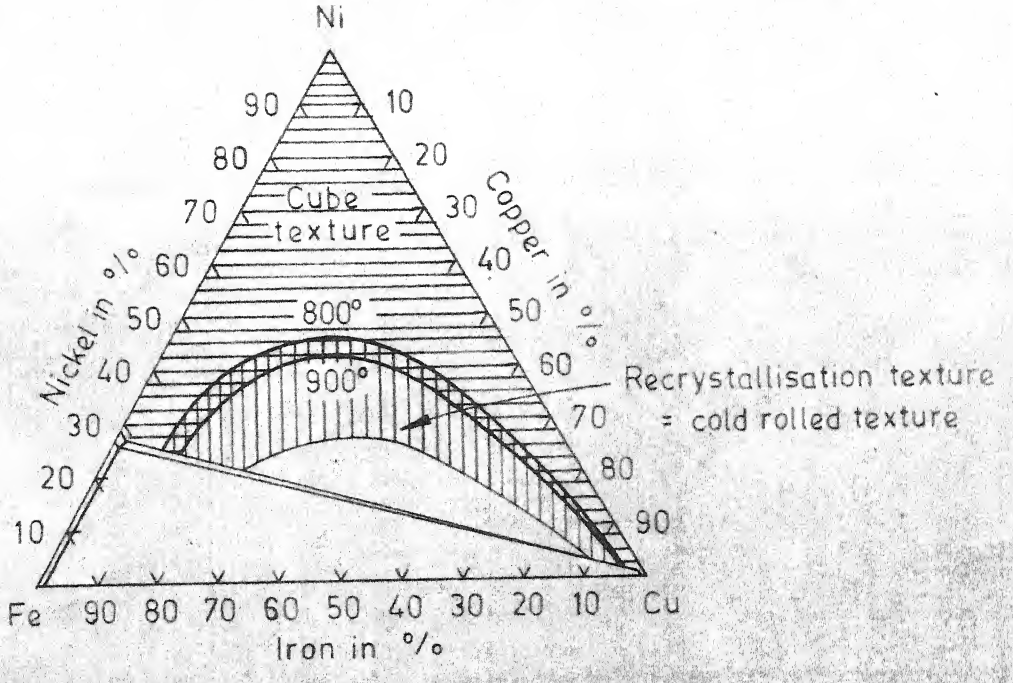
Ni
90
80
70
60
50
40
30
20
10
Nickel in %
10
20
30
40
50
60
70
80
90
Copper in %
Cube
texture
800°
900°
Recrystallisation texture
= cold rolled texture
Fe 90 80 70 60 50 40 30 20 10 Cu
Iron in %

Fig. 12

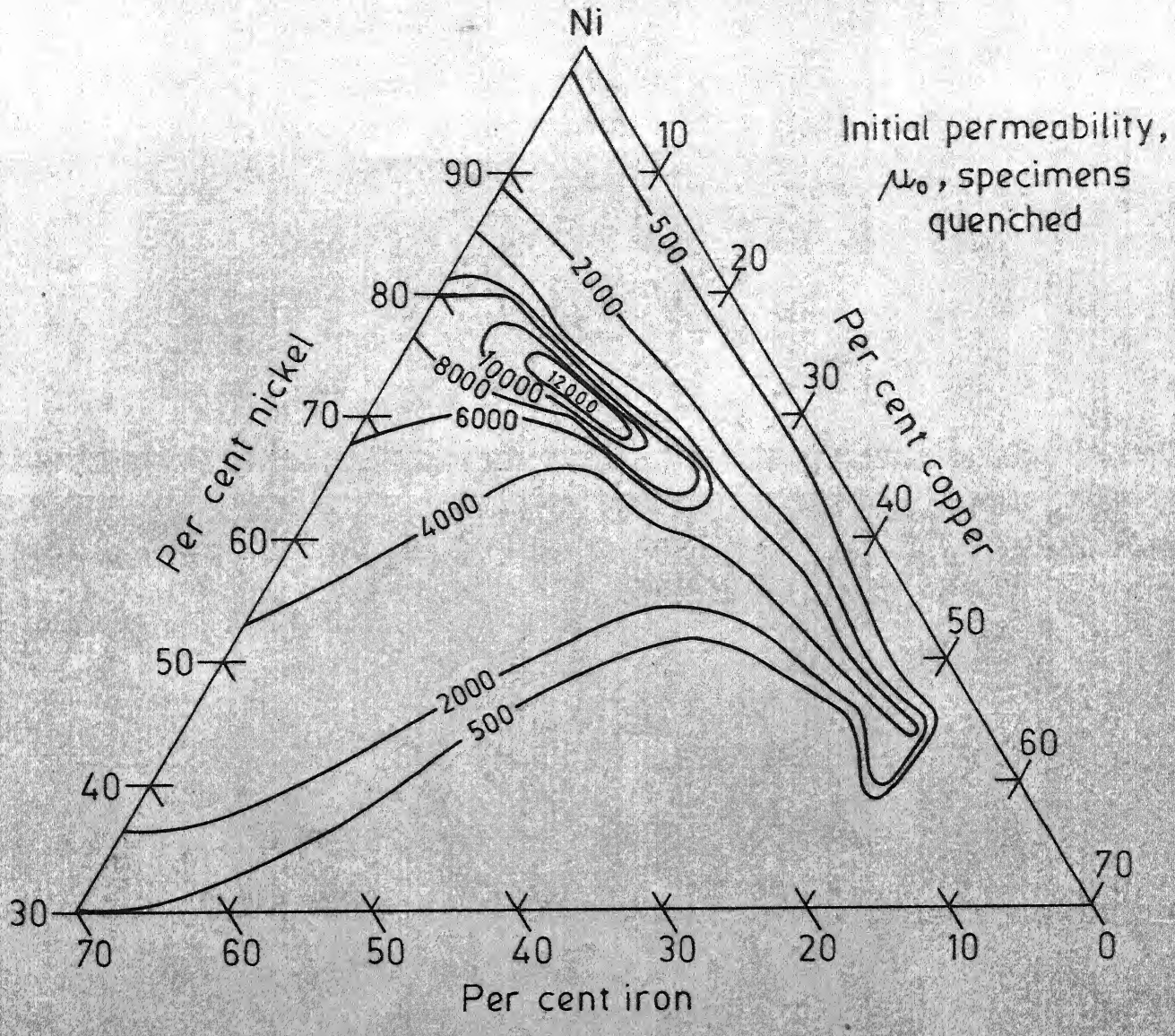
Ni
Initial permeability, μ_0, specimens quenched
Per cent nickel
Per cent copper
Per cent iron
10
90
20
80
30
70
40
60
50
50
60
40
70
30
0
10
20
30
40
50
60
70
500
2000
4000
6000
8000
10000
12000
2000
500

Fig. 13

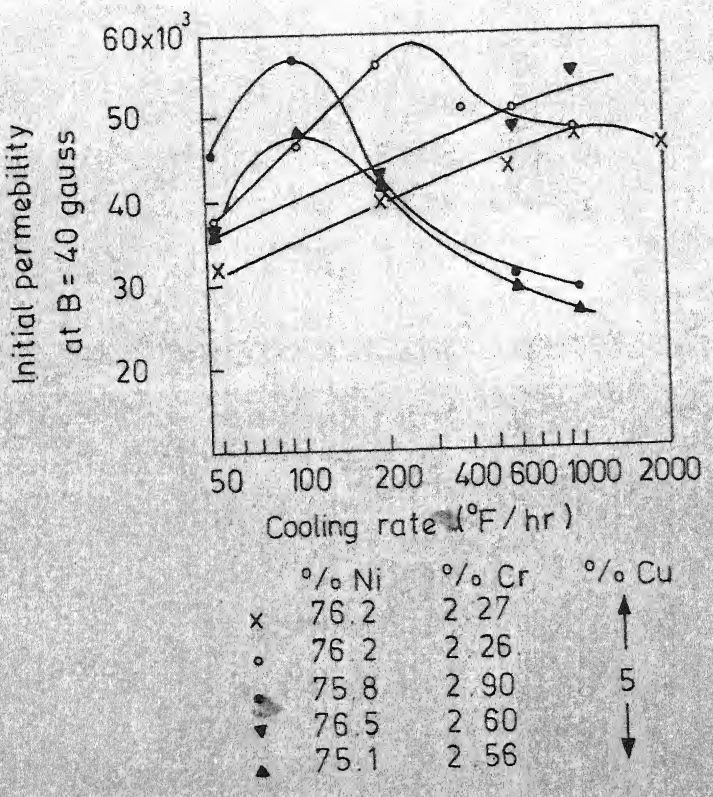
60x10³
50
40
30
20
Initial permeability
at B = 40 gauss
50 100 200 400 600 1000 2000
Cooling rate (°F / hr)
% Ni
% Cr
% Cu
x 76.2 2.27
o 76.2 2.26
● 75.8 2.90
▼ 76.5 2.60
▲ 75.1 2.56
5

Fig. 14

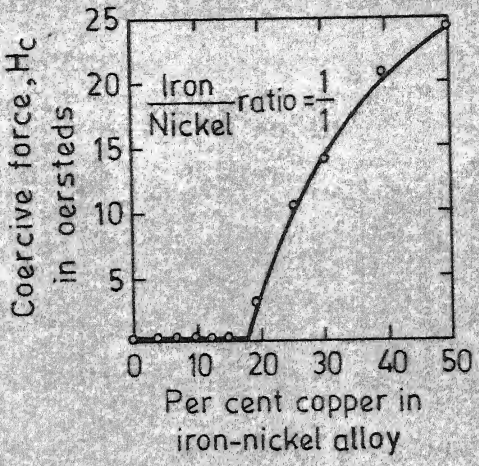
Coercive force, H_c in oersteds
25
20
15
10
5
Iron / Nickel ratio = 1/1
0 10 20 30 40 50
Per cent copper in iron-nickel alloy

Fig. 15

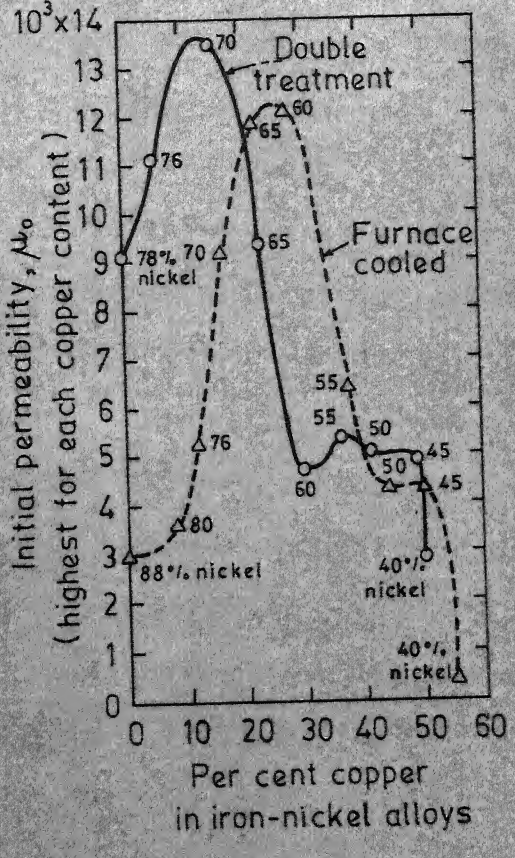
$10^3 \times 14$
Initial permeability, μ_o (highest for each copper content)
Double treatment
Furnace cooled
78% nickel
88% nickel
40% nickel
40% nickel
0 10 20 30 40 50 60
Per cent copper in iron-nickel alloys

Fig. 16

influenced by the cooling rate as is the $K_1 = 0$ line. λ tends toward isotropy, with increasing cooling rate.

It was found[26] that the cooling rate and bake temperature are functions of Fe, Cu and Mo contents. As the Fe content of Fe-Ni-Cu-Mo alloy decreases, faster cooling rate is required to develop high permeability. Addition of Cu and Mo increases permeability of Fe-Ni alloys. Addition of Cu and Mo to Fe-Ni alloys is expected to lower down order-disorder temperature[26]. The magnitude and sign of first anisotropy constant K_1 at room temperature of alloy containing 77 pct. Ni - 14 pct. Fe - 5 pct. Cu - 4 pct. Mo by weight are shown to be dependent on the degree of short range order. Among Mo and Cu bearing permalloys, the only remarkable one is the 1040 alloy which was first discovered by Neumann 1934. It contains 14 pct. Cu, 3 pct. Mo, 72 pct. Ni and rest iron. The most remarkable property of this alloy is the high μ_o of about 40000, compared to 4-79 Mo permalloy.

Major and Martin[27] found the improvements in magnetic properties of cube textured alloys containing 13.95 wt. pct. Fe, 4.86 wt. pct. Cu, 4.20 wt. pct. Mo and balance Ni over a randomly oriented alloy of same compositions (Figs. 18-21). It was concluded that secondary recrystallization could be obtained by first annealing the 0.1'' thick sheet and then cold rolling to 0.006'' and 0.004'' in order to give 94 pct. and 96 pct. cold reduction respectively.

FIGURE CAPTION

Figure 17 : Nickel corner of Ni-Fe-Mo alloys in which Cu is substituted for Fe. Line A alloys are highly responsive to magnetic annealing[25].

Figure 18 : Permeability at 40G vs. annealing temperature curves for oriented and random samples of 94 pct. cold rolled alloy containing 13.95 pct. Fe, 4.86 pct. Cu, 4.20 pct. Mo, bal. Ni[27].

Figure 19 : Permeability at 40 G vs annealing temperature curves for oriented and random samples of 96 pct. cold rolled alloy containing 13.95 pct. Fe, 4.86 pct. Cu, 4.20 pct. Mo, bal.Ni[27].

Figure 20 : Squareness ratio vs annealing temperature curves for oriented and random samples of 94 pct. cold rolled alloy containing 13.95 pct. Fe, 4.86 pct. Cu, 4.20 pct. Mo, bal. Ni[27].

Figure 21 : Squareness ratio vs. annealing temperature curves for oriented and random samples of 96 pct. cold rolled alloy containing 13.95 pct. Fe, 4.86 pct. Cu, 4.20 pct. Mo, bal. Ni[27].

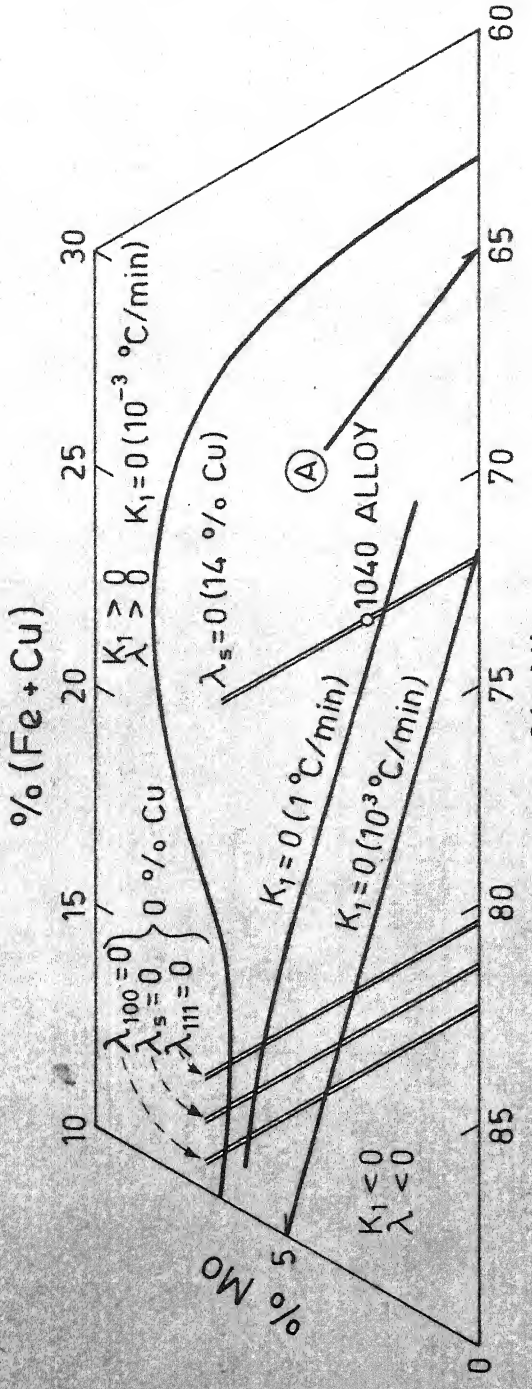
% (Fe + Cu)
% Ni
% Mo
10
15
20
25
30
60
65
70
75
80
85
0
5
$\lambda_{100}=0$
$\lambda_s=0$
$\lambda_{111}=0$
0 % Cu
$K_1 \geq 0$
$K_1=0\,(10^{-3}$ °C/min)
$\lambda_s=0$ (14 % Cu)
A
1040 ALLOY
$K_1=0$ (1 °C/min)
$K_1=0\,(10^3$ °C/min)
$K_1<0$
$\lambda<0$

Fig. 17

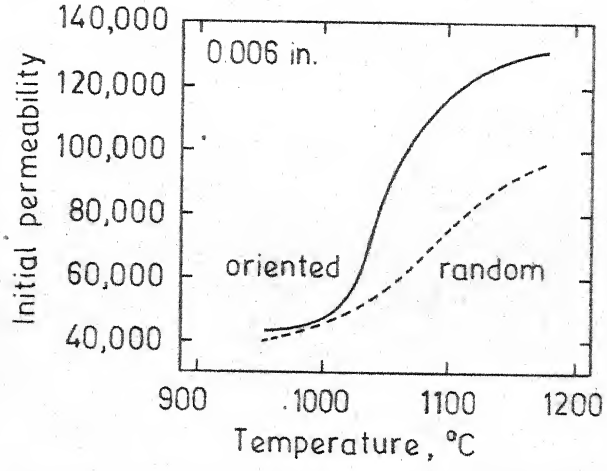
140,000
120,000
100,000
80,000
60,000
40,000
Initial permeability
0.006 in.
oriented
random
900
1000
1100
1200
Temperature, °C

Fig. 18

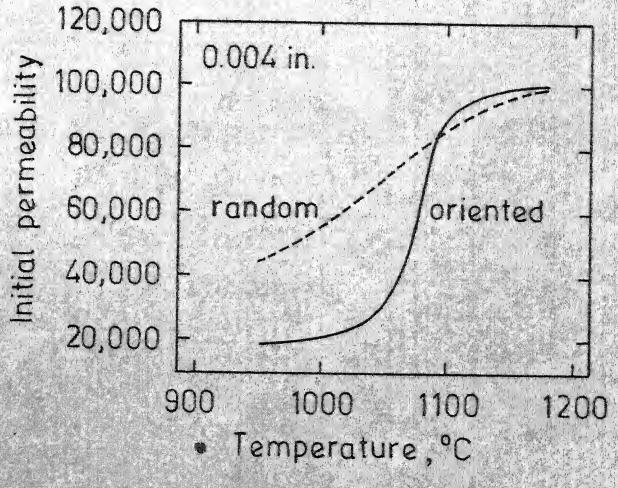
120,000
100,000
80,000
60,000
40,000
20,000
Initial permeability
0.004 in.
random
oriented
900
1000
1100
1200
Temperature, °C

Fig. 19

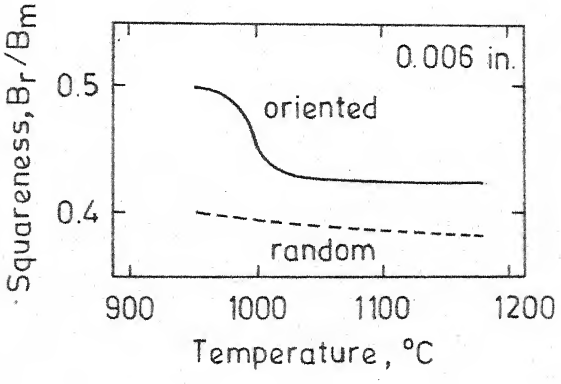
Squareness, B_r/B_m
0.5
0.4
0.006 in.
oriented
random
900
1000
1100
1200
Temperature, °C

Fig. 20

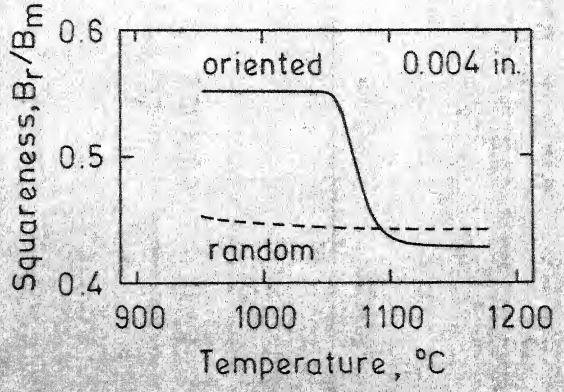
Squareness, B_r/B_m
0.6
0.5
0.4
oriented
0.004 in.
random
900
1000
1100
1200
Temperature, °C

Fig. 21

Table I : Some properties of common commercial permalloys[29].

Permalloy composition and heat treatment	Permeability Initial (μ_o)	Permeability Maximum (μ_m)	H_c (θ_e)	B_s (Gauss)	W_h (ergs/cm^3)	T_c (^oC)	ρ ($\mu\Omega$ cm)	d (g/cm^3)	UTS (kg/mm^2)	pct. elongation
1	2	3	4	5	6	7	8	9	10	11
45 Permalloy (45Ni-55 Fe) (1050^oC annealed)	2500	25000	0.3	16000	1200	440	45	8.17	45.5-56.0	40
68 Permalloy (68 Ni - 32 Fe) (1000^oC, magnetic cooled)	1200	250000	0.03	13000	120	600	20	8.45	-	-
78 Permalloy (78.5Ni - 21.5Fe (1050^oC, 600^oC quenched)	8000	100000	0.05	10800	580	600	16	8.60	52,5-63.0	50
4-79 Permalloy (4Mo, 79Ni,17Fe) (1100^oC,controlled cooling rate)	20000	100000	0.05	8700	200	460	55	8.72	59.5	-
Supermalloy (5Mo,79Ni-16Fe) (1300^oC,H_2 annealed, controlled cooling rate)	100000	1000000	0.002	7900	8	400	60	8.77	-	-

Table I (Contd.)

1	2	3	4	5	6	7	8	9	10	11
Mumetal (5Cu,2Cr,77Ni, 16Fe) ($1175^{o}C, H_2$ annealed)	20000	100000	0.05	6500	-	430	62	8.58	49.0^{φ}	25^{φ}
1040 Alloy (3Mo,14Cu,72Ni, 11Fe) ($1100^{o}C, H_2$ annealed)	40000	100000	0.02	6000	200	290	56	8.76	-	-

φ These mechanical data are for Mumetal possibly containing no chromium.

H_c = Coercieve force, B_s = saturation induction W_h = Hysteresis loss,

T_c = Curie temperature, ρ = Electrical resistivity, d = Density,

UTS = Ultimate tensile strength.

I.4 Statement of the Problem

The literature review presented in previous sections indicates that the magnetic properties of permalloys can be improved through the development of perfect cube texture and through suitable heat treatments e.g. magnetic annealing or controlled cooling etc. The development of textured magnetic materials thus can be divided in two parts - (1) development of magnetic material through the development and perfection of cube texture in permalloys and (2) development of better magnetic properties in textured permalloys through suitable heat treatment. The permalloys chosen for this study are the copper bearing permalloys and it was decided to attempt development of strong cube texture in these alloys first before attempting to improve the magnetic properties by heat treatment.

Alloys chosen for the present study are 5 pct. Cu and 14 pct. Cu containing 75 pct. Ni-Fe alloys with small additions (upto 2 pct.) of Ti and Cr. Based on the results obtained by Sarkar[28] for the 48 permalloy, the alloys are to be cold rolled with pct. reduction in thickness varying between 95 pct. to 98 pct. and the annealing is proposed to be done at a fixed temperature of 1050°C for varying lengths of time using argon or hydrogen atmosphere. After developing proper texture in these alloys, it is proposed to study the

magnetic properties of the textured alloys by using a vibrating sample magnetometer and a permeameter. An attempt will also be made to improve the magnetic properties through treatments like magnetic cooling and controlled quenching treatments.

CHAPTER II

EXPERIMENTAL PROCEDURE

CHAPTER II

EXPERIMENTAL PROCEDURE

The present study has been made with copper bearing Fe-Ni alloys containing small amounts of additional alloying elements Cr and Ti. The intended composition of the alloys used for this study are shown in Table II. The experimental procedure adopted for this study is given in detail in the following sections.

II.1 Alloy Preparation

Alloys were prepared using 99.9 pct. pure Fe, Ni and Cu supplied by Semi Elements, USA, 99.9 pct. pure Cr supplied by Union Carbide, USA and Ti chips supplied by BARC, Bombay. Allloys were melted in a 6 kilo-watt Ajax induction melting unit fitted with a sealed end quartz tube melting chamber. About 200 gms of each alloy was melted in argon atmosphere using recrystallized alumina crucibles. A graphite cruicible with graphite cover was used as susceptor. Before melting the furnace chamber was evacuated to about 50μ of Hg and flushed with argon. This process was repeated twice to drive out air from the melting chamber. Since the melting point of the alloys were in the range of 1450° to 1475°C, therefore, the temperature of the charge was raised upto

1500-1550°C. The melt was allowed to solidify in the cruicible itself. Ingots thus obtained were of about 1'' dia and about 2½'' long and usually had surface blow holes. Melting losses in all cases were found to be in the range of 0.2 to 0.4 pct. Before further processing, the ingots were turned to remove the surface blow holes. The ingots were homogenized at 1150° to 1175°C for 1 hour. The homogenized alloys were chemically analysed to findout chemical composition which are shown in Table III. The intended and actual composition for all alloys except one alloy were found reasonably close to each other. The alloy X° was found to contain larger amount of copper than intended. This is possibly due to accidental improper weighing out of copper for the charge for melting.

II.2 Fabrication of alloys

II.2.1 Hot Rolling

In order to break the cast structure and reduce the the thickness, each ingot was hot rolled. The ingots were soaked at temperatures between 1150 and 1175°C for 1 hour and then hot rolled in order to avoid cracking of specimens. In the initial stages, two to three passes were allowed after each soaking but later on when sample thickness was reduced,

Table II : Alloy designation for different Cu bearing permalloys

Alloy designation is given as α^{m} pn

where α = P,Q,R, ... etc. signify nominal alloy composition

p = a,b,c,d, ... etc. signify pct. reduction in thickness

m = 0,1,2, ... etc. signify melt number

n = 0,1,2,3,4,.... etc. signify hrs of anneal of cold rolled strips at 1050°C

Alloy designation followed by (H_2) indicates hydrogen anneal. If nothing is mentioned after alloy designation, it indicates argon anneal.

Pct. reduction in thickness for different designation of p

	pct. reduction in thickness				
	95	96	97	98	99
p	a	b	c	d	e

Table II (Contd.)

Nominal alloy composition for different designations of α

α	Alloy element content (nominal) in wt. pct.					
	Ni	Mn	Cu	Cr	Ti	Fe
P	75	0.5	5	-	-	19.5
R	75	0.5	14	-	-	10.5
T	75	0.5	5	2	-	17.5
U	75	0.5	5	-	2	17.5
V	75	0.5	5	1	1	17.5
W	75	0.5	14	1	1	8.5
X	75	0.5	10	-	2	12.5
Y	75	0.5	14	-	2	8.5

Table III: Analysed Chemical Composition of Cu bearing Permalloys.

Element in wt. pct. \ Alloy designation	T^o	U^o	V^o	V^1	X^o_{xx}	W^o	Y^o
Fe	18.0	19.5	18.5	18.0	18.7	9.6	9.0
Cu	4.7	4.5	4.9	4.5	11.0	13.0	12.8
Ti	-	1.5	0.9	0.9	1.45	0.9	1.7
Cr	1.9	-	0.8	0.8	-	0.78	-
Mn	0.55	0.54	0.53	0.55	0.55	0.55	0.55
Ni$^{\varphi}$	74.85	73.96	74.37	75.25	68.3	75.17	75.95

$^{\varphi}$ Ni content is obtained by difference.

xx Intended composition of X^o is same as of U^o alloy but the actual chemical analysis of this alloy (X^o) has indicated higher Cu content. (11.0 pct.) possibly due to improper weighing of copper in the alloy charge.

not more than one pass was allowed after each soaking of about 15-20 minutes. This procedure was found to produce hot rolled slab without cracks. Reduction per pass varied between 0.02" and 0.01". Final thickness of hot rolled slabs of different alloys varied according to the final pct. age cold reduction desired and the final sheet thickness desired. The final hot rolled thickness of different specimens are shown in Table IV. After attaining the final hot rolled thickness, the hot rolled slabs were heated for 10-15 minutes at 1000°C and quenched in cold water.

II.2.2 Cold Rolling

The water quenched hot rolled slabs were first cleaned with coarse emergy paper in order to remove thin oxide layer formed on the surface during hot rolling. The edges were ground off to remove the side cracks. Cold rolling was done at room temperature. The minimum thickness of the specimen which was attained after cold rolling as a single sheet was in the range of 0.010-0.011". Further reduction in thickness was done by pack rolling i.e. rolling three strips together. The final cold rolled, thickness of sheets varied between 0.0035" to 0.005" according to the desired pct. age cold reduction. The starting and final thickness alongwith pct. reduction of each specimen is shown in Table IV. Thickness

of hot rolled slabs, where it was more than that was required, were reduced to the required value by grinding the surface of hot rolled slabs. Final cold reduction in thickness varied in the range of 96-98 pct.

II.3. Physical property measurement

II.3.1 Mechanical Testing

Mechanical properties play important role in governing the workability of the material. Therefore mechanical properties were found out using Instron 1195 mechanical testing machine. Cold rolled sheets of 0.04" thickness were annealed at 1050°C for 1 hour before preparing the test specimens. The dimensions of the test specimens used are shown in Fig. 25. Gauge length used was 0.787" (20 mm). The load elongation diagram was drawn automatically on a strip chart recorder and the total elongation was also noted from the dial of the testing machine. Using this plot, various properties like pct. elongation, total elongation, proof stress and ultimate tensile stress were found out for each specimen.

II.3.2 Electrical Resistivity Measurement

Higher is the electrical resistivity of a soft magnetic alloy lower will be its eddy current loss. Hence it is an important property of soft magnetic alloys which should be

Table IV : Hot and cold rolled thickness of alloy strips

Alloy Designation	Hot rolled thickness$^{\varphi}$ (inch)	Cold rolled^{+} thickness Initial (inch)	Final (inch)
$T^{o}b$	0.132	0.124	0.005
$T^{o}c$	0.132	0.120	0.0035
$U^{o}b$	0.138	0.124	0.005
$U^{o}c$	0.138	0.120	0.0035
$V^{o}b$	0.130	0.121	0.0048
$V^{o}c$	0.130	0.120	0.0036
$W^{1}d$	0.165	0.165	0.0033
$X^{o}d$	0.176	0.175	0.0035
$W^{o}b$	0.163	0.125	0.005
$W^{o}c$	0.163	0.160	0.0048
$Y^{o}b$	0.160	0.125	0.005
$Y^{o}c$	0.160	0.160	0.0048

φ Hot rolled between 1050° to 1150°C.

+ Cold rolling done at room temperature.

determined. About 3" long and 0.05" wide specimens were cut out from cold rolled sheets. The specimens were sealed in evacuated fused silica capsules and annealed at 950°C for ½ hour. Surface of annealed specimens were cleaned with emery paper and etched with 1 pct. HNO_3 solution.

Specimen holder used for putting the resistivity specimens is shown in Fig. 22. Current through the specimens was standardized through the measurement of potential drop across a NBS standard resistances. Voltage drop across the specimen was measured to find out the electrical resistance of each specimen. A Leeds and Northrup Type K-3 Universal Potentiometer and Keithley Null Detector were used in measuring the potential and getting the null point respectively.

II.3.3 Differential Thermal Analysis (DTA)

When disordering of atoms takes place in a chemically ordered alloy, there is absorption of energy. This fact has been utilized in an attempt to determine the order-disorder temperature of Cu-bearing permalloys. Samples of cylindrical shape of 0.1" dia. and 0.2" long were prepared. An axial blank hole was made in each specimen so that it could sit on the thermocouple tip properly. Since for DTA work, one standard alloy is required in which no energy absorption or

evolution takes place, a 90 at. pct. Ni, 10 at pct. Cr alloy was considered as a standard specimen because it does not show any type of transformation above 100°C (its curie temperature being close to room temperature).

Since the alloys had various amounts of alloying elements and that the alloying elements may lower the transition temperature of alloys, especially for those containing higher amounts of Cu, it was necessary to give long heat treatment to the alloys. To ensure that the alloys have sufficient chance to go through ordering reaction a stepwise lower temperature annealing schedule was used. The alloys were annealed in evacuated and sealed fused silicate tubes at 950°C for 2 hrs. and then it was followed by a step anneal: 450°C for 406 hrs. → 400°C for 170 hrs → 350°C for 490 hrs. → 250°C for 250 hrs. and finally the alloys were cooled in air without breaking the vacuum seal. These specimens were used after thorough cleaning of the specimens (especially the blank hole) for DTA work. A locally fabricated DTA apparatus was used for measuring order-disorder temperature. DTA specimen together with the standard specimens were heated in an air-tight furnace tube in purified argon atmosphere. Gas flow rate was controlled to 2-3 bubbles per minute. The emf of the (Pt vs Pt-10 pct. Rh) differential thermocouple was fed to a L and N microvolt amplifier and recorded in an

Omniscribe two pen strip chart recorder. A Pt vs Pt-10 pct. Rh thermocouple was used for specimen temperature measurement and for controlling the heating rate. The temperature measuring thermocouple was connected to the second pen of the recorder to serve both these purposes. The furnace was heated up at the rate of 2°C/minute using Indotherm 457 programmer-controller.

II.4 Texture development

II.4.1 Heat Treatment

The cold rolled strips were cut into about $1\frac{1}{4}$'' long X about $1\frac{1}{4}$'' wide size. These strips were annealed in flowing purified argon gas using the furnace shown in Fig. 23. Annealing temperature employed for all cases was 1050 ± 2°C and annealing time varied from 1 to 6 hours. After the furnace attained the desired temperature the specimens were loaded on the specimen tray and kept at the cooler part of the furnace. The furnace tube was evacuated to 20μ of Hg and then it was flushed with argon gas. This procedure was repeated three four times and then finally gas was allowed to flow at the rate of 2 to 3 bubbles per minute. The specimen was then pushed into the hot zone and the time was noted. At the end of the desired annealing time, the specimen

tray was pulled out into the cooler region of the furnace without stopping the gas flow and it was kept there for 10 to 15 minutes before the furnace tube was opened to air for taking out the annealed specimens. Some specimens were also annealed in purified hydrogen gas in order to study the effect of annealing environment on the texture development. For this purpose a Hydrogen-Aron gas purification train (Fig. 24) was used.

II.4.2 Texture determination

The texture produced after cold rolling and after annealing was studied using a transmission texture goniometer[31]. Since this technique needed uniformly thinned specimens, each specimen was thinned to the desired thickness of 0.002" using a chemical thinning solution a mixture of conc. HNO_3 and 5 pct. HF in 8:1 ratio[28]. Thinning of specimens to the desired thickness took 8-10 minutes for each specimen and the variation in thickness was well within 0.0002".

II.4.2.1 Determination of θ_{111}

Since Bragg angle for (hkl) reflection (θ_{hkl}) is required for fixing the position of scintillation counter at $2\theta_{hkl}$ and for calculating intensity correction factor, θ_{hkl}

FIGURE CAPTION

Figure 22 : Electrical resistivity measuring specimen holder.

Figure 23 : Heat treatment furnace.

Figure 24 : Hydrogen gas purification train and Argon and Hydrogen gas mixer arrangement.

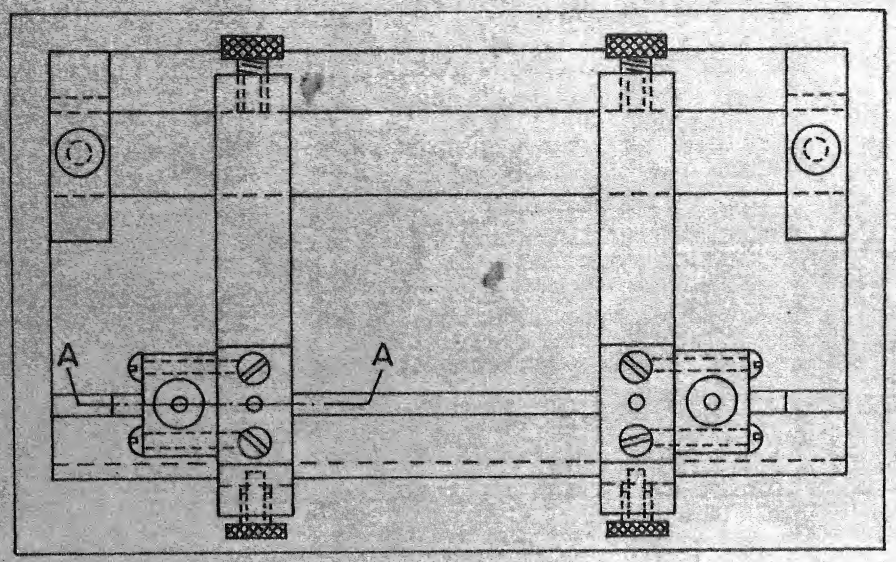

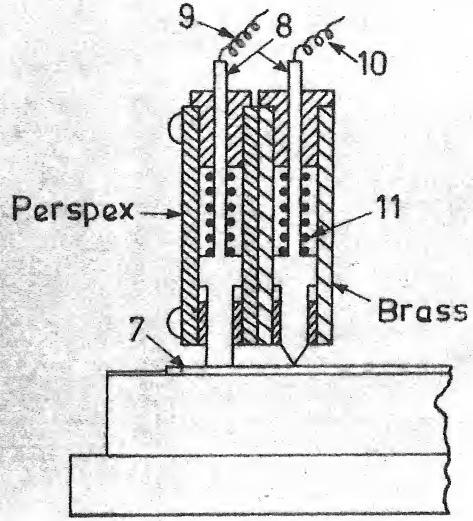

Section AA

No.	Description
1	Wooden base
2	Perspex base
3	Perspex stand
4	Holding screw
5	Stainless steel pin
6	Guide rod, perspex
7	Specimen
8	Contact pins, S.S.
9	Current lead
10	Potential lead
11	Cu-Be spring
12	Brass arm

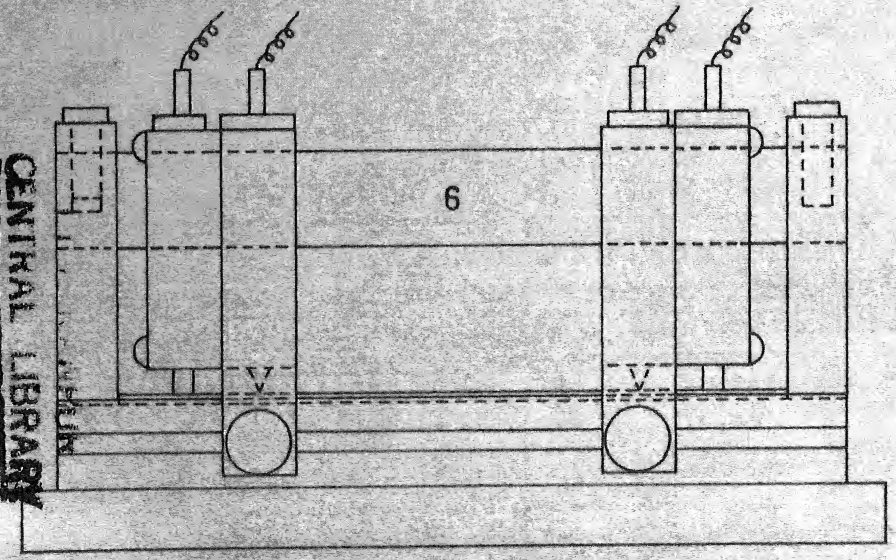

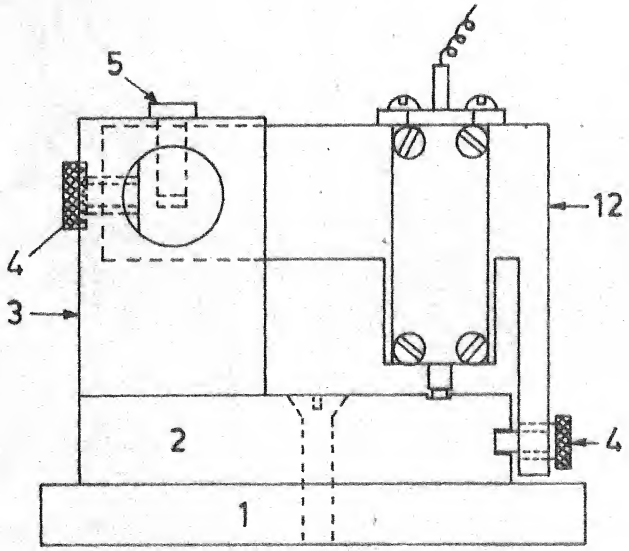

Fig. 22 - Electrical resistivity measuring specimen holder.

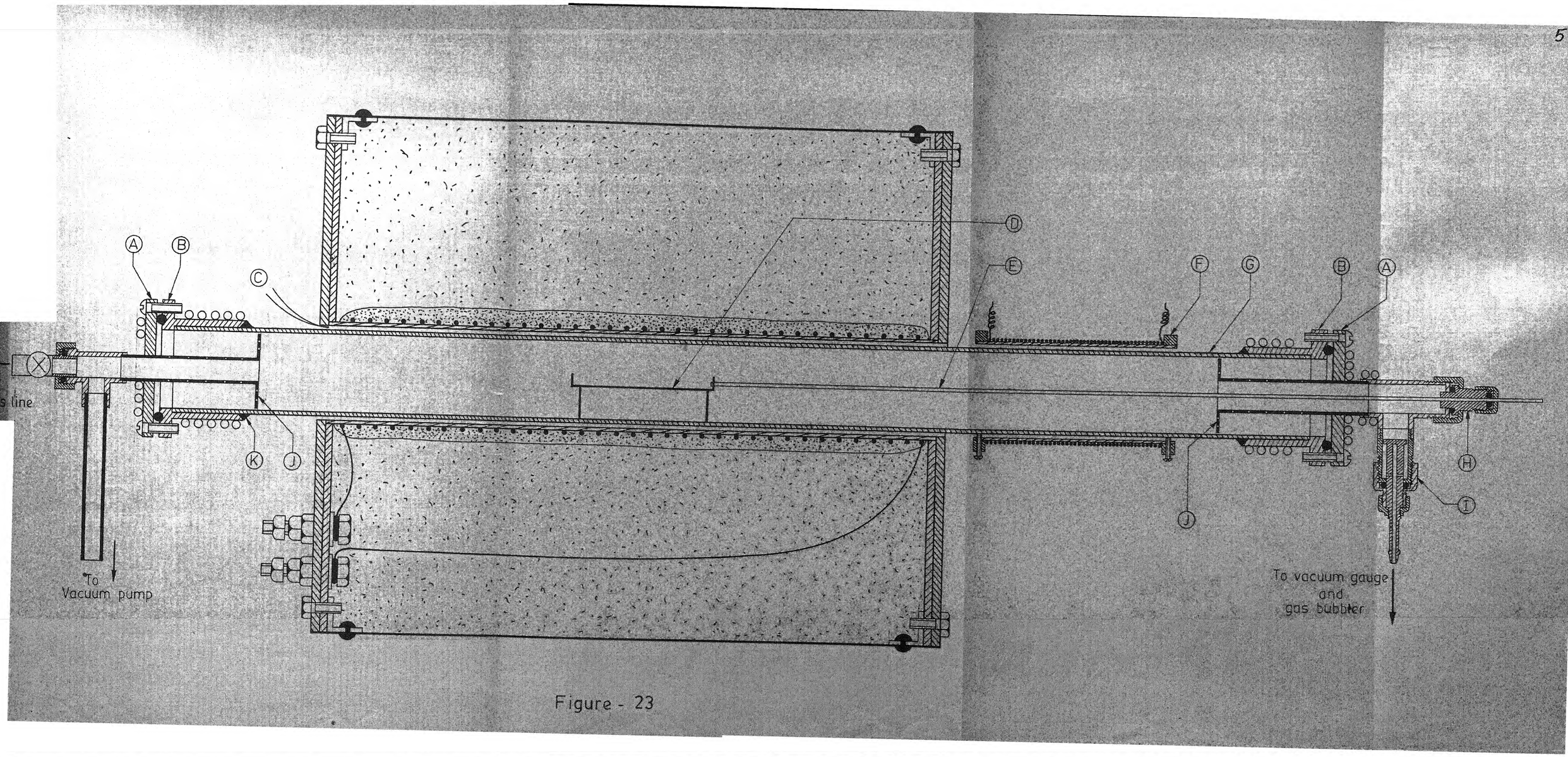
A
B
C
D
E
F
G
B
A
K
J
H
I
J
To
Vacuum pump
To vacuum gauge
and
gas bubbler

Figure - 23

was determined for each alloy using x-ray diffractometer. For the present study (111) pole figures were needed and hence θ_{111} for each alloy was determined. Specimens for this purpose were prepared by using powder obtained by filing each alloy with a jeweller's file and annealing the powder at 950°C for 30 minutes. Mo-radiation was used to determine θ_{111} because the same radiation was chosen for texture study. Value of θ_{111} was also used for calculating density for each alloy.

II.4.2.2 Determination of μt of specimen using Mo-radiation

μt value, where μ is the linear absorption coefficient for x-rays for a specimen and t is the specimen thickness, is required for calculating intensity correction factor[31]. The intensity correction is needed because due to rotation of specimen, there is change in path length of x-rays and volume of material is not also uniform. μt of each specimen was determined by using a strong diffracted beam from a parmaquartz specimen ($2\theta = 12.09^{\circ}$). The intensity of the diffracted x-ray beam with and without the specimen in the path of the diffracted x-ray beam was measured. Using the formula $I_t = I_o \exp(-\mu t)$, where I_o is the intensity of diffracted beam without the specimen in its path and I_t is the intensity of the transmitted beam through the specimen, μ_t for each alloy was calculated.

Table V : Diffractometer conditions used for texture determination

Radiation	-	MoK_{α}
Counter	-	Scintillation counter
Voltage	-	45 KV
Ampere	-	15 mA
Slit system at the source	-	3^{o} MR solan slit
Slit system at the counter	-	MR sollarslit with 0.2^{o} receiving slit
Scalar counting time	-	40 seconds
Filter used	-	Zr filter

I.4.2.3 Pole figure determination

The counter was fixed at the correct $2\theta_{111}$ angle for the sample to receive the diffracted beam corresponding to the (111) reflection. The specimen in the goniometer was positioned initially with the rolling direction vertical i.e. concident with the diffractometer axis and with the plane of the specimen bisecting the angle between the incident and diffracted beams[28]. This corresponded to $\alpha = 0^{\circ}$ and $\phi = 0^{\circ}$. The diffractometer conditions used for measurement of intensity of diffracted beam is given in Table V.

Intensity of diffracted beam from the specimen was recorded manually for each rotation of specimen around the vertical axis of the goniometer (α) and around the normal to the rolling plane (ϕ). The value of α varied from 0° to 50° and the value of ϕ varied from 0° to 90°. Intensity readings were taken at intervals of 5° for both ϕ and α rotations. Intensity of (111) reflection was recorded for 40 seconds. Since the counter should not be exposed to strong radiations (i.e. counts should not exceed 10000 CPS) and for the alloys studied the intensity values often exceeded this limit, intensity control of diffracted beam was necessary. Besides controlling KV and mA of the x-ray tube, a Zr filter was always used in the path of the diffracted beam. This not only reduced the counts to the desiredlimit but also

reduced scatter in the data by eliminating the scattered radiations incident on the counter. The recorded intensity data were corrected using correction factor table given by Sarkar[28]. For cold rolled texture corrected intensity was divided by 10 and then these values were plotted on polar net drawn at 2° intervals whereas for annealed texture each corrected intensity value was divided by the smallest corrected intensity in the investigated part of pole figure, then this relative intensity was plotted on polar net. Contoor lines passing through equiintensity points were drawn in the pole figure to indicate pole densities. The pole figures were interpretted with the help of available standard projections for cubic crystals.

II.5 Magnetic Tests

II.5.1 Curie Temperature (T_c) measurement

It is well known that ferromagnetic materials become paramagnetic above curie temperature. This fact was utilized in measuring T_c. Specimen 0.1''dia. x 0.125''long was heated in a heater assembly of PAR model 150 A vibrating sample magnetometer attached to an electromagnet. Current was fed to the heater assembly using a IC regulated Power supply (0-30V, 5A). Heating rate used was $3^{\circ}C$ to $5^{\circ}C$ per minute. The furnace chamber was evacuated below 0.2μ of Hg before the

specimen was heated up. The curve between M and T was recorded automatically using a x-y recorder. The existing heater assembly could be heated upto about 550°C only. Curie temperature determination was done in the residual field (~ 40 Oe) of the electromagnet.

II.5.2 Magnetic Measurements

II.5.2.1 Magnetic measurements using PAR model 150A vibrating sample magnetometer

The existing power supply for the electromagnet attached with the PAR vibrating sample magnetometer was found to be suitable for large magnetic fields. It was not possible to use it for small field strength adjustments needed for the soft magnetic materials like permalloys. Therefore, a separate DC regulated power supply having 0-30V, 5A ranges with fine control of current (minimum possible current adjustment of about 10 mA) was used to energise the magnet. Using this power supply, it was possible to increase the magnetic field at intervals of about 4 Oe. About 1A current was sufficient to get 500 Θ_e field. A differential Gaussmeter having a minimum range of 50 Θ_e full scale and a maximum range of 25 K Θ_e was used to record the magnetic field. Least count of the gauss meter used was 1 Θ_e.

The magnetic measurement using the magnetometer was carried out for annealed specimens and for quenched specimens.

Annealed specimens of 1/8'' long x 1/8" wide size were cut along the rolling direction from the specimens used for texture determination. At first the most suitable temperature for quenching of each alloy specimen was determined. The specimens were sealed in evacuated pyrex tube, annealed at $10^{o}C$ interval for 45 mts at various temperatures in the range between T_c and $T_c + 50^{o}C$ and cooled in three different ways (i) quenched in water (ii) air cooled and (iii) quenched in water at $85^{o}C$. The relative value of B during magnetisation of the specimen was found using a solenoid and fluxmeter. These quenching experiments indicated the best quenching temperature to be $T_c + 10^{o}C$ and cooling rate corresponding to hot water ($85^{o}C$) quenching. Therefore one specimen of each alloy was annealed at a temperature $10^{o}C$ above T_c of the specimen and then it was quenched in hot water at $85^{o}C$. This specimen was also used for magnetic measurements.

The specimens were placed between the electromagnets in such a way that the rolling direction becomes parallel to the magnetic field of the electromagnet. Before putting the specimen in the magnetometer, the magnetic field was increased slowly to 500 θ_e and then the current was slowly reduced to zero value. This gave in each case a residual field of about 40 θ_e. The specimen was then placed between the electromagnets and the magnetic moment value during the

magnetisation of specimen was recorded manually with increasing magnetic field. After reaching 500 θ_e field strength, the magnet current was reduced slowly to note down the magnetic moment values during the demagnetization cycle. After reaching the residual field, the magnet current direction was reversed and the demagnetisation cycle was continued to - 100 θ_e field strength. For most of the cases no further data was obtained. For a few specimens, however, a complete B-H loop was determined.

II.5.2.2 Magnetic measurement using Permeameter

The specimen used for magnetometer was too small and hence it may not give representative magnetic properties of a larger annealed sheet. Therefore a permeameter was fabricated so that a single sheet specimens of 4'' long x 0.354'' wide can be used for magnetic tests. There are three coils in the permeater - a magnetising coil, a H coil and a B coil. The current is fed to the magnetising coil using a regulated DC Power supply. The minimum field strength possible to obtain with the permeater was 0.2 θ_e and the maximum field strength was 70 θ_e. Based on the texture data obtained for the different specimens, 4'' long x 0.354'' wide strips were cut from the cold rolled sheets which gave the best annealed textures. These strips were annealed at 1050^{o}C for the

required annealing periods for which the best textures were produced in each of the alloys. After setting the specimen in the B coil of the permeameter specimen holder the permeater was first demagnetised to give zero residual field. The specimen was then magnetised by increasing the current in the magnetising coil and after attaining maximum field strength the specimen demagnetisation was done. Both the magnetisation and demagnetisation curves were obtained. The magnetic induction (B) due to the specimen was obtained by using RFL 803 Fluxmeter.

II.5.3 Magnetic cooling

A preliminery magnetic cooling treatment was carried out to find the response of Cu bearing permalloys to magnetic cooling. For this purpose, annealed strips used for permeameter measurements were heated to 700°C in flowing argon gas and then the furnace was switched off at 700°C. The specimens were cooled in the magnetic field of 8 θ_e from 700°C to 250°C. After this the specimens were pulled out in the cooler parts of the furnace and were allowed to cool to room temperature in presence of the magnetic field. These specimens cooled in magnetic field were used for determination of magnetisation and demagnetisation curves using the permeameter.

CHAPTER III

RESULTS

CHAPTER III

RESULTS

Copper bearing permalloys having intended compositions mentioned in Table II were prepared by induction melting and then processed through hot rolling and cold rolling followed by annealing in controlled atmosphere. Processing details have been presented in an earlier chapter (Table IV). The experimental results obtained through physical property measurements, texture determination and magnetic measurements have been described in the following sections.

III.1 Physical property measurement

III.1.1 Density

Density of each alloy was calculated on the basis of the actual chemical composition and the measured $2\theta_{111}$ angle determined for each alloy. Calculated density values have been tabulated in Table VII. The calculated density of T^{o} alloy (8.61 gm/cm^3) is very close to 8.58 gm/cm^3 as quoted by Bozorth[29]. Density of 5 pct. Cu containing alloys ranges between 8.6 and 8.7 gm/cm^3 whereas the density of 14 pct. Cu containing alloys is more, ranging between 8.91 and 8.93 gm/cm^3 because of higher copper content.

III.1.2 Mechanical Test

Mechanical properties for alloys studied are presented in Table VI. For one alloy, load-elongation diagram obtained during mechanical testing is also shown in Fig. 25. The nature of the load elongation curve is similar for all other alloys. Proof strength was calculated for 0.2 pct. elongation for each alloy specimen. Mechanical test data reveals that addition of Ti and Cr to 5 pct. and 14 pct. Cu containing permalloys improves their pct. elongation compared to the alloys not having Ti or Cr and thus makes these alloys more ductile.

III.1.3 Electrical Resistivity Measurement

Electrical resistivity data for various alloys are presented in Table VII. Electrical resistivity plays an important role in minimising eddy current loss. The data presented in Table VII reveals that addition of Cr increases the electrical resistivity of Cu bearing permalloys than when Ti is added. Electrical resistivity of 14 pct. Cu containing alloys is more compared to 5 pct. Cu containing alloys because of their larger Cu content. Since no data is available for copper bearing permalloys containing only 75 pct. Ni and 5 pct. or 14 pct. Cu it is not possible to find the effect of Ti on the electrical resistivity of these alloys.

III.1.4 Differential Thermal Analysis (DTA)

DTA plots between differential emf and temperature for all alloys did not show any peak indicating that no appreciable ordering could be produced through the step anneal. This may be because of two reasons. Since the ordering reaction in Fe-Ni system is very sluggish, it is possible that the addition of alloying elements like Ti and Cr make the reaction still more sluggish so that not appreciable degree of order could be produced by the step anneal. It is also possible that the temperatures used and the corresponding times allowed at each temperature was not sufficient for producing appreciable degree of order. These results thus indicate that practically no chemical order sets in the alloys during the processing of these alloys.

III.1.5 Curie temperatures (T_c) of Cu bearing permalloys

T_c of different alloys investigated are presented in Table VII. In the existing apparatus it was not possible to measure T_c above 550°C. T_c of alloy containing 75 pct. Ni, 25 pct. Fe is 600°C[29] whereas T_c of alloy containing 5 pct. Cu alongwith 75 pct. Ni, 25 pct. Fe is found to be $\sim$ 530°C (Fig. 10). Data presented in Table VII indicate that addition of alloying elements such as Ti and Cr decreases T_c further. Addition of Cr to 5 pct. and 14 pct. Cu containing permalloys

FIGURE CAPTION

Figure 25 : Load-elongation diagram for P^{o} alloy.

Figure 26 : Curie temperature plots for V^{1} and W^{o} alloy.

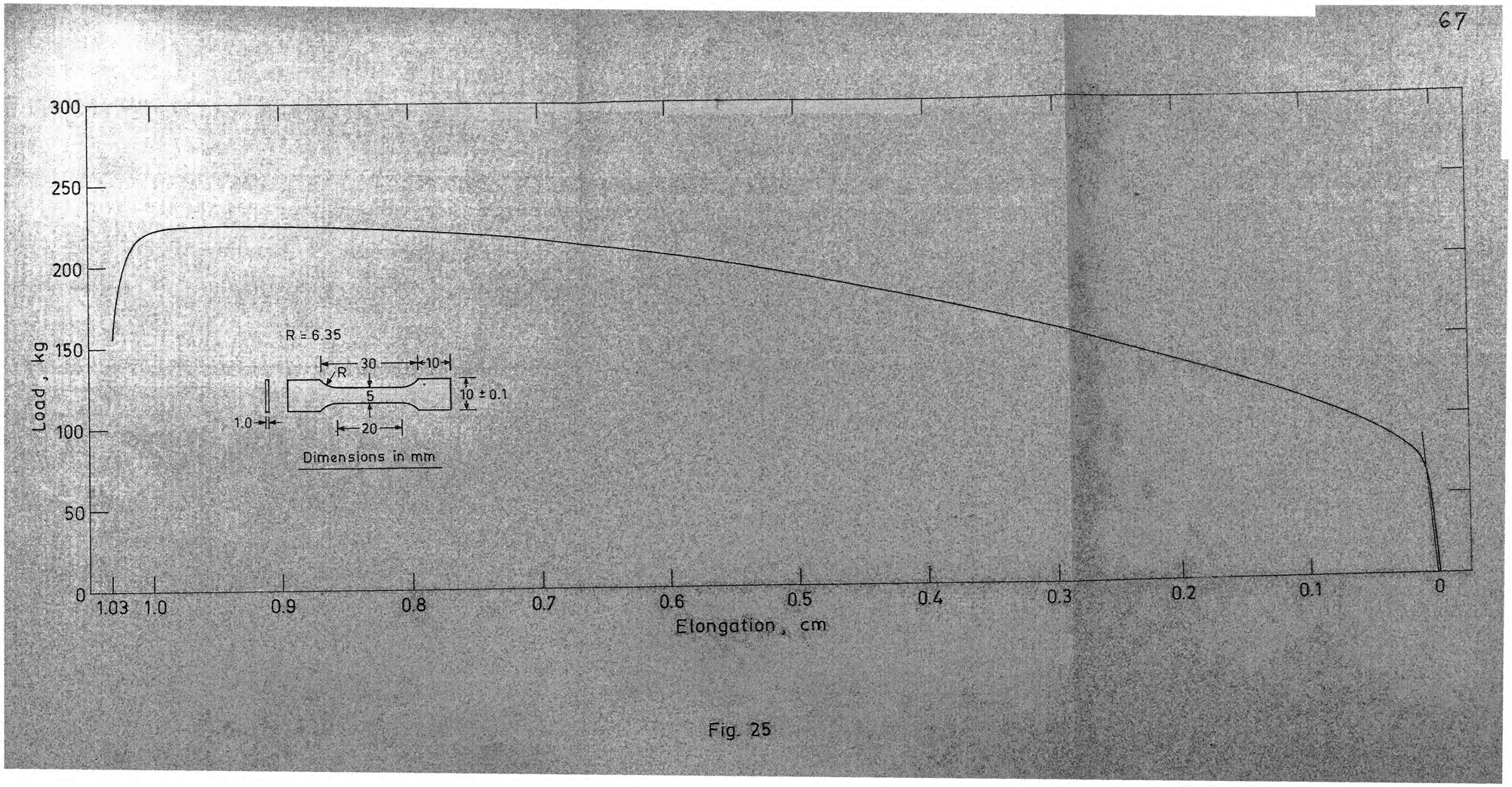
300
250
200
150
100
50
0
Load , kg
R = 6.35
30
10
R
5
10 ± 0.1
1.0
20
Dimensions in mm
1.03
1.0
0.9
0.8
0.7
0.6
0.5
0.4
0.3
0.2
0.1
0
Elongation , cm

Fig. 25

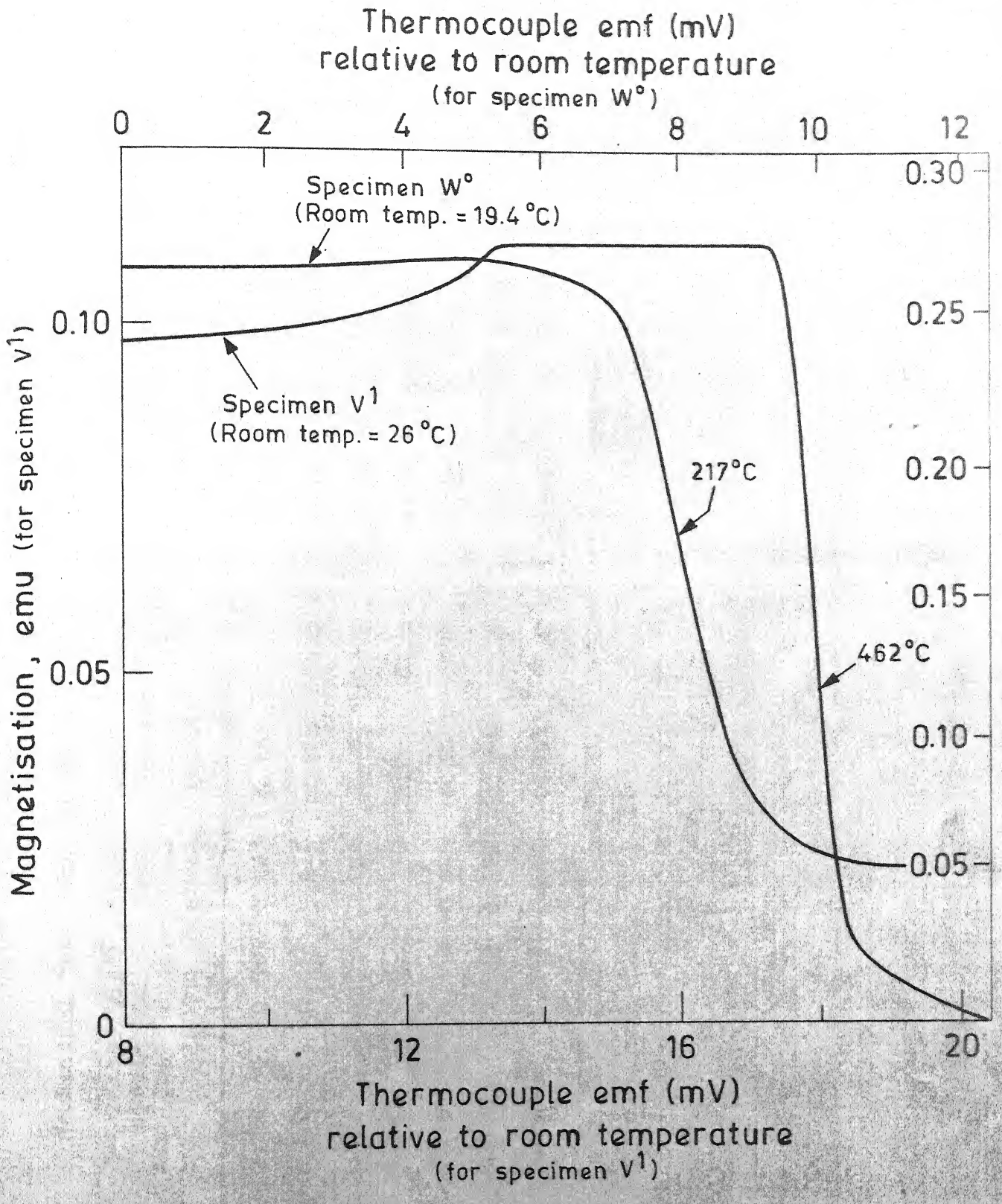
Thermocouple emf (mV)
relative to room temperature
(for specimen W°)
0
2
4
6
8
10
12
Specimen W°
(Room temp. = 19.4 °C)
0.10
0.05
0
Magnetisation, emu (for specimen V¹)
Specimen V¹
(Room temp. = 26 °C)
217°C
462°C
0.30
0.25
0.20
0.15
0.10
0.05
Magnetisation, emu (for specimen W°)
8
12
16
20
Thermocouple emf (mV)
relative to room temperature
(for specimen V¹)

Fig. 26

Table VI : Mechanical test data for Cu bearing permalloys.

Alloy Designation	Thickness of specimen (cms)	Width of specimen (cms)	Cross-sectional area (cms^2)	Total elongation (cms)	pct. elongation	Proof stress (kgm/cm^2)	Ultimate tensile stress (kgm/cm^2)
P^o	0.085	0.505	0.043	0.955	47.7	1568	5264
T^o	0.089	0.500	0.045	0.926	46.3	1676	5244
V^o	0.084	0.504	0.042	1.04	52.0	1537	5732
X^o	0.097	0.500	0.048	1.05	52.5	1754	5601
R^o	0.089	0.504	0.045	0.86	43.0	1561	4966
W^o	0.073	0.506	0.037	0.858	42.9	1353	4844
Y^o	0.087	0.507	0.044	0.953	47.6	1247	5128

Table VII : Some Physical and Crystallographic Properties of Cu bearing permalloys.

Alloy Designation	$2\theta^{o}_{111}$	Lattice parameter (A^{o})	Density (gm/cm^{3})	Electrical resistivity ($\mu\Omega$ cm)	Curie temperature (^{o}C)
T^{o}	19.90	3.55	8.6	66.3	430$^{\varphi}$
U^{o}	19.97	3.54	8.7	40.4	489
V^{1}	19.90	3.55	8.6	49.9	458
W^{o}	20.08	3.52	8.9	58.3	217
Y^{o}	20.06	3.53	8.9	47.6	258

$^{\varphi}$ This value has been quoted by Bozorth[29].

appears to decrease T_c to a larger extent than when Ti alone is added. A very large decrease ($\sim$400°C) in T_c for the 14 Cu alloys containing Ti and Cr is not wholly due to the large copper content of the alloys. On addition of 14 pct. Cu to Fe-75 Ni alloy, the estimated decrease in T_c is $\sim$ 200°C. Hence, a major part of the large decrease in T_c of the 14 Cu alloys appears to be due to the small additions of Ti and Cr.

III.2 Texture development

III.2.1 $2\theta_{111}$ determination

Bragg angle for (111) reflection was determined for each alloy using x-ray diffractometer. The results are presented in Table VII. The values of $2\theta_{111}$ varies between 19.9° and 20.08°. As seen from the data, the variation of $2\theta_{111}$ with composition is not very large for the alloys studied.

III.2.2 Texture determination

Texture determination was done using a transmission texture goniometer. Cold rolled and annealed textures are generally presented as the pole figures showing the actual distribution of intensity of (111) reflection. Since different pole figures have to be compared, absolute intensity values have no real use. It is generally normalized relative to random specimen. But random specimen for transmission

technique is very difficult to prepare. Therefore relative intensity values were found out at different pole locations in pole figures using another method (See Appendix I for the pole locations in pole figures). It has been found that for cold rolled textures the intensity value at location E remains constant (above a certain pct. reduction in thickness) with increase in pct. cold reduction[34]. Therefore, for the cold rolled textures the intensity values relative to that at location E have been tabulated in Table VIII. Pole figures showing cold rolled textures are shown in Figs. 27 to 39.

The annealed textures were studied after annealing the cold rolled strips at 1050°C for different lengths of time. Pole figures for the annealed textures are shown in Figs. 40 to 75. Location 6 in the pole figures of annealed textures indicate the intensity due to cube orientation. Intensity at location 7 or 8 is due to grains having twin orientation relative to the cube oriented grains. In a well developed cube texture the intensity at locations 7 or 8 are always present (Fig. 5). For well developed cube texture the ratio of intensity at location 6 and location 7 or 8 should be very high. For example, in the case of pure copper this ratio is 40:1 (Fig. 5). Thus to judge whether a strong cube texture has been produced or not this ratio of intensity between locatin 6 and location 7 or 8 may be used. In the present study the same

FIGURE CAPTION

Figure 27 : (111) pole figure of 96 pct. CR 5Cu alloy ($P^{o}b0$).

Figure 28 : (111) pole figure of 97 pct. CR 14Cu alloy ($R^{o}c0$).

Figure 29 : (111) pole figure of 96 pct. CR 5Cu alloy ($T^{o}b0$).

Figure 30 : (111) pole figure of 97 pct. CR 5Cu alloy ($T^{o}c0$).

Figure 31 : (111) pole figure of 96 pct. CR 5Cu alloy ($U^{o}b0$).

Figure 32 : (111) pole figure of 97 pct. CR 5Cu alloy ($U^{o}c0$).

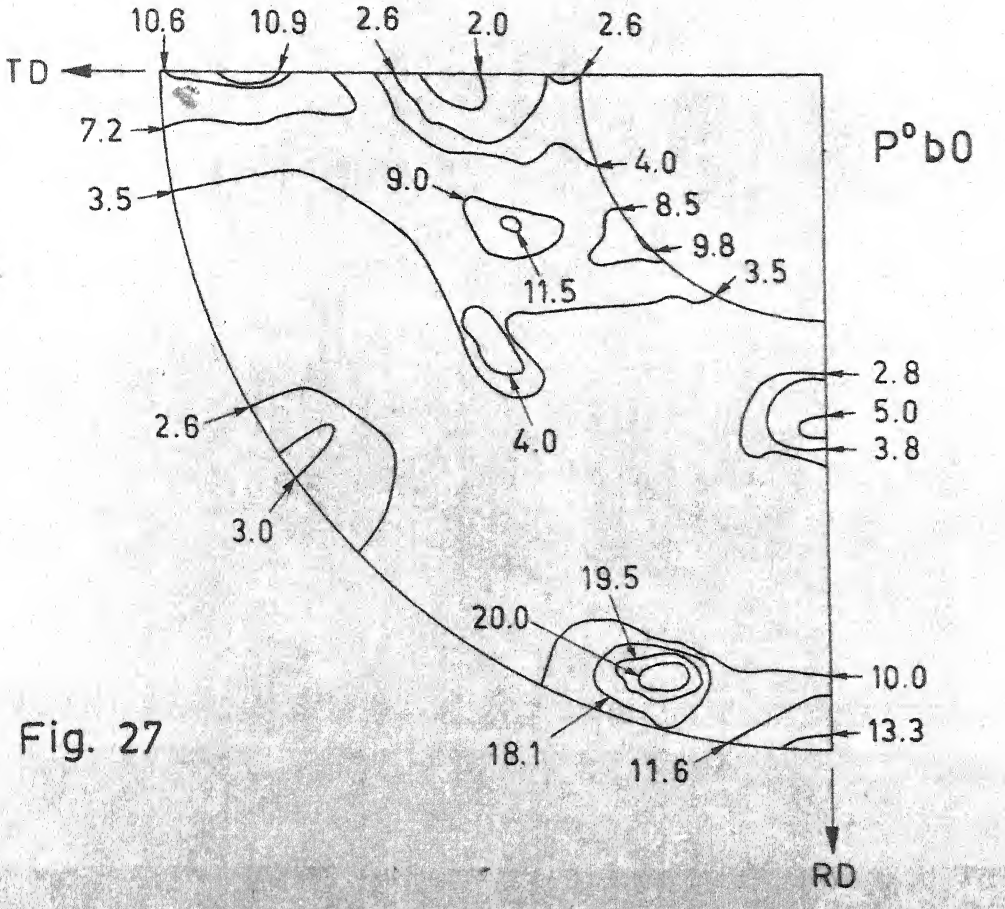
10.6
10.9
2.6
2.0
2.6
TD
7.2
4.0
P°b0
9.0
3.5
8.5
9.8
11.5
3.5
2.8
5.0
3.8
2.6
4.0
3.0
19.5
20.0
10.0
13.3
18.1
11.6
RD

Fig. 27

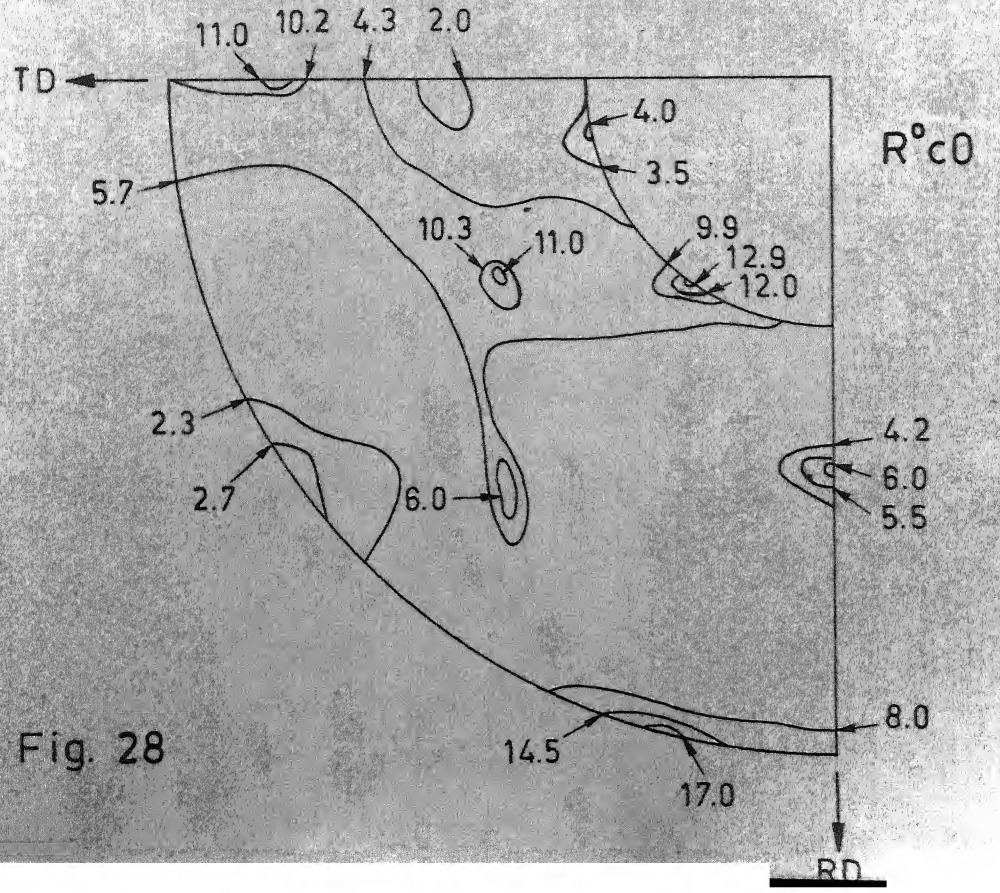
11.0
10.2
4.3
2.0
TD
4.0
R°c0
3.5
5.7
10.3
11.0
9.9
12.9
12.0
2.3
4.2
6.0
2.7
6.0
5.5
8.0
14.5
17.0
RD

Fig. 28

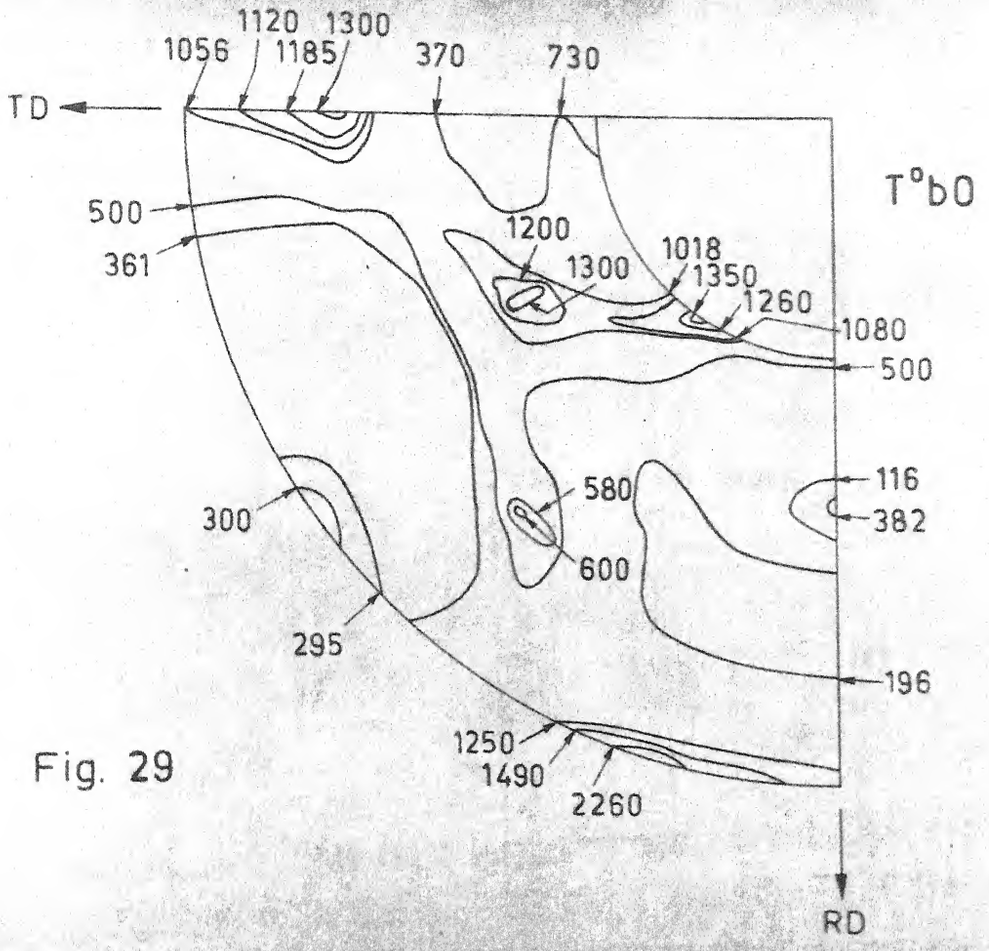
1120
1300
1056
1185
370
730
TD
T°bO
500
361
1200
1018
1300
1350
1260
1080
500
116
580
382
300
600
295
196
1250
1490
2260
RD

Fig. 29

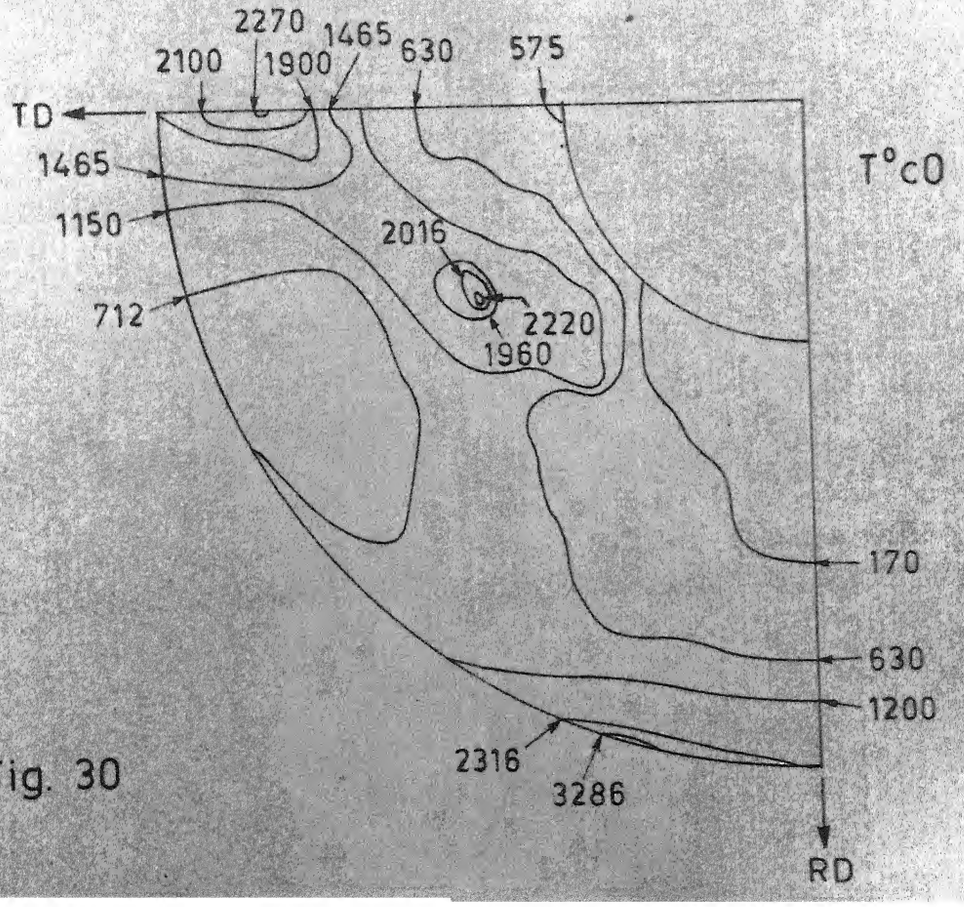
2270
1465
2100
1900
630
575
TD
T°cO
1465
1150
2016
712
2220
1960
170
630
1200
2316
3286
RD

Fig. 30

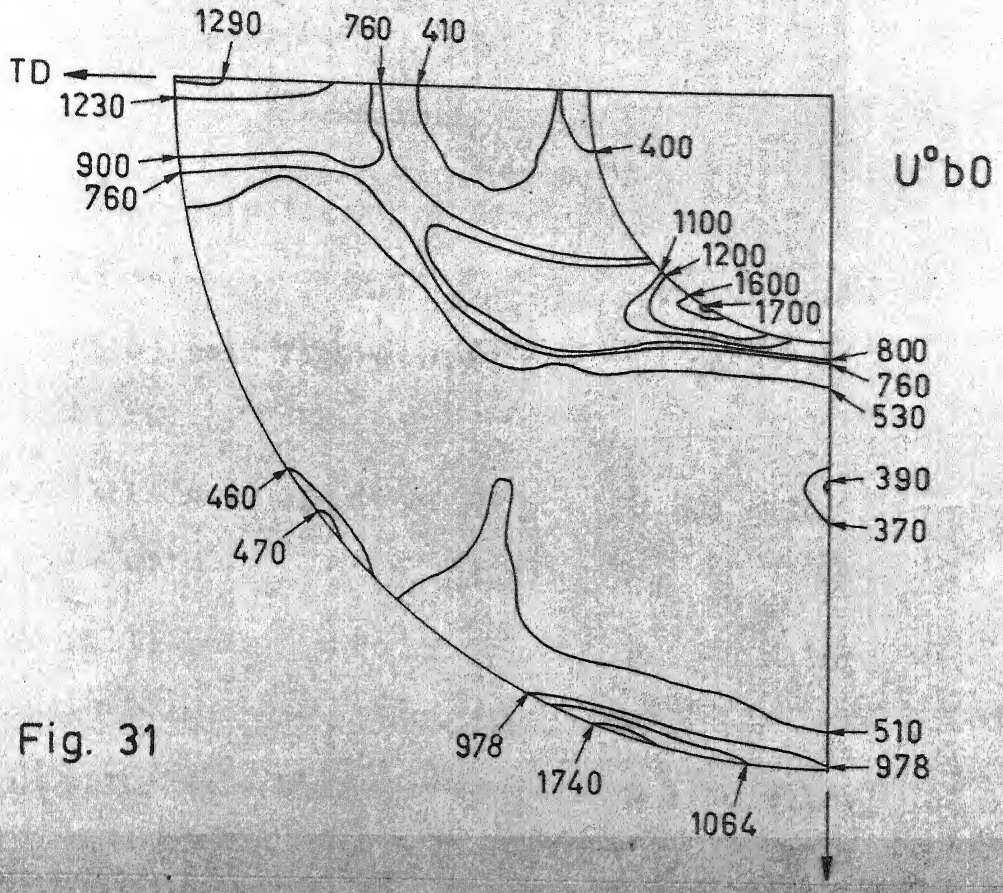
1290
760
410
TD
1230
900
760
400
U°bO
1100
1200
1600
1700
800
760
530
390
370
460
470
978
1740
1064
510
978

Fig. 31

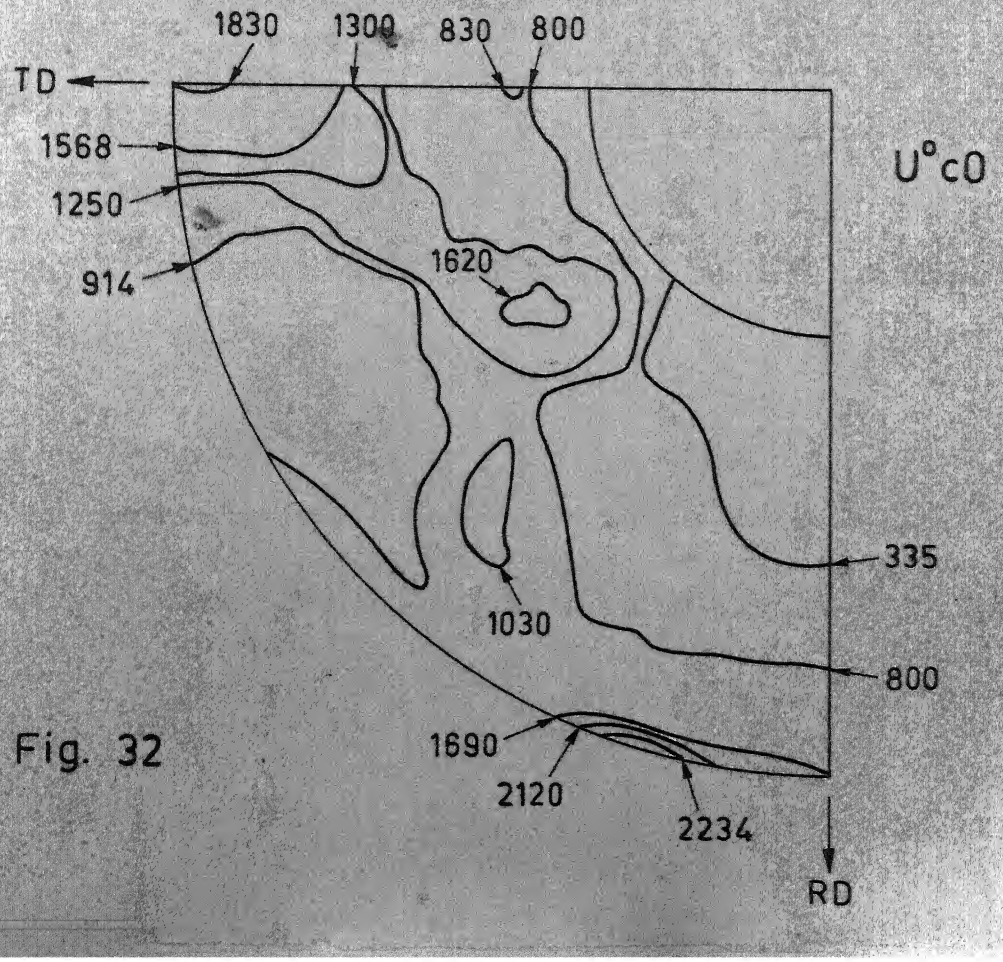
1830
1300
830
800
TD
1568
1250
914
1620
U°cO
335
1030
800
1690
2120
2234
RD

Fig. 32

FIGURE CAPTION

Figure 33 : (111) pole figure of 96 pct. CR 5Cu alloy ($V^{o}b0$).

Figure 34 : (111) pole figure of 97 pct. CR 5Cu alloy ($V^{o}c0$).

Figure 35 : (111) pole figure of 98 pct. CR 5Cu alloy ($V^{1}d0$).

Figure 36 : (111) pole figure of 96 pct. CR 14Cu alloy ($W^{o}b0$).

Figure 37 : (111) pole figure of 97 pct. CR 14Cu alloy ($W^{o}c0$).

Figure 38 : (111) pole figure of 96 pct. CR 14Cu alloy ($Y^{o}b0$).

Figure 39 : (111) pole figure of 97 pct. CR 14Cu alloy ($Y^{o}c0$).

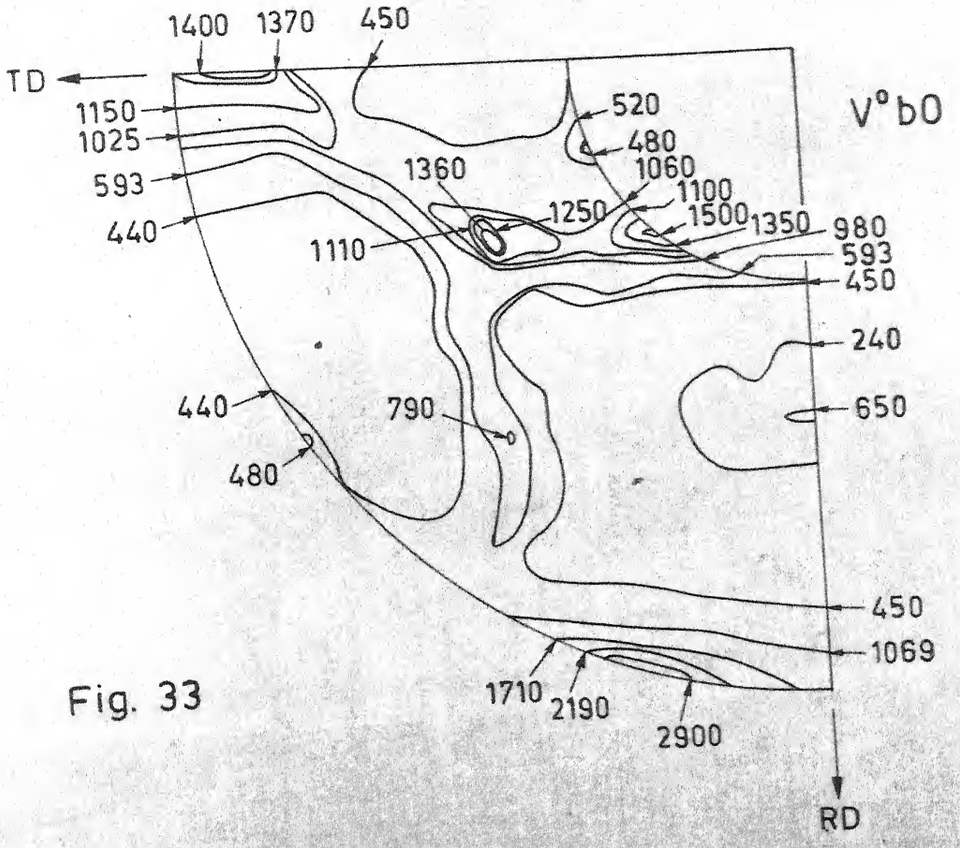
1400
1370
450
TD
1150
1025
593
440
520
480
1060
1100
1500
1350
980
593
450
1360
1250
1110
240
650
440
790
480
450
1069
1710
2190
2900
RD
V°bO

Fig. 33

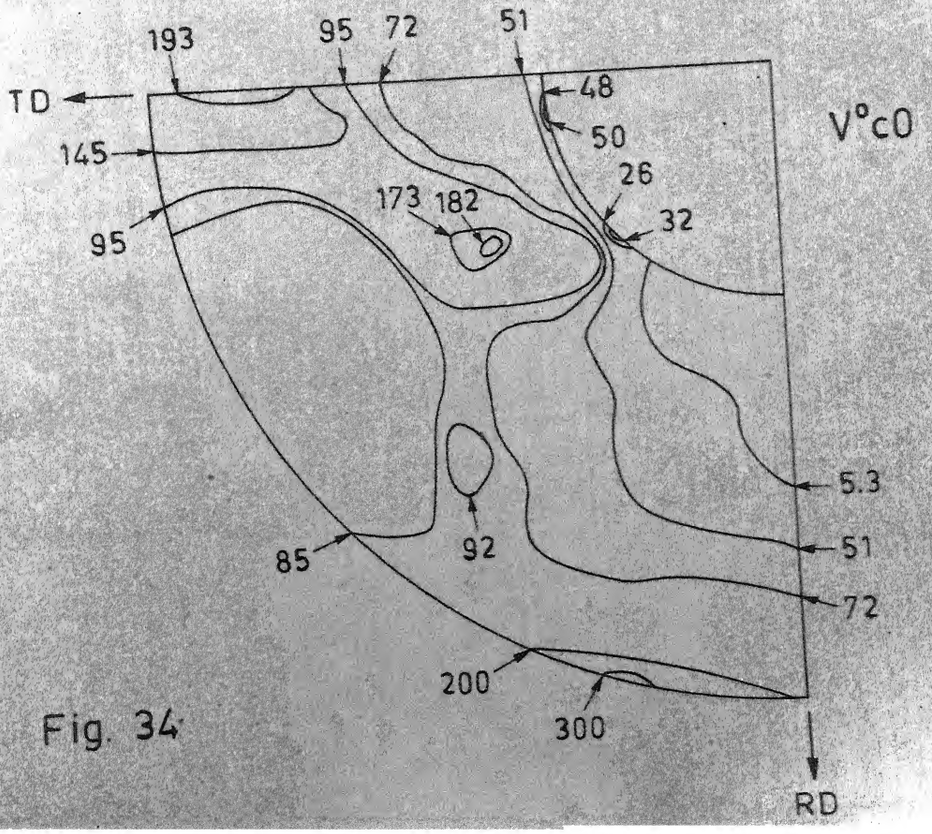
193
95
72
51
TD
48
50
145
26
173
182
95
32
5.3
92
85
51
72
200
300
RD
V°cO

Fig. 34

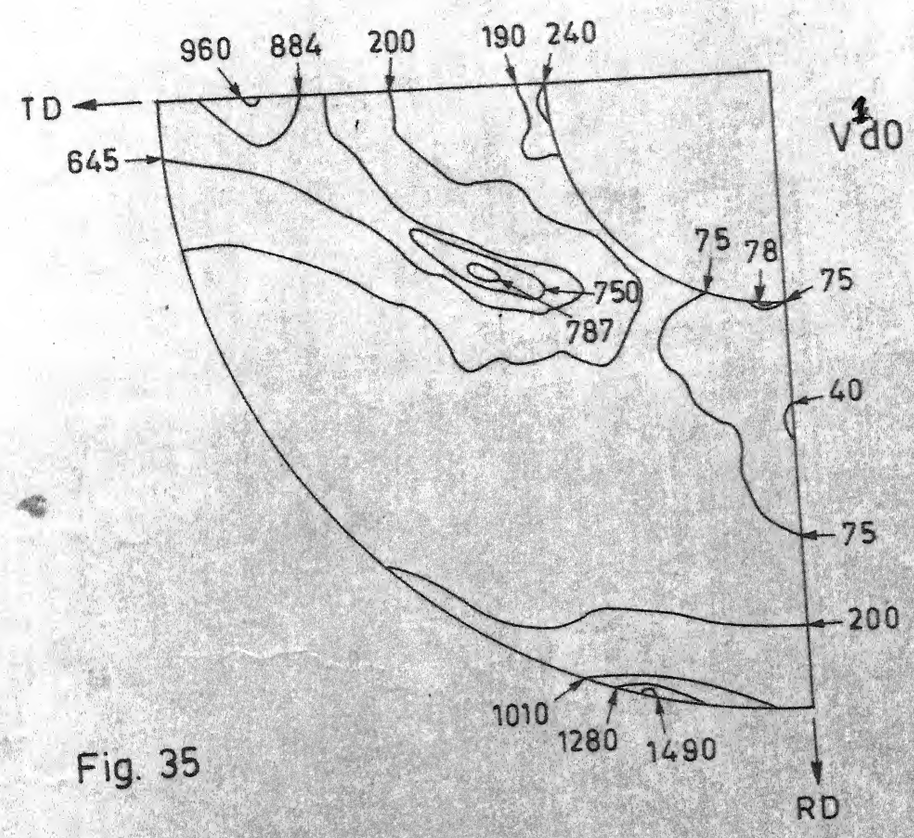
960
884
200
190
240
TD
645
Vd0
75
78
75
750
787
40
75
200
1010
1280
1490
RD

Fig. 35

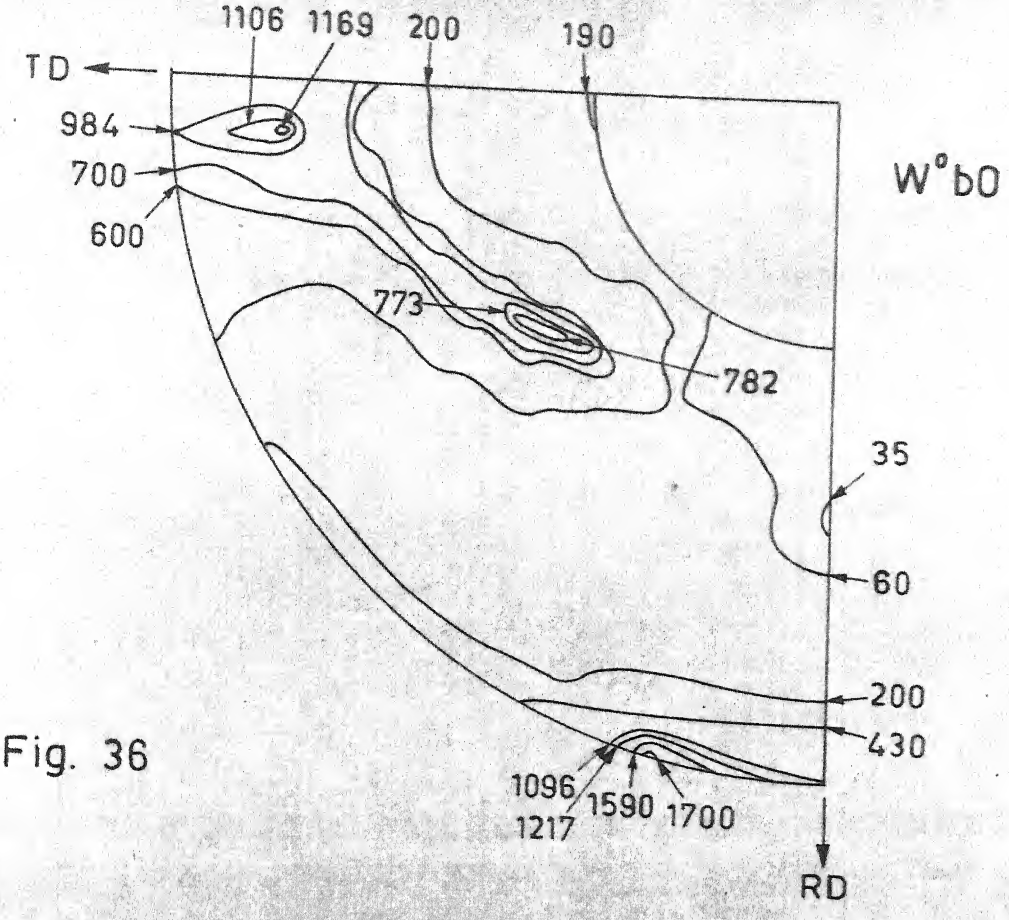
1106
1169
200
190
TD
984
700
600
773
782
W°bO
35
60
200
430
1096
1217
1590
1700
RD

Fig. 36

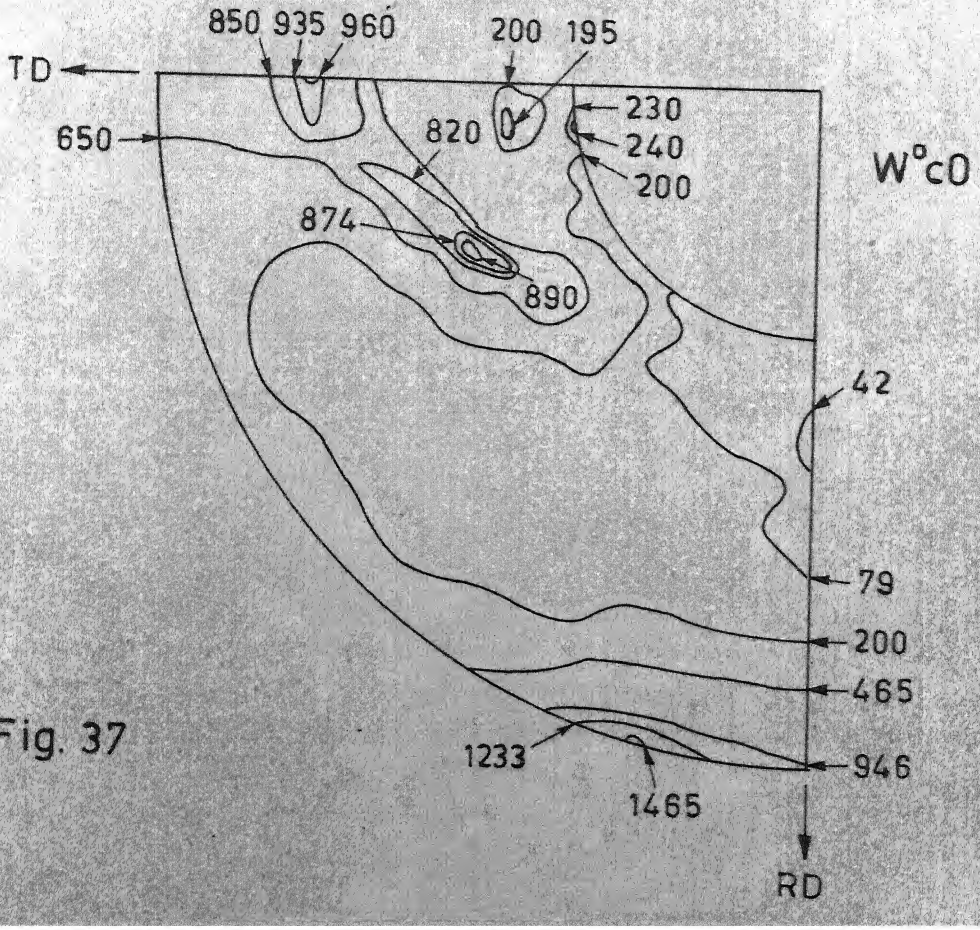
850
935
960
200
195
TD
650
820
230
240
200
874
890
W°cO
42
79
200
465
1233
1465
946
RD

Fig. 37

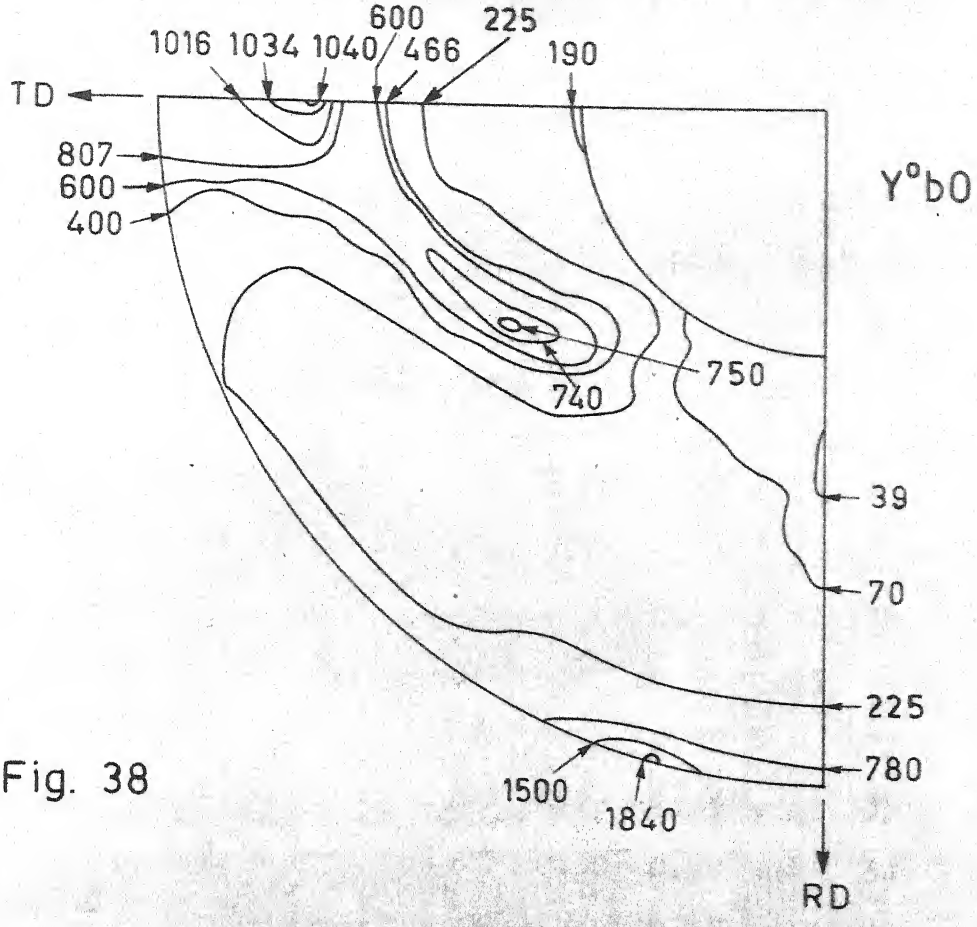
1016
1034
1040
600
466
225
190
TD
807
600
400
Y°bO
750
740
39
70
225
780
1500
1840
RD

Fig. 38

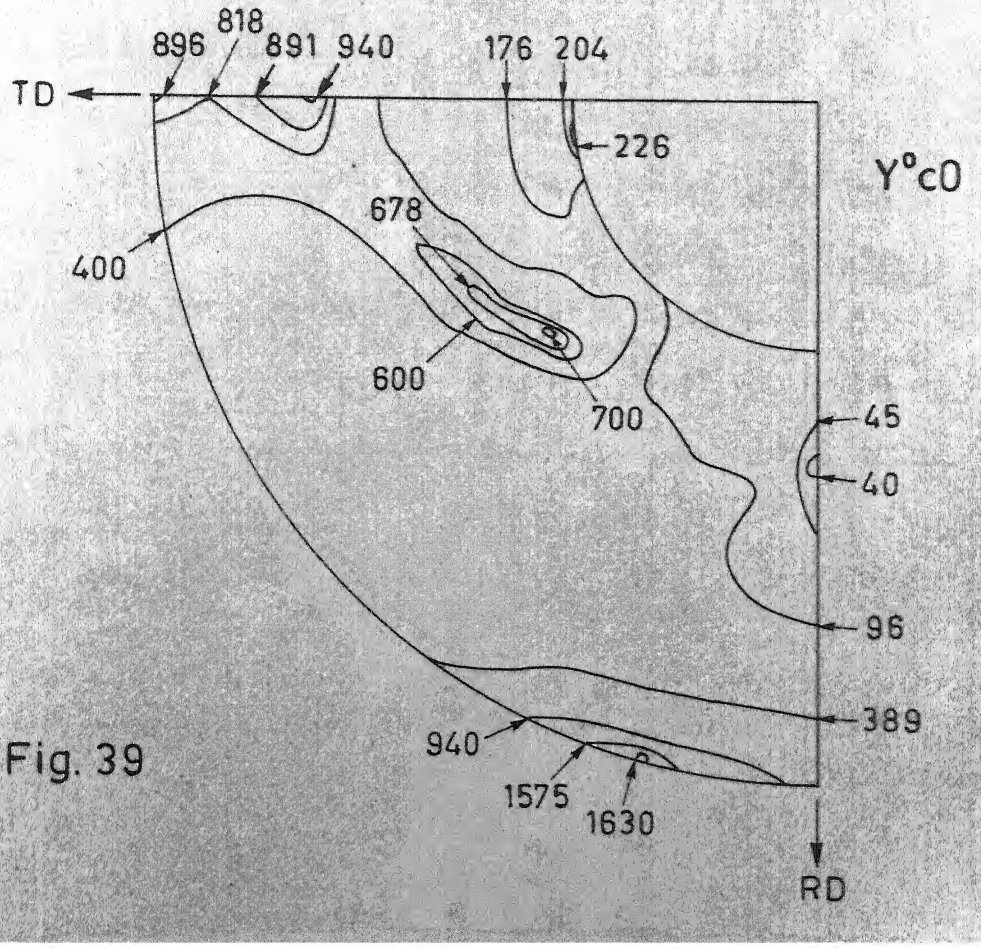
896
818
891
940
176
204
TD
226
Y°cO
678
400
600
700
45
40
96
389
940
1575
1630
RD

Fig. 39

Table VIII : Effect of composition and process variables on cold rolled texture of Cu bearing permalloys.

Alloy Designation	Relative (111) reflection intensity at different locations relative to E								Fig. No.
	A	B	C	D	E	F	G	H	
$P^{o}bO$	0.55	0.13	0.49	0.25	1.00	0.20	0.56	0.15	27
$T^{o}bO$	0.56	0.16	0.60	0.26	1.00	0.27	0.56	0.13	29
$T^{o}cO$	0.69	0.18	-	-	1.00	-	0.68	0.22	30
$U^{o}bO$	0.74	0.22	0.98	0.22	1.00	-	-	0.26	31
$U^{o}cO$	0.70	0.30	-	-	1.00	0.40	0.60	-	32
$V^{o}bO$	0.47	-	0.50	0.21	1.00	0.26	0.45	-	33
$V^{o}cO$	0.67	-	0.10	-	1.00	0.30	0.60	-	34
$V^{1}dO$	0.64	-	-	-	1.00	-	0.53	0.13	35
$X^{o}dO$	0.61	0.16	-	-	1.00	-	0.46	-	-
$R^{o}cO$	0.65	-	0.76	0.35	1.00	0.35	0.65	0.16	28
$W^{o}bO$	0.69	0.11	-	-	1.00	-	0.46	-	36
$W^{o}cO$	0.66	0.14	-	-	1.00	-	0.61	-	37
$Y^{o}bO$	0.57	0.10	-	-	1.00	-	0.41	-	38
$Y^{o}cO$	0.58	0.14	-	-	1.00	-	0.43	-	39

FIGURE CAPTION

Figure 40 : (111) pole figure of 96 pct. CR 5Cu alloy ($P^{o}b4$) annealed at 1050°C for 4 hrs.

Figure 41 : (111) pole figure of 97 pct. CR 14Cu alloy ($R^{o}c4$) annealed at 1050°C for 4 hrs.

Figure 42 : (111) pole figure of 96 pct. CR 5Cu alloy ($T^{o}b2$) annealed at 1050°C for 2 hrs.

Figure 43 : (111) pole figure of 96 pct. CR 5Cu alloy ($T^{o}b4$) annealed at 1050°C for 4 hrs.

Figure 44 : (111) pole figure of 97 pct. CR 5Cu alloy ($T^{o}c2$) annealed at 1050°C for 2 hrs.

Figure 45 : (111) pole figure of 97 pct. CR 5Cu alloy ($T^{o}c2$ (H_2)) annealed at 1050°C for 2 hrs. in hydrogen.

Figure 46 : (111) pole figure of 97 pct. CR 5Cu alloy ($T^{o}c4$) annealed at 1050°C for 4 hrs.

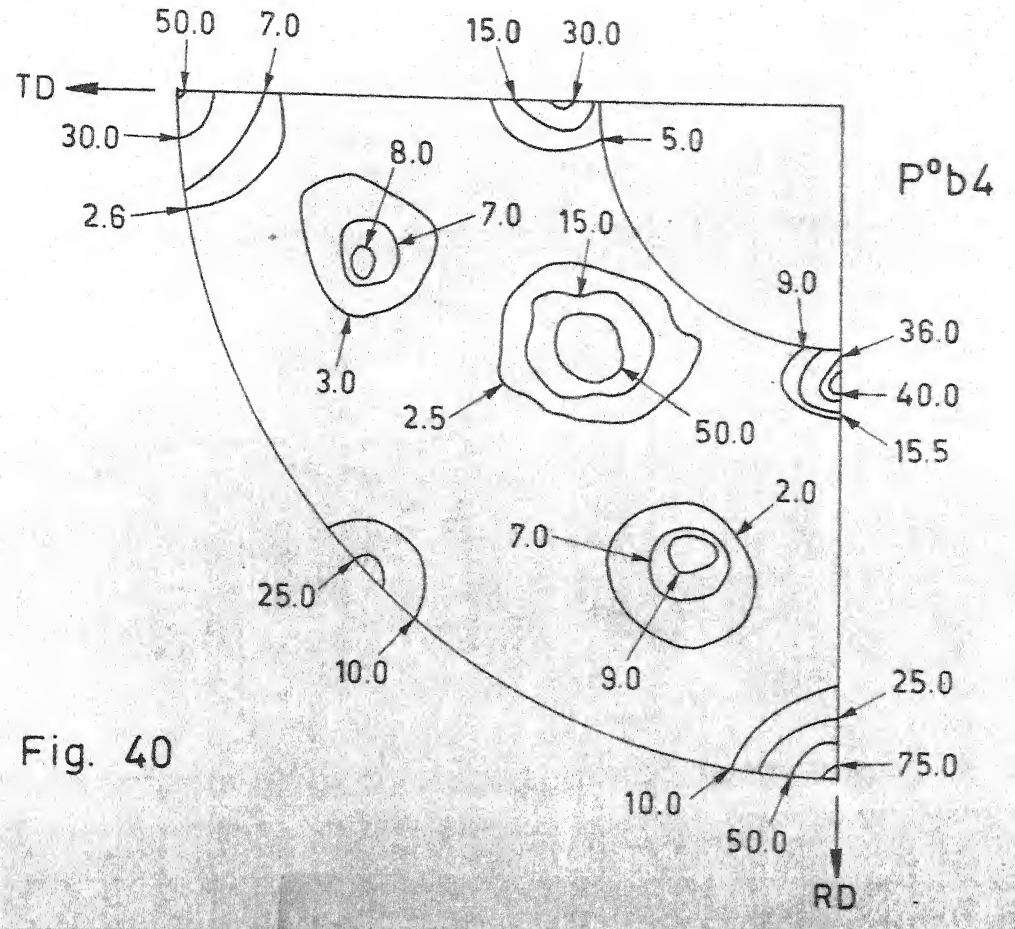
50.0
7.0
15.0
30.0
TD
30.0
5.0
8.0
2.6
7.0
15.0
P°b4
9.0
3.0
36.0
2.5
40.0
50.0
15.5
2.0
7.0
25.0
9.0
10.0
25.0
75.0
10.0
50.0
RD

Fig. 40

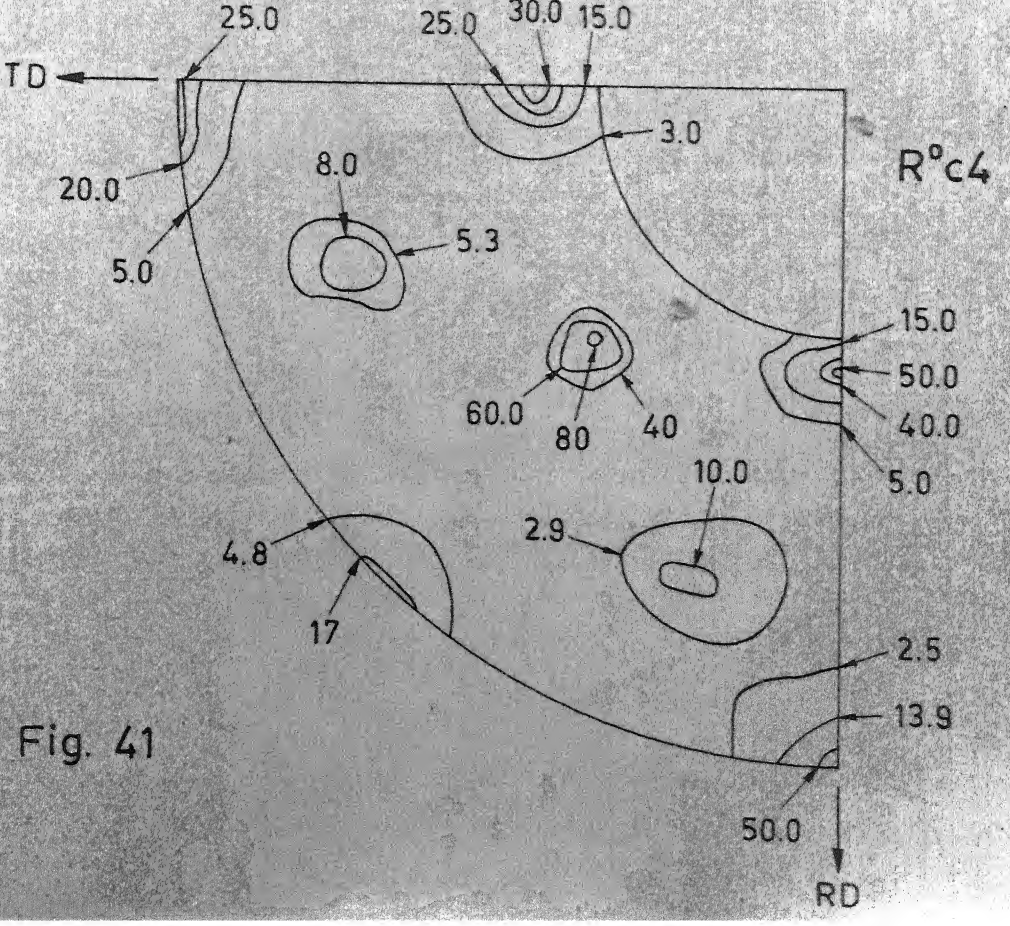
25.0
25.0
30.0
15.0
TD
3.0
20.0
8.0
R°c4
5.3
5.0
15.0
50.0
60.0
80
40
40.0
5.0
10.0
2.9
4.8
17
2.5
13.9
50.0
RD

Fig. 41

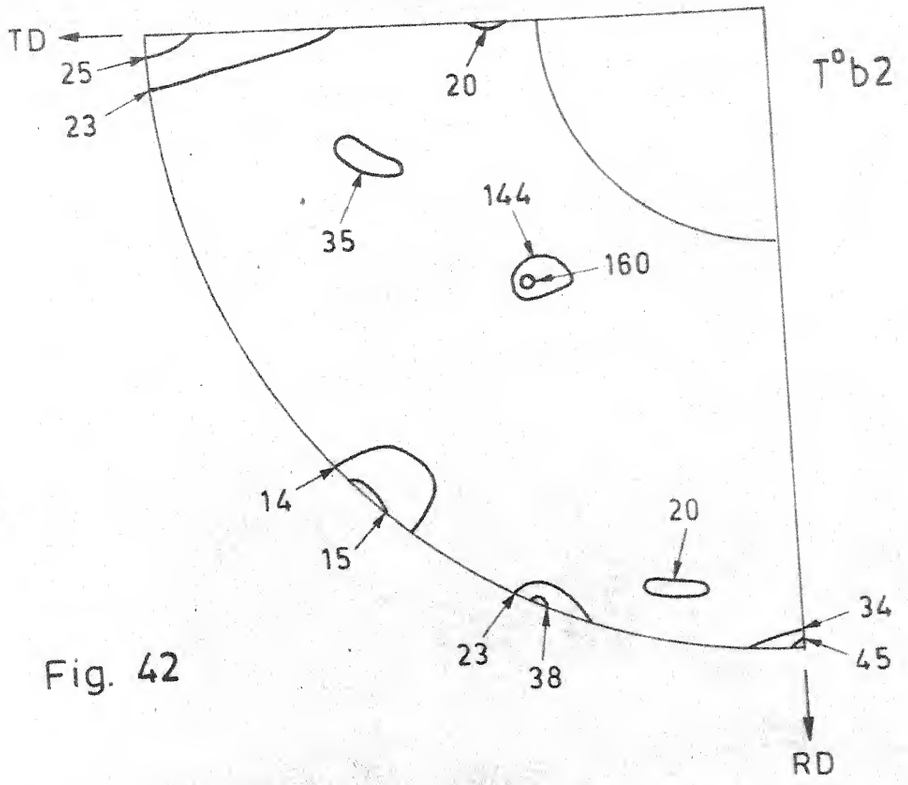
TD
25
23
20
T°b2
35
144
160
14
15
20
34
45
23
38
RD

Fig. 42

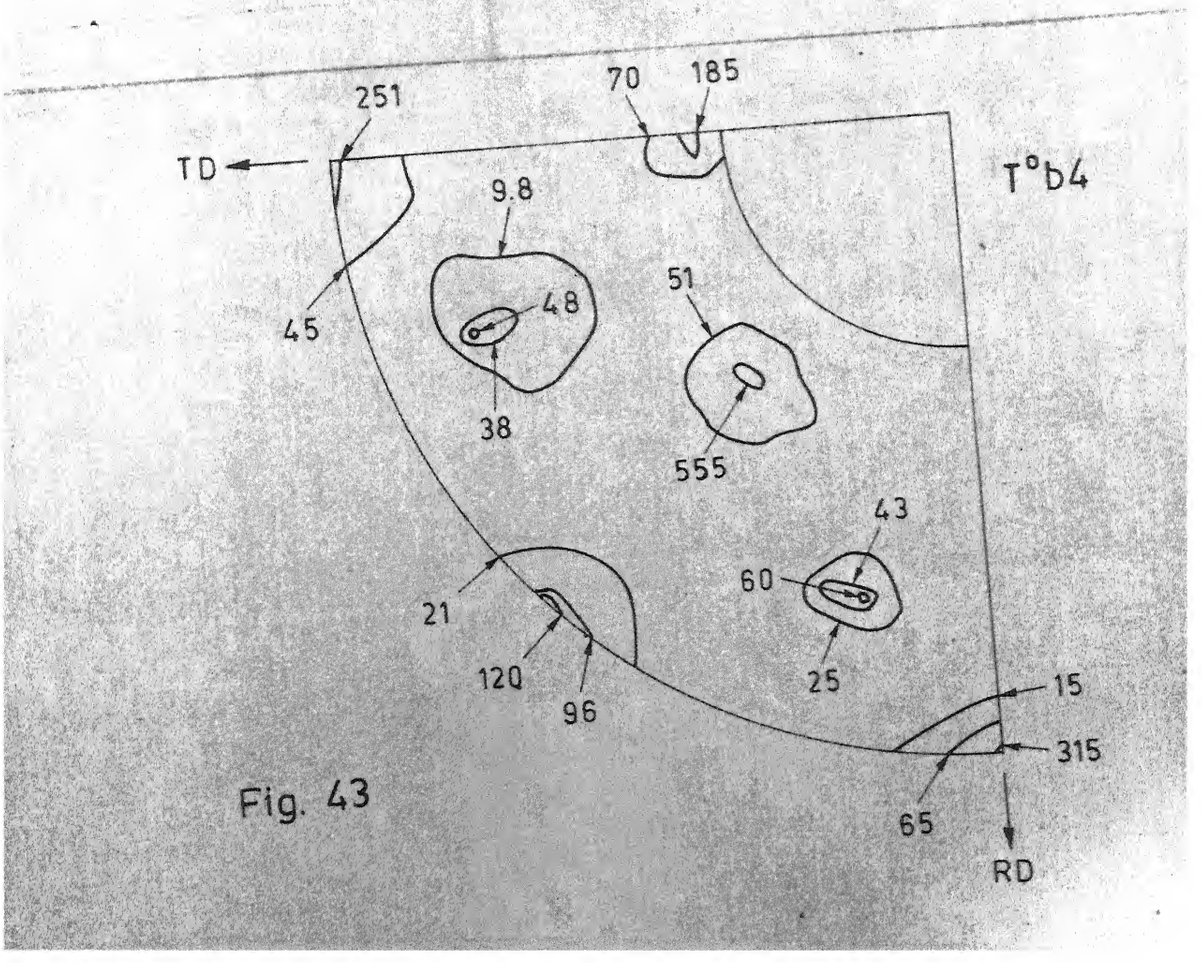
251
70
185
TD
T°b4
9.8
45
48
38
51
555
43
60
21
120
96
25
15
315
65
RD

Fig. 43

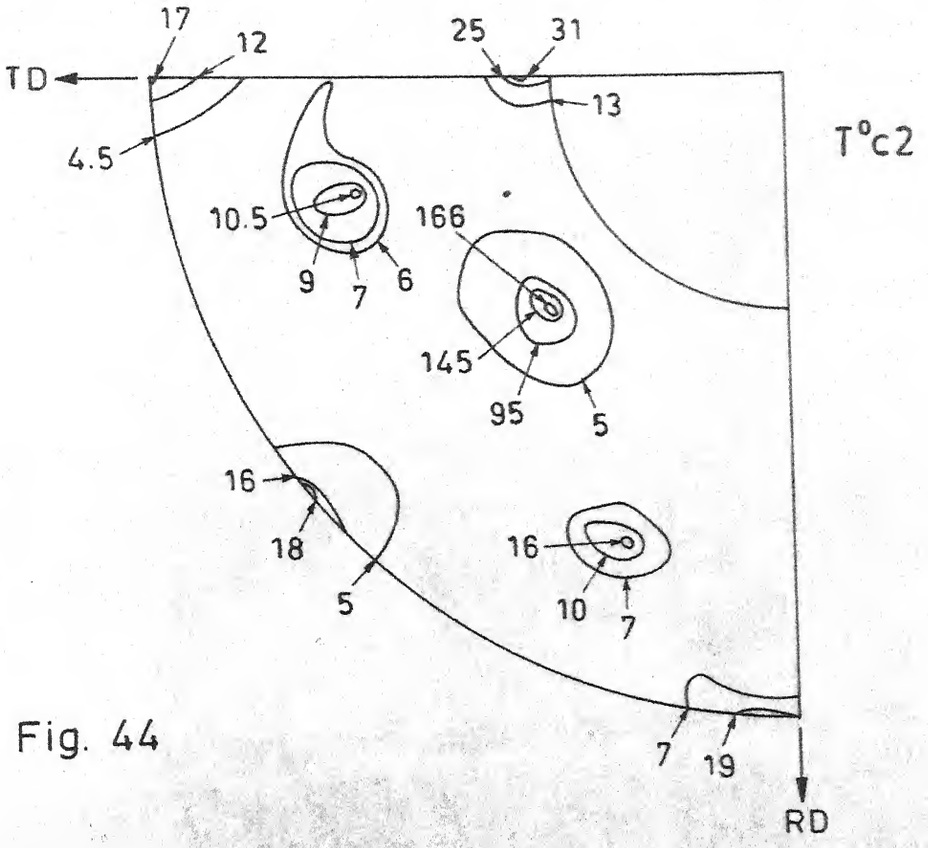
17
12
25
31
TD
13
T°c2
4.5
10.5
166
9
7
6
145
95
5
16
18
5
16
10
7
7
19
RD

Fig. 44

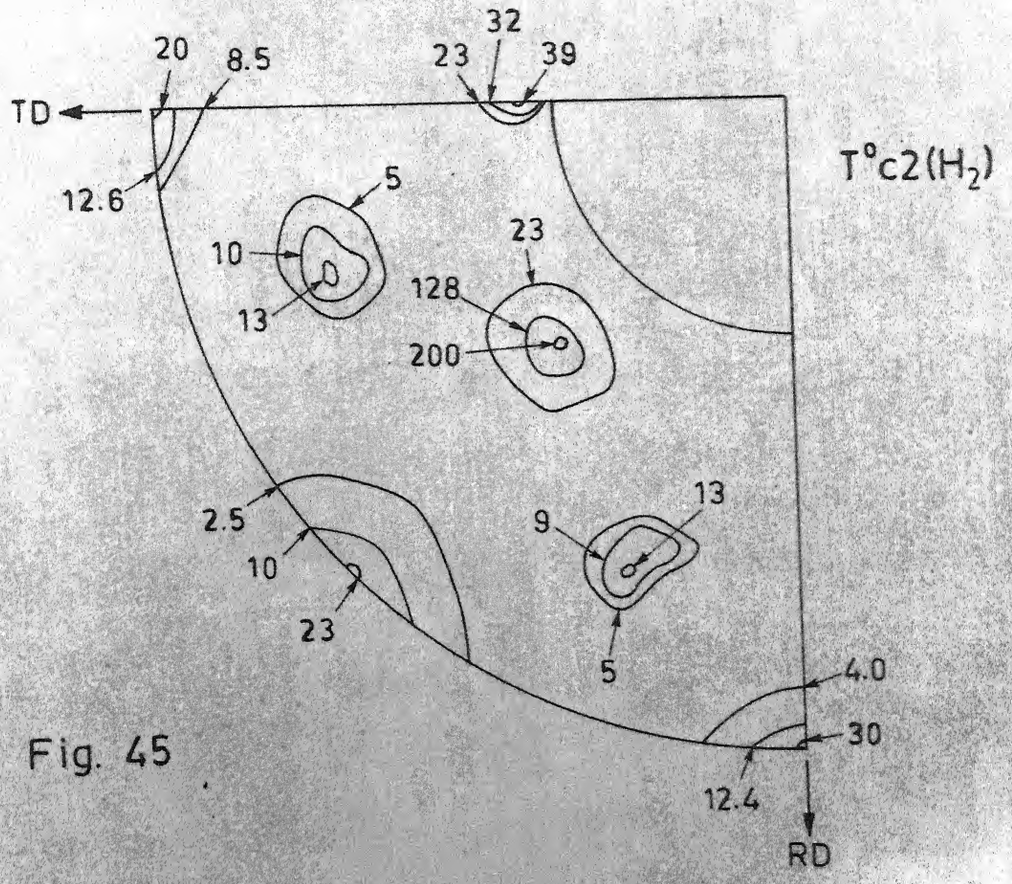
32
20
8.5
23
39
TD
T°c2(H2)
12.6
5
10
23
13
128
200
2.5
13
9
10
23
5
4.0
30
12.4
RD

Fig. 45

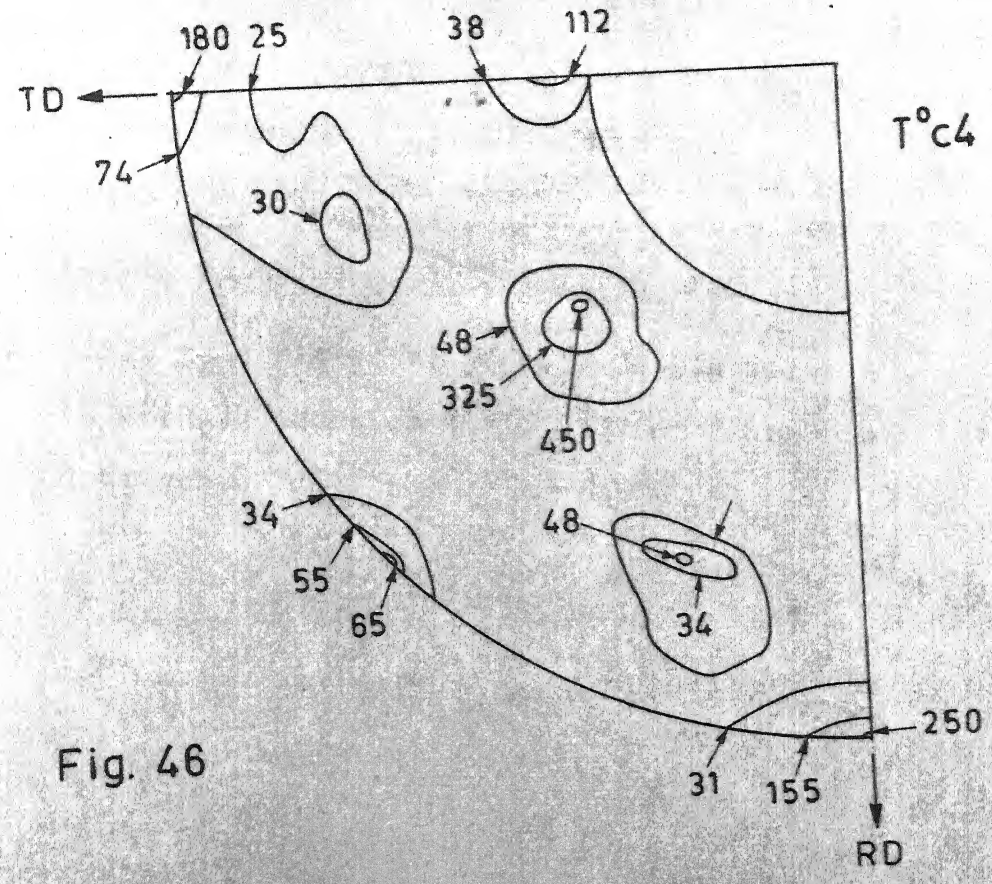

Fig. 46

FIGURE CAPTION

Figure 47 : (111) pole figure of 96 pct. CR 5Cu alloy ($U^{o}b2$) annealed at 1050°C for 2 hrs.

Figure 48 : (111) pole figure of 96 pct. CR 5Cu alloy ($U^{o}b4$) annealed at 1050°C for 4 hrs.

Figure 49 : (111) pole figure of 97 pct. CR 5Cu alloy ($U^{o}c2$) annealed at 1050°C for 2 hrs.

Figure 50 : (111) pole figure of 97 pct. CR 5Cu alloy ($U^{o}c4$) annealed at 1050°C for 4 hrs.

Figure 51 : (111) pole figure of 97 pct. CR 5Cu alloy ($U^{o}c6$) annealed at 1050°C for 6 hrs.

Figure 52 : (111) pole figure of 97 pct. CR 5Cu alloy ($U^{o}c2(H_2)$) annealed at 1050°C for 2 hrs. in hydrogen.

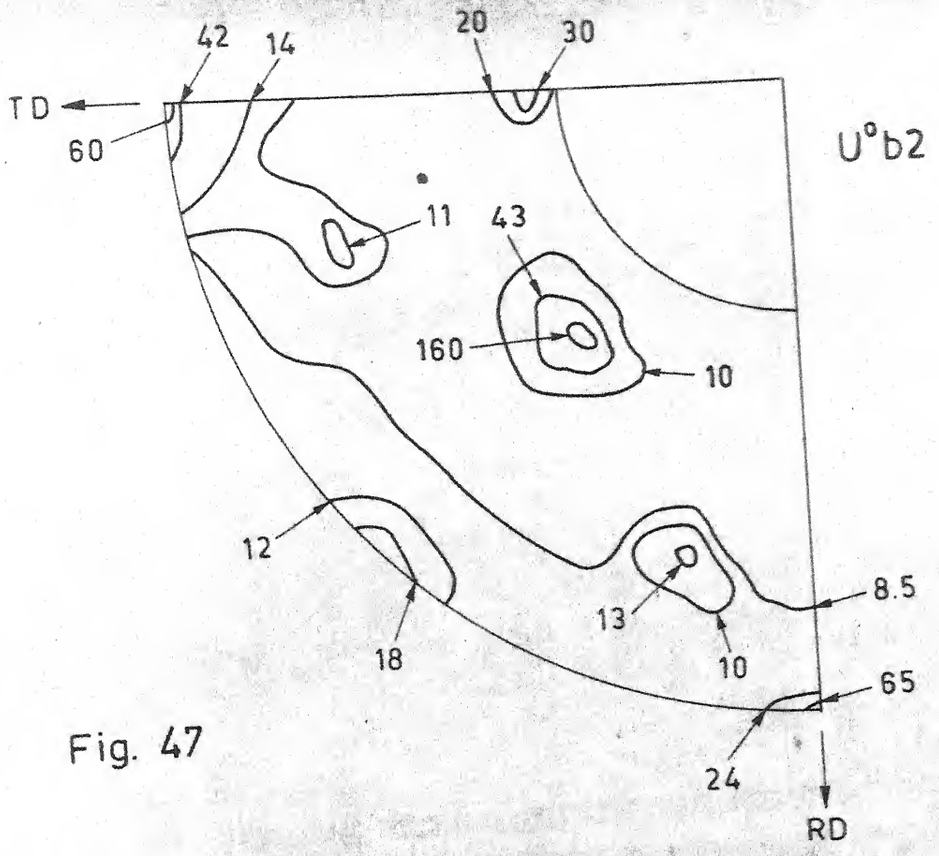
42
14
20
30
TD
60
U°b2
11
43
160
10
12
8.5
13
18
10
65
24
RD

Fig. 47

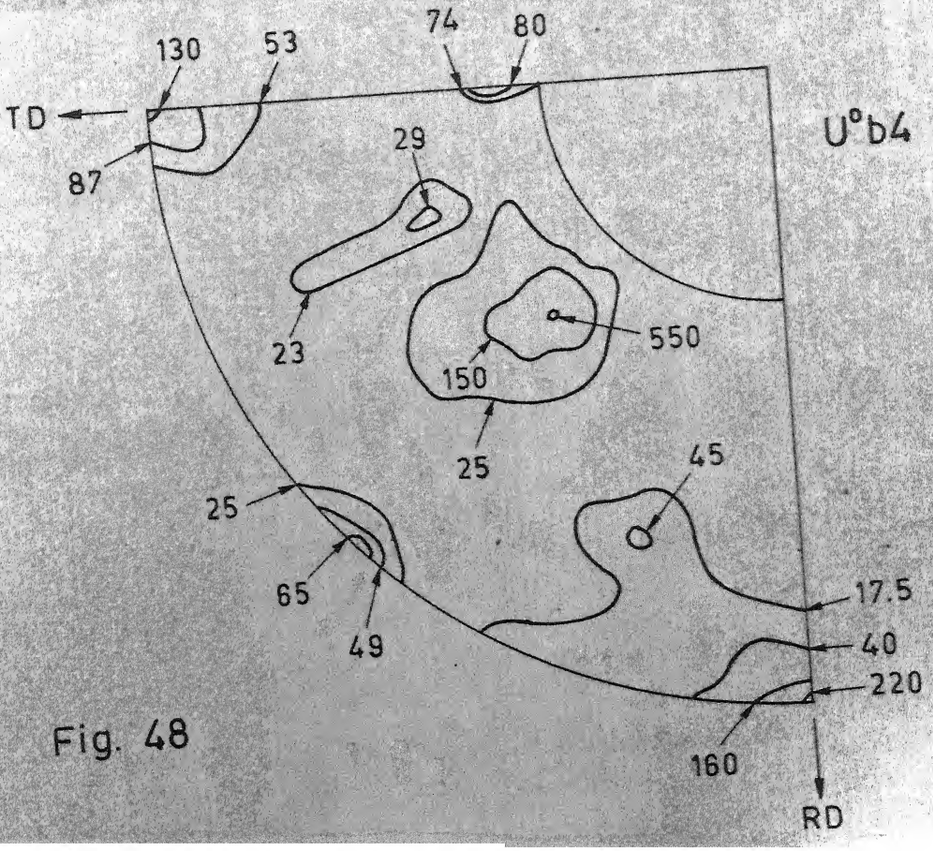
130
53
74
80
TD
87
U°b4
29
23
550
150
25
45
25
65
49
17.5
40
220
160
RD

Fig. 48

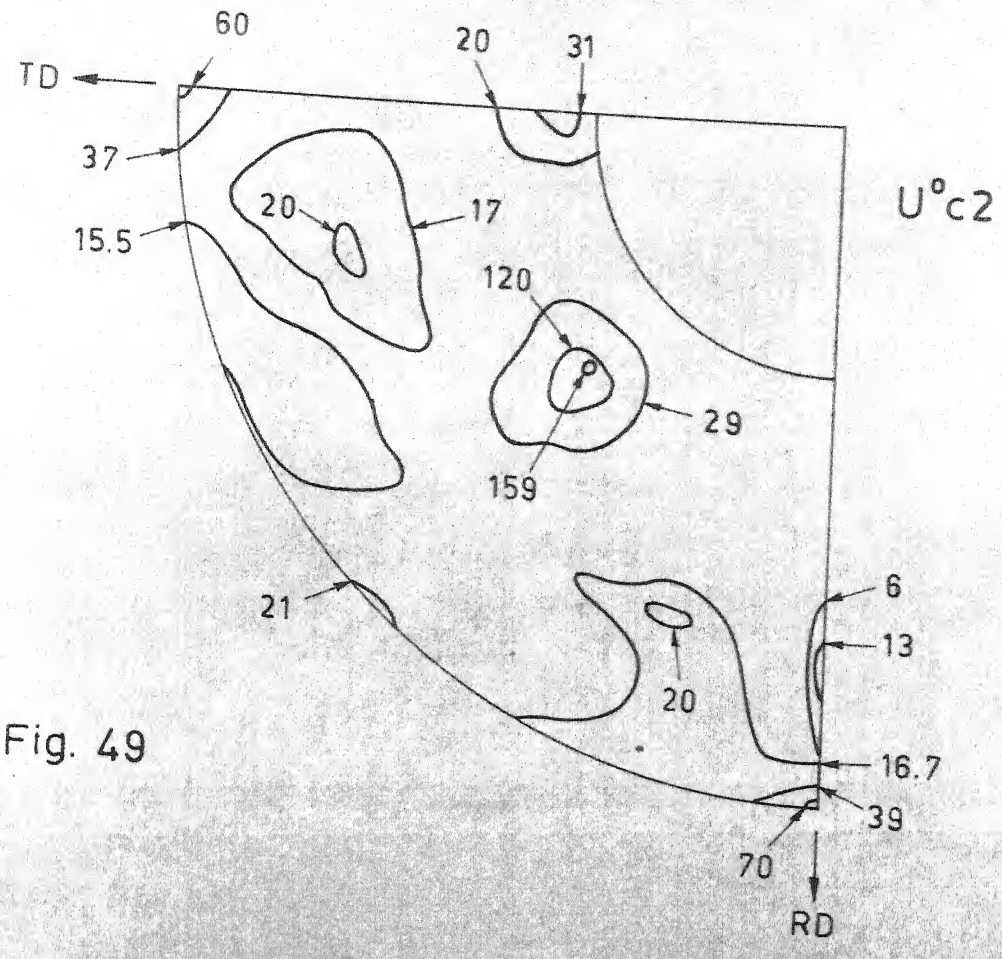
60
TD
20
31
37
20
17
15.5
U°c2
120
29
159
21
6
13
20
16.7
39
70
RD

Fig. 49

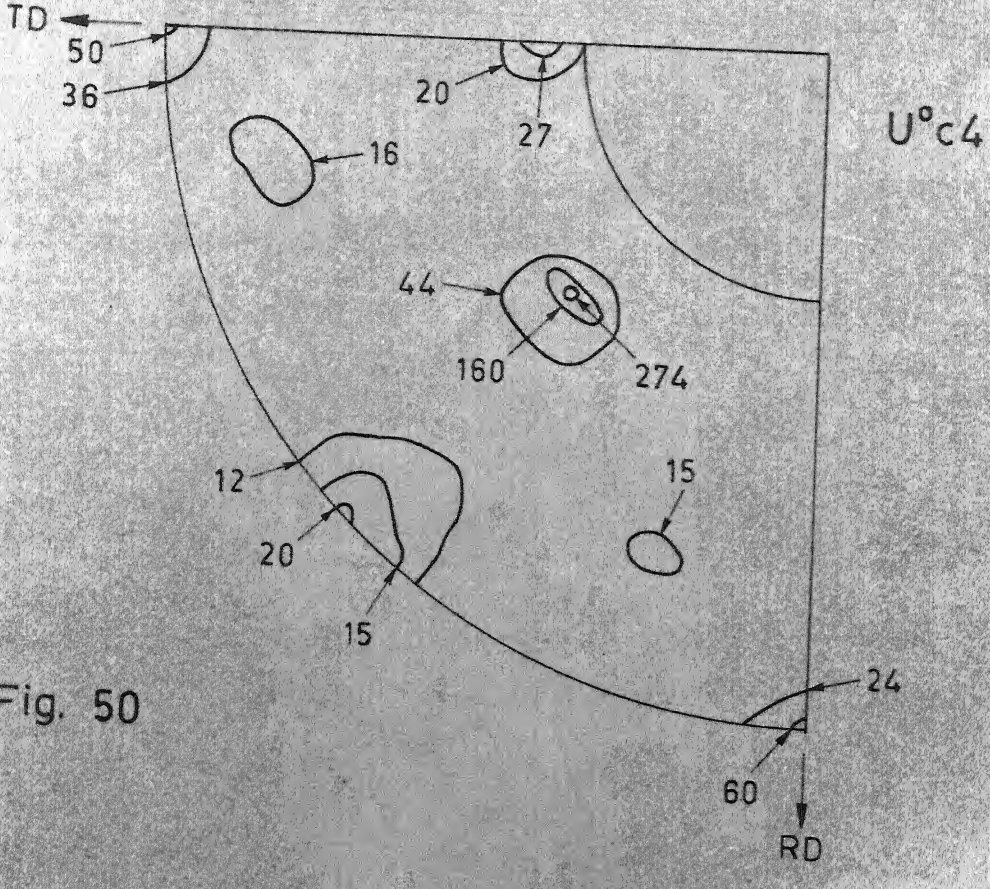
TD
50
36
20
27
U°c4
16
44
160
274
12
15
20
15
24
60
RD

Fig. 50

FIGURE CAPTION

Figure 53 : (111) pole figure of 96 pct. CR 5Cu alloy ($V^{o}b2$) annealed at 1050°C for 2 hrs.

Figure 54 : (111) pole figure of 96 pct. CR 5Cu alloy ($V^{o}b4$) annealed at 1050°C for 4 hrs.

Figure 55 : (111) pole figure of 96 pct. CR 5Cu alloy ($V^{o}b6$) annealed at 1050°C for 6 hrs.

Figure 56 : (111) pole figure of 96 pct. CR 5Cu alloy ($V^{o}c2(H_2)$) annealed at 1050°C for 2 hrs in hydrogen.

Figure 57 : (111) pole figure of 97 pct. CR 5Cu alloy ($V^{o}c1$) annealed at 1050°C for 1 hr.

Figure 58 : (111) pole figure of 97 pct. CR 5Cu alloy ($V^{o}c2$) annealed at 1050°C for 2 hrs.

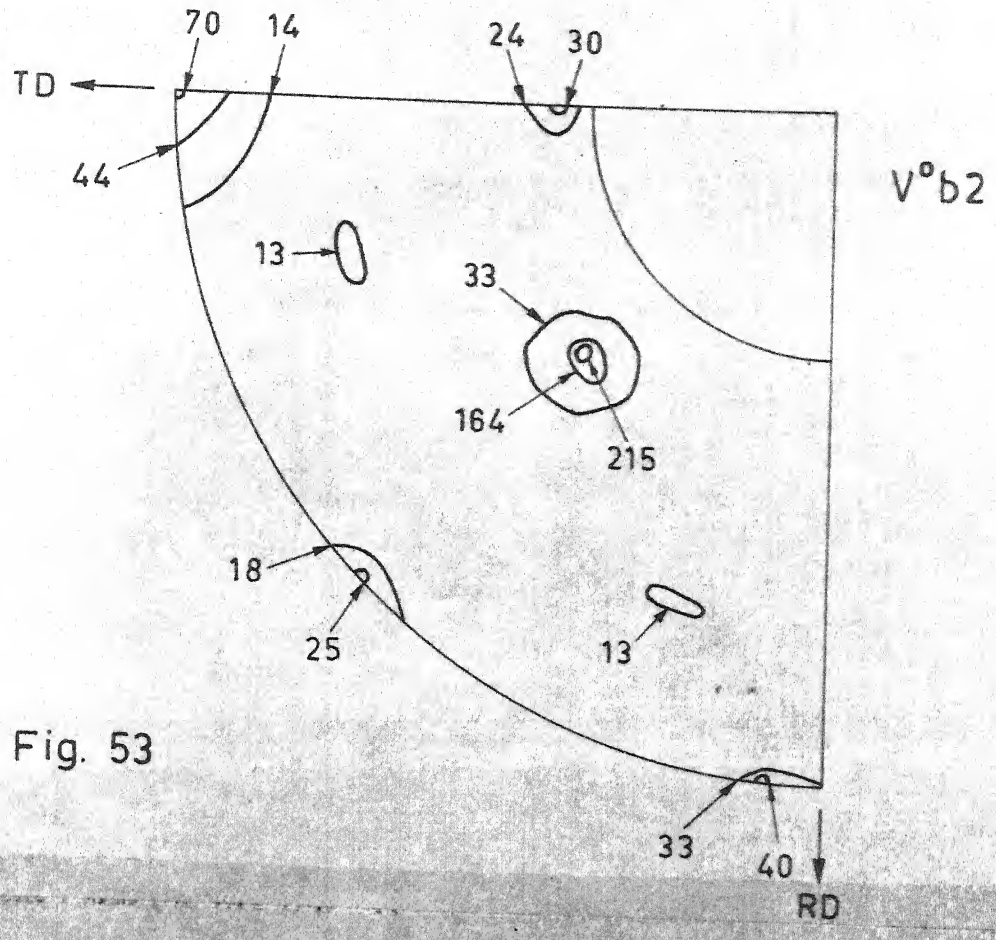
70
14
24
30
TD
44
V°b2
13
33
164
215
18
25
13
33
40
RD

Fig. 53

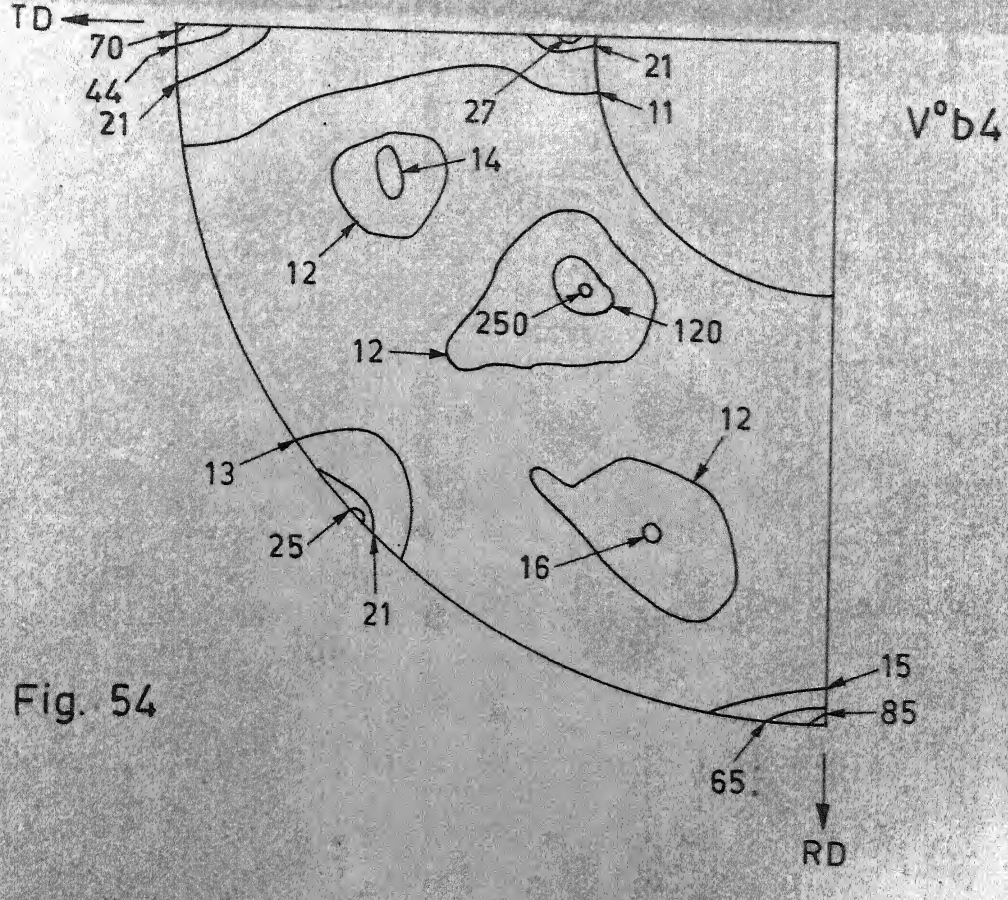
TD
70
44
21
21
27
11
V°b4
14
12
250
120
12
12
13
25
21
16
15
85
65
RD

Fig. 54

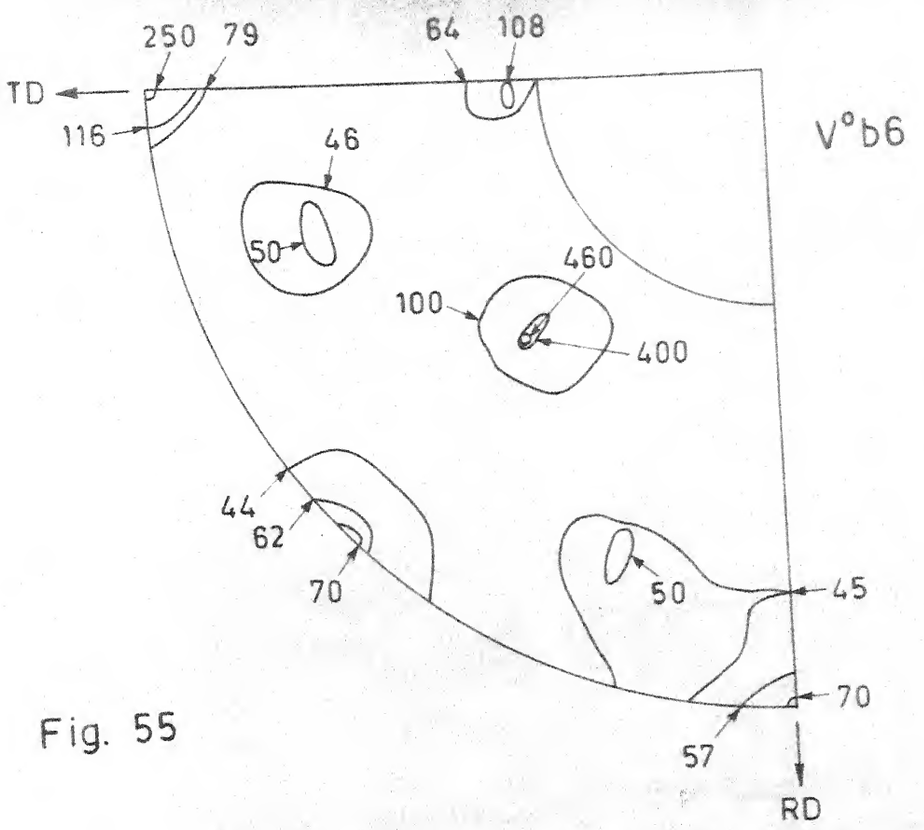
250
79
64
108
TD
116
46
50
460
100
400
44
62
70
50
45
70
57
RD
V°b6

Fig. 55

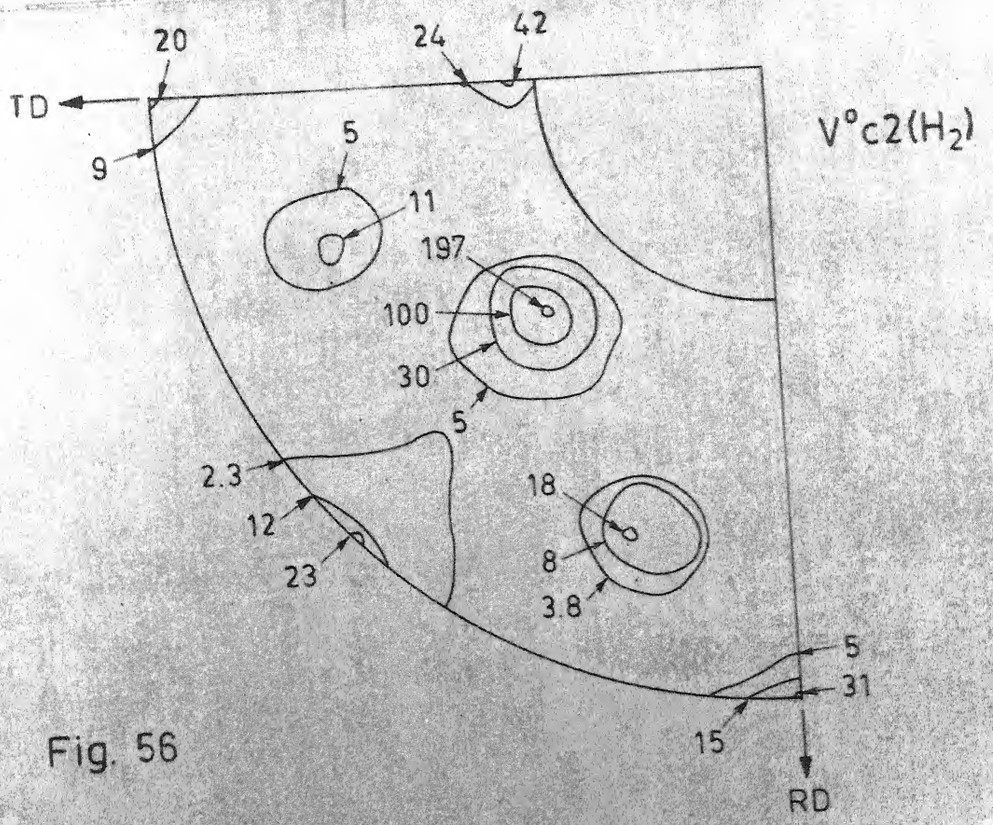
20
24
42
TD
9
5
11
197
100
30
5
2.3
12
23
18
8
3.8
5
31
15
RD
V°c2(H2)

Fig. 56

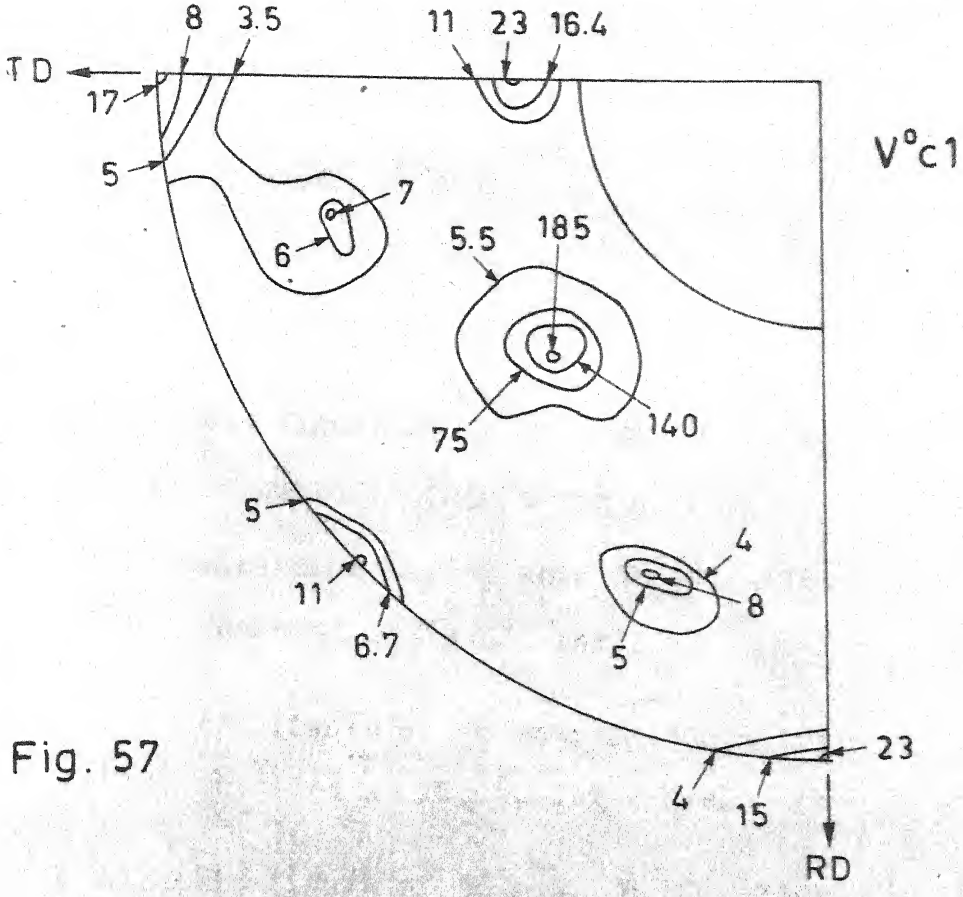
8
3.5
11
23
16.4
TD
17
5
V°c1
7
6
5.5
185
75
140
5
11
6.7
4
8
5
23
4
15
RD

Fig. 57

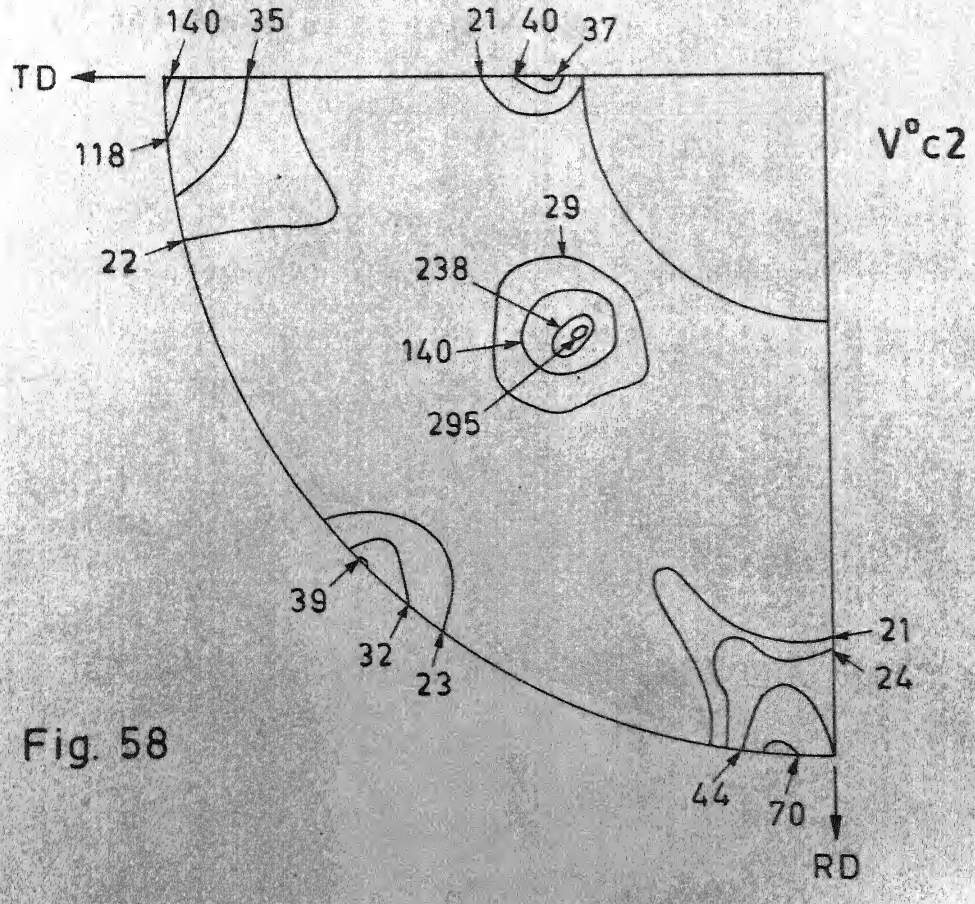
140
35
21
40
37
TD
118
V°c2
29
22
238
140
295
39
32
23
21
24
44
70
RD

Fig. 58

FIGURE CAPTION

Figure 59 : (111) pole figure of 97 pct. CR 5Cu alloy ($V^{o}c4$) annealed at 1050°C for 4 hrs.

Figure 60 : (111) pole figure of 98 pct. CR 5Cu alloy ($V^{1}d1$) annealed at 1050°C for 1 hr.

Figure 61 : (111) pole figure of 98 pct. CR 5Cu alloy ($V^{1}d2$) annealed at 1050°C for 2 hrs.

Figure 62 : (111) pole figure of 98 pct. CR 5Cu alloy ($V^{1}d4$) annealed at 1050°C for 4 hrs.

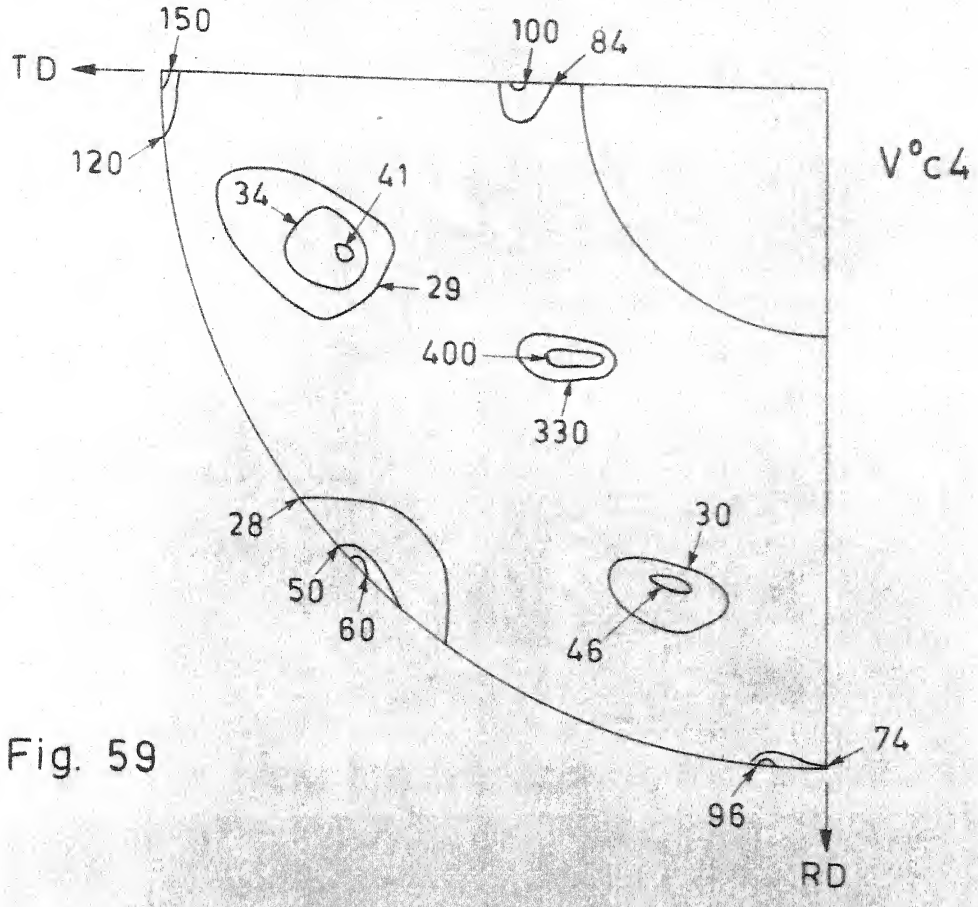
150
TD
100
84
120
41
34
29
400
330
V°c4
28
50
60
30
46
74
96
RD

Fig. 59

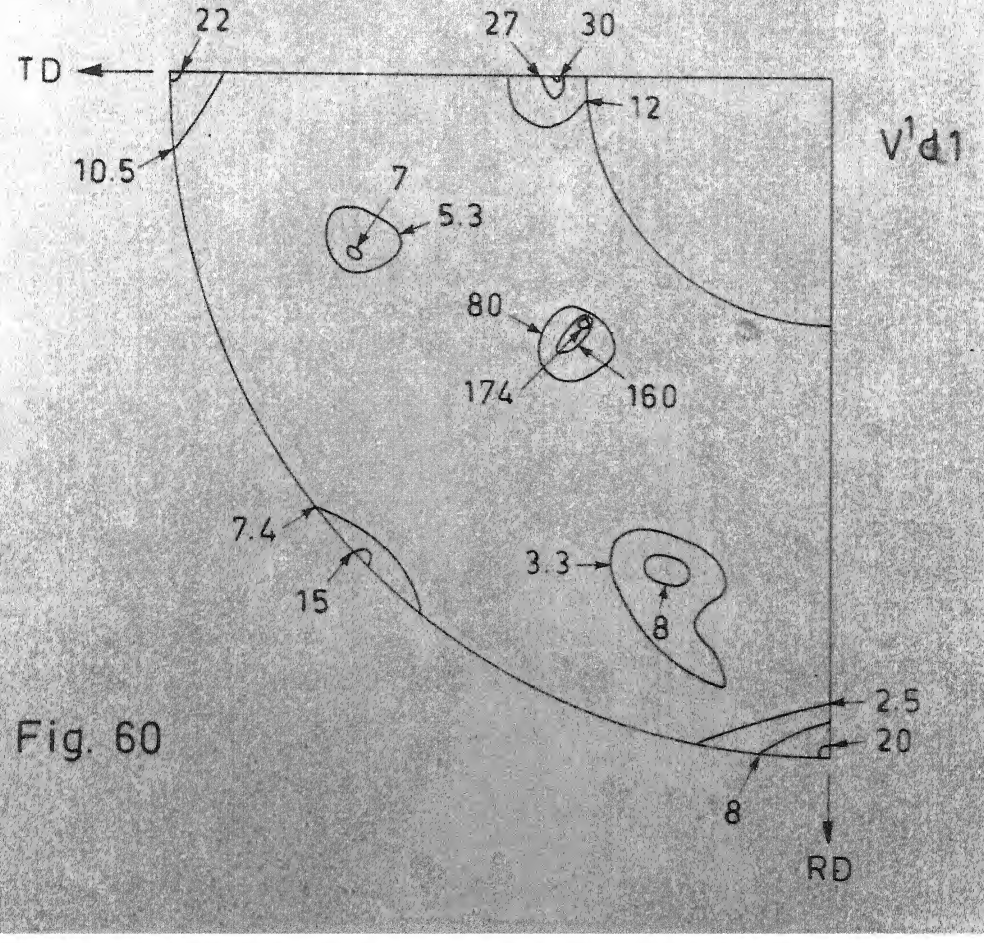
22
TD
27
30
12
10.5
7
5.3
80
174
160
V¹d1
7.4
15
3.3
8
2.5
20
8
RD

Fig. 60

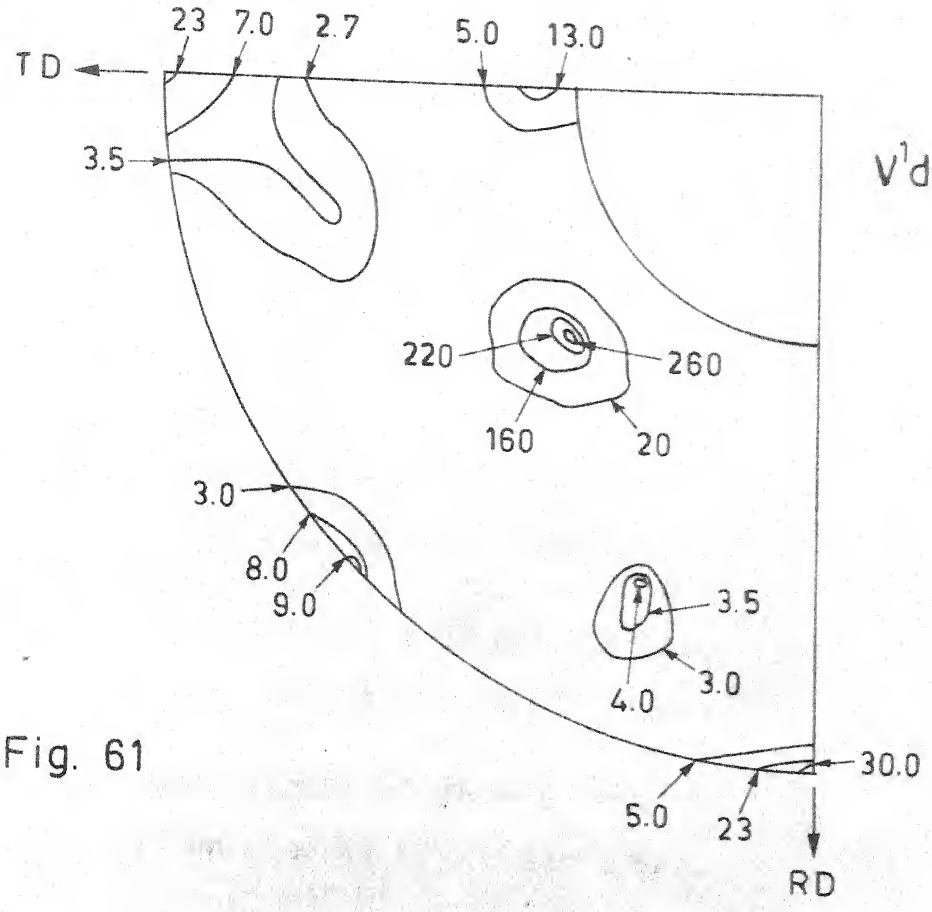
TD
23
7.0
2.7
5.0
13.0
3.5
V'd2
220
260
160
20
3.0
8.0
9.0
3.5
3.0
4.0
30.0
5.0
23
RD

Fig. 61

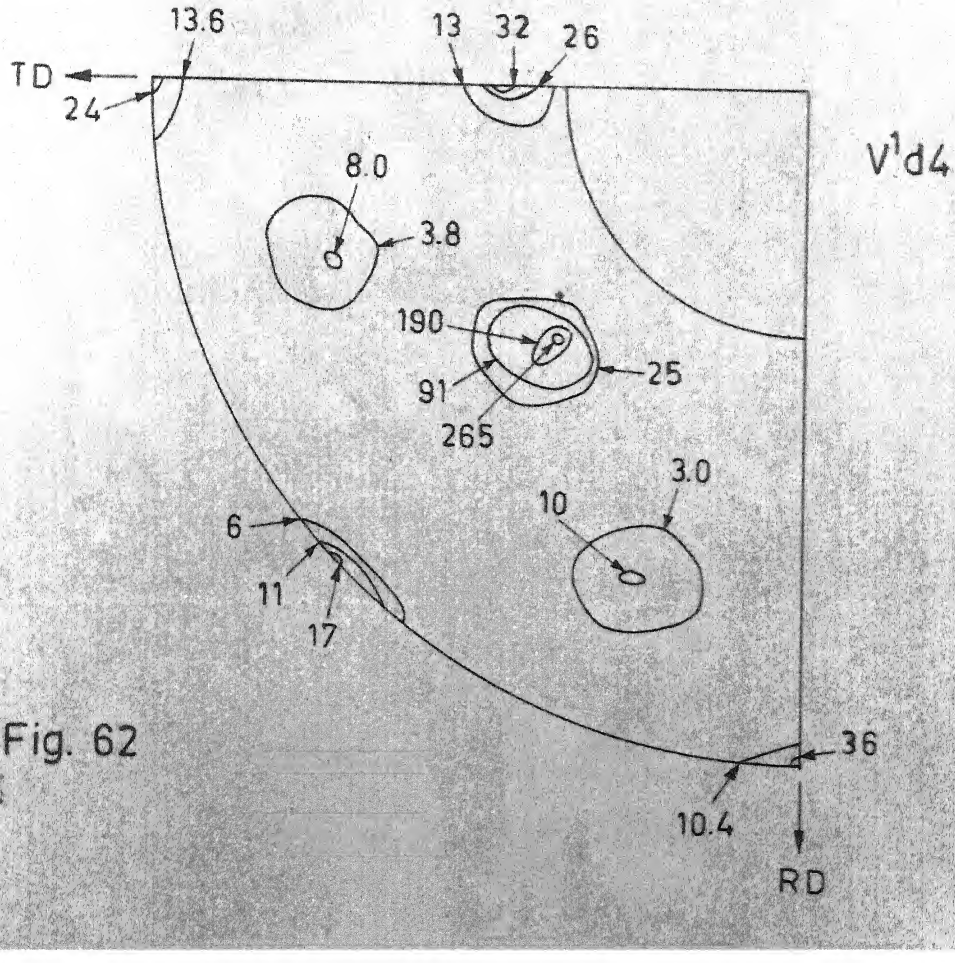
TD
13.6
24
13
32
26
V'd4
8.0
3.8
190
25
91
265
3.0
10
6
11
17
36
10.4
RD

Fig. 62

FIGURE CAPTION

Figure 63 : (111) pole figure of 96 pct. CR 14Cu alloy ($W^{o}b2$) annealed at 1050°C for 2 hrs.

Figure 64 : (111) pole figure of 96 pct. CR 14Cu alloy ($W^{o}b4$) annealed at 1050°C for 4 hrs.

Figure 65 : (111) pole figure of 97 pct. CR 14Cu alloy ($W^{o}c2$) annealed at 1050°C for 2 hrs.

Figure 66 : (111) pole figure of 97 pct. CR 14Cu alloy ($W^{o}c4$) annealed at 1050°C for 4 hrs.

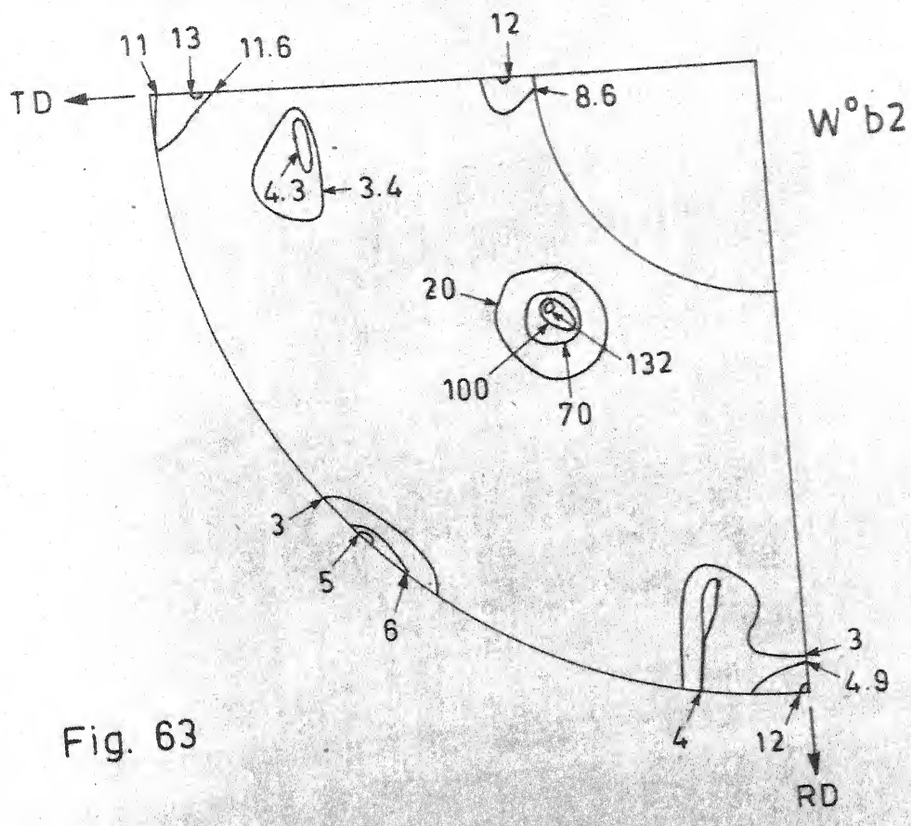
11
13
11.6
12
TD
8.6
W°b2
4.3
3.4
20
132
100
70
3
5
6
3
4.9
4
12
RD

Fig. 63

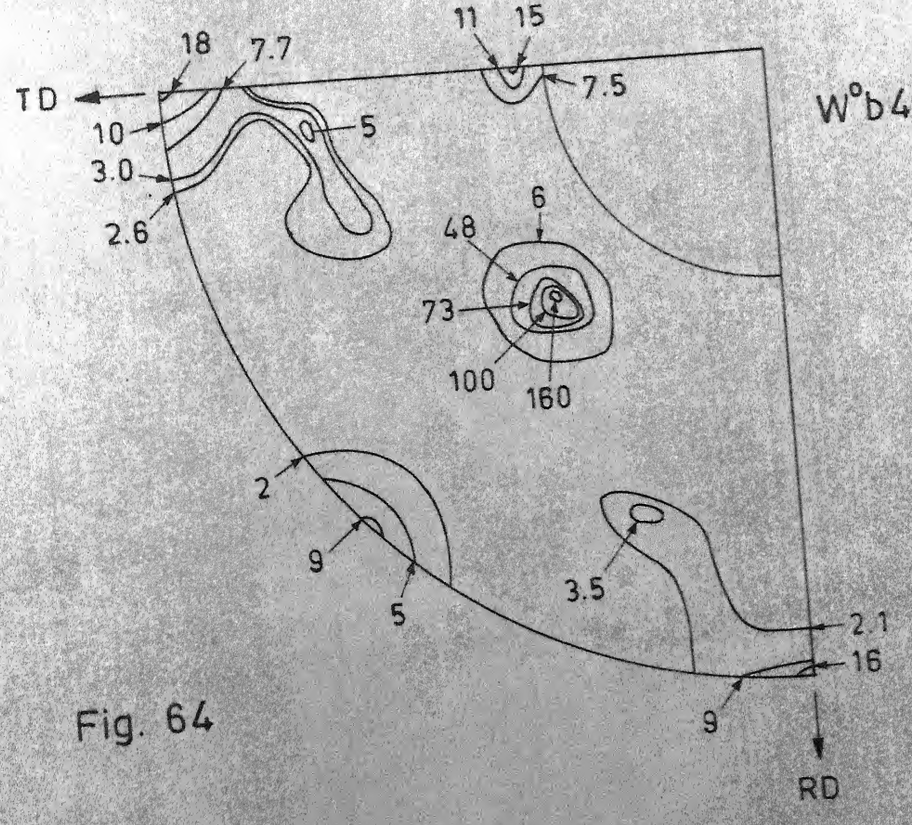
18
7.7
11
15
TD
7.5
W°b4
10
5
3.0
2.6
6
48
73
100
160
2
9
5
3.5
2.1
16
9
RD

Fig. 64

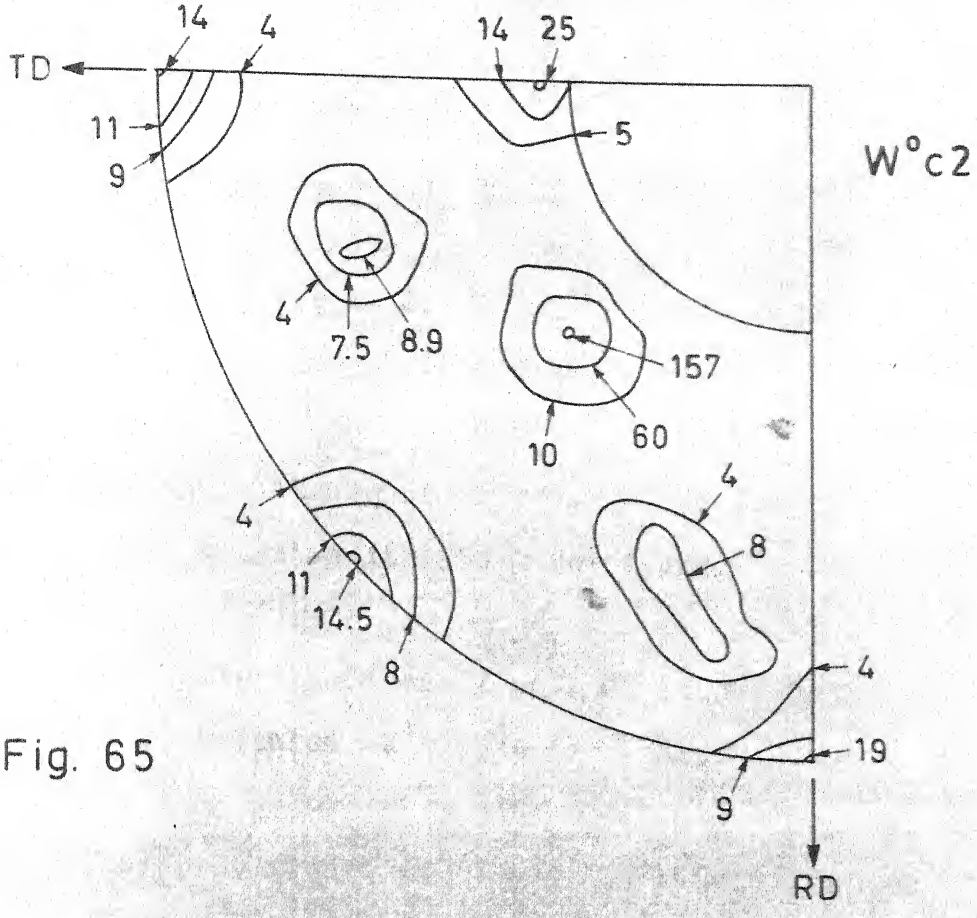
TD
14
4
14
25
11
9
5
W°c2
4
7.5
8.9
157
10
60
4
4
8
11
14.5
8
4
19
9
RD

Fig. 65

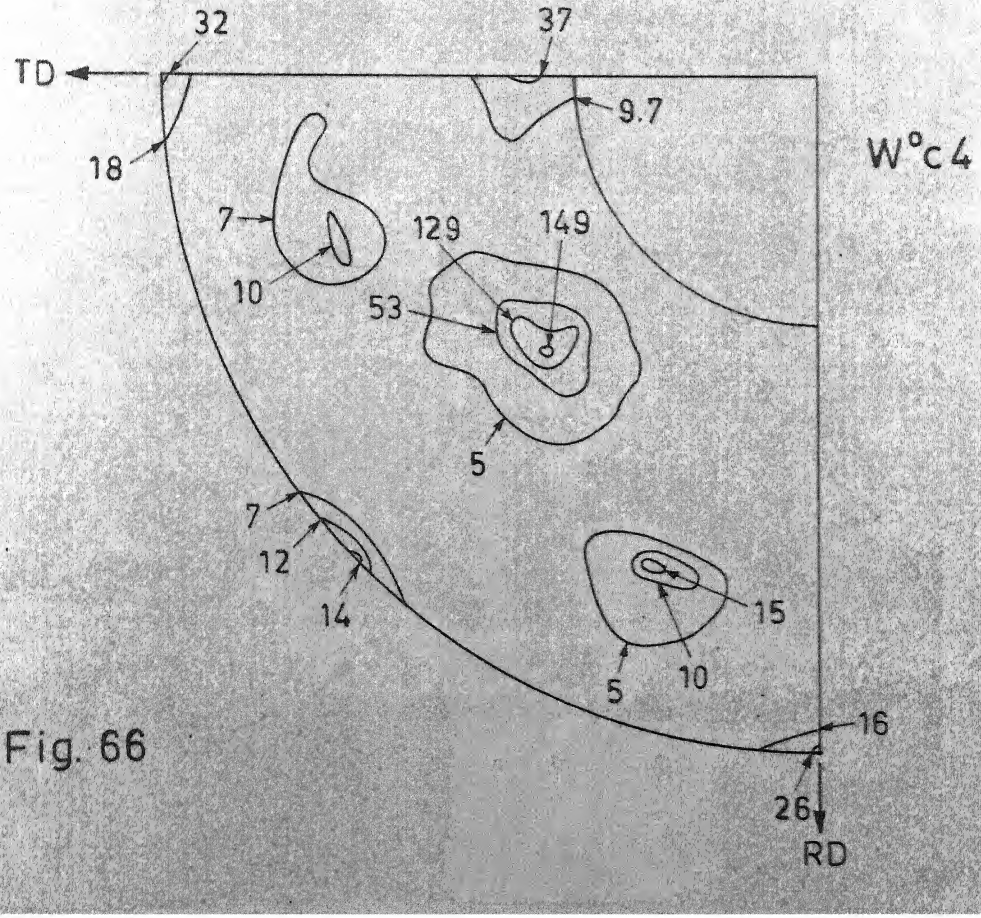
TD
32
37
9.7
18
W°c4
7
10
129
149
53
5
7
12
14
15
5
10
16
26
RD

Fig. 66

FIGURE CAPTION

Figure 67 : (111) pole figure of 96 pct. CR 14Cu alloy ($Y^{o}b2$) annealed at 1050°C for 2 hrs.

Figure 68 : (111) pole figure of 96 pct. CR 14Cu alloy ($Y^{o}b4$) annealed at 1050°C for 4 hrs.

Figure 69 : (111) pole figure of 97 pct. CR 14Cu alloy ($Y^{o}c2$) annealed at 1050°C for 2 hrs.

Figure 70 : (111) pole figure of 97 pct. CR 14Cu alloy ($Y^{o}c4$) annealed at 1050°C for 4 hrs.

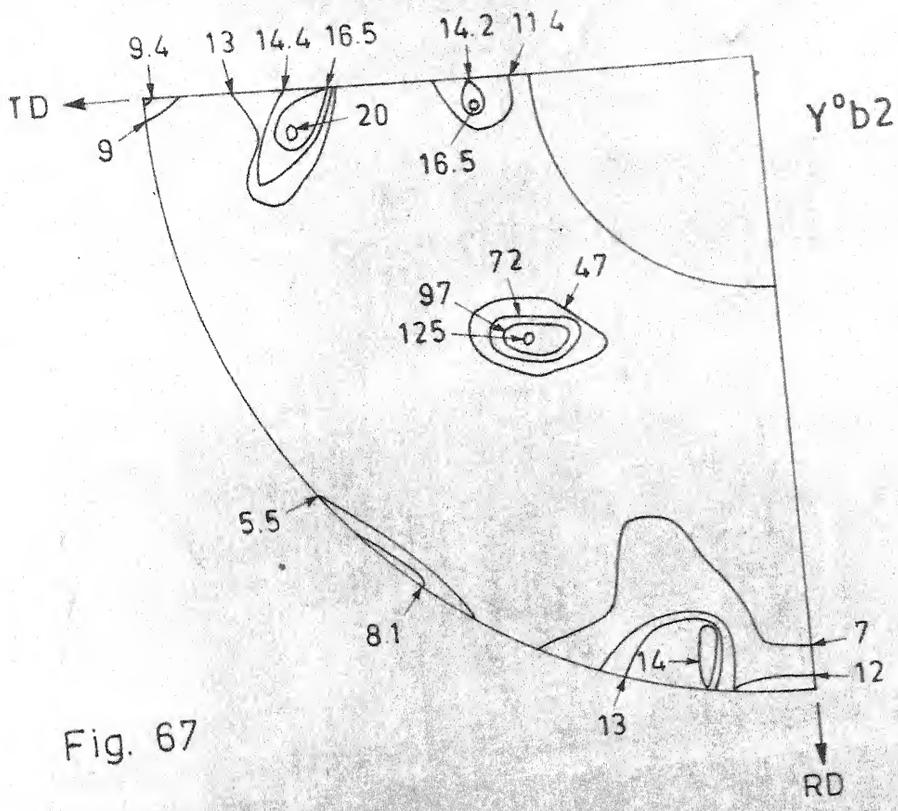
9.4
13
14.4
16.5
14.2
11.4
TD
9
20
16.5
Y°b2
72
47
97
125
5.5
8.1
7
14
12
13
RD

Fig. 67

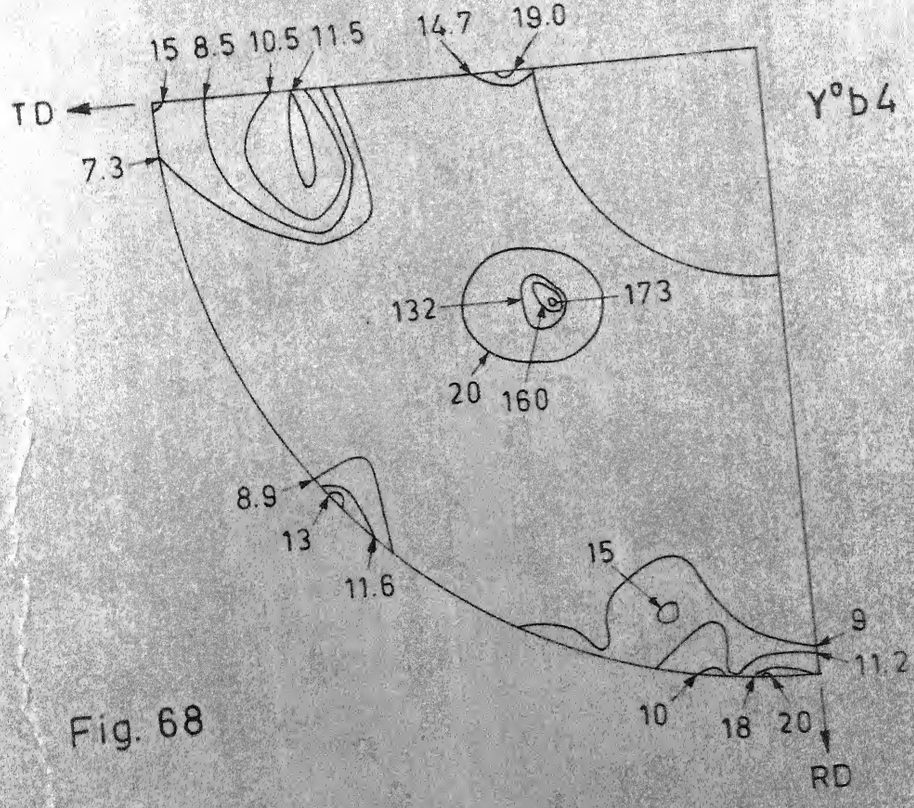
15
8.5
10.5
11.5
14.7
19.0
TD
7.3
Y°b4
132
173
20
160
8.9
13
11.6
15
9
11.2
10
18
20
RD

Fig. 68

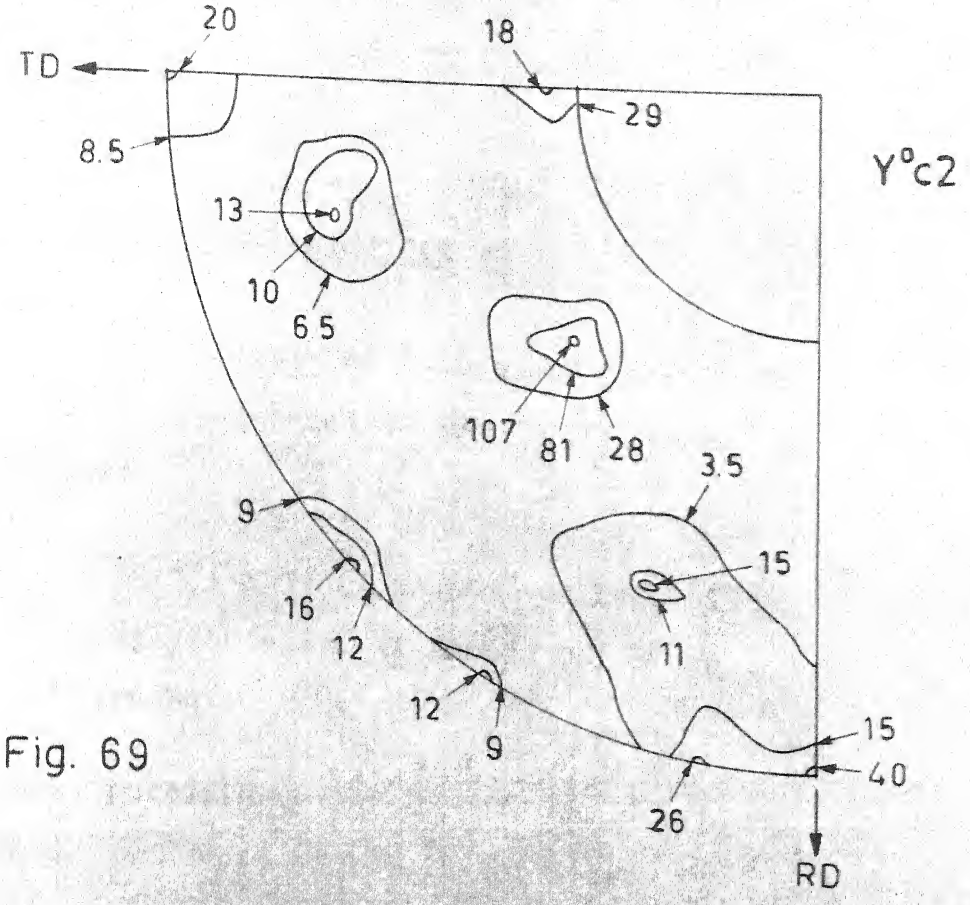
20
18
TD
29
8.5
Y°c2
13
10
6.5
107
81
28
3.5
9
15
16
12
11
12
9
15
40
26
RD

Fig. 69

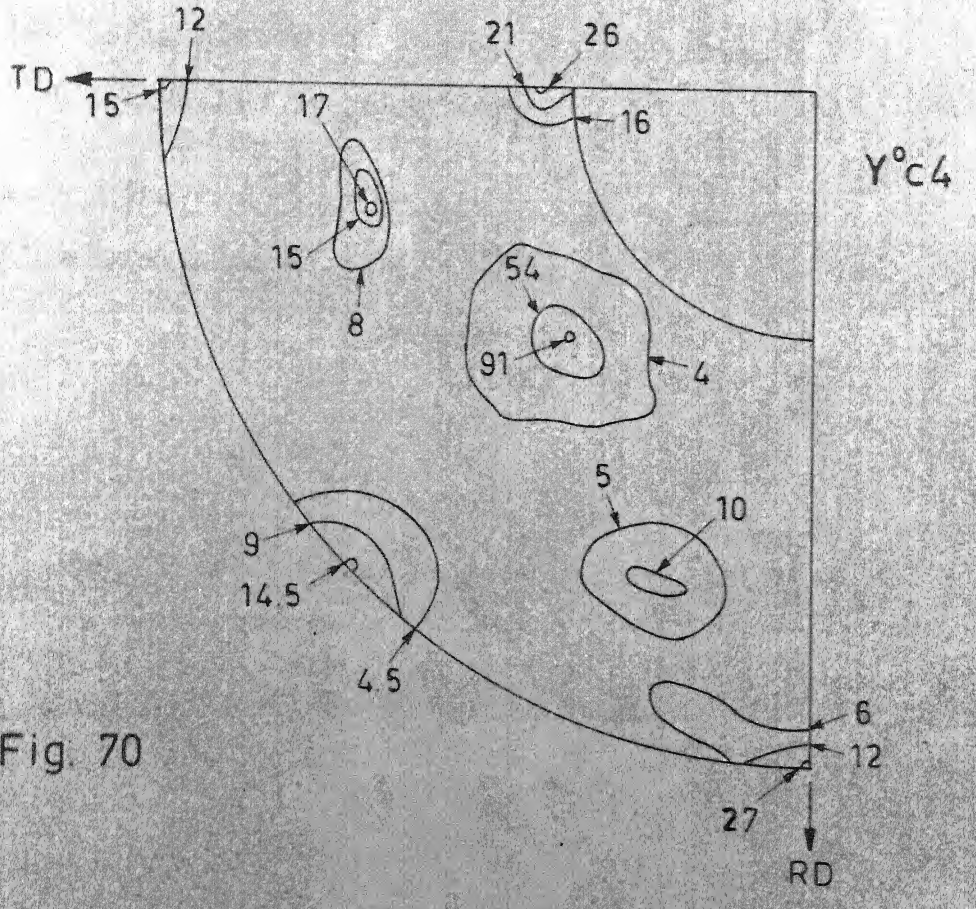
12
21
26
TD
15
17
16
Y°c4
15
8
54
91
4
5
10
9
14.5
4.5
6
12
27
RD

Fig. 70

FIGURE CAPTION

Figure 71 : (111) pole figure of 96 pct. CR 14Cu alloy ($Y^{o}b2(H_2)$) annealed at 1050°C for 2 hrs. in hydrogen.

Figure 72 : (111) pole figure of 96 pct. CR 14Cu alloy ($W^{o}b2(H_2)$) annealed at 1050°C for 2 hrs. in hydrogen.

Figure 73 : (111) pole figure of 98 pct. CR 10Cu alloy ($X^{o}d1$) annealed at 1050°C for 1 hr.

Figure 74 : (111) pole figure of 98 pct. CR 10Cu alloy ($X^{o}d2$) annealed at 1050°C for 2 hrs.

Figure 75 : (111) pole figure of 98 pct. CR 10 Cu alloy ($X^{o}d4$) annealed at 1050°C for 4 hrs.

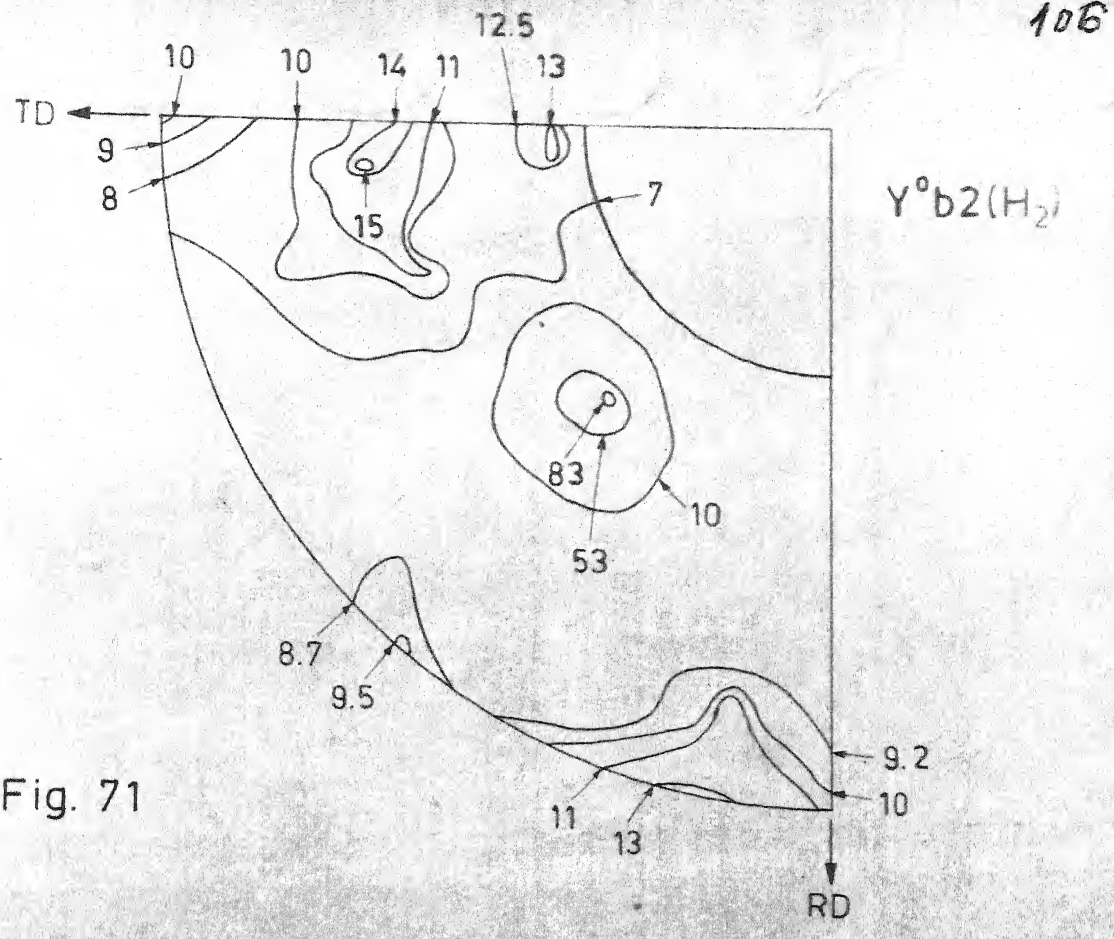
TD
10
10
14
11
12.5
13
9
8
15
7
83
10
53
8.7
9.5
9.2
10
11
13
RD
Y°b2(H2)

Fig. 71

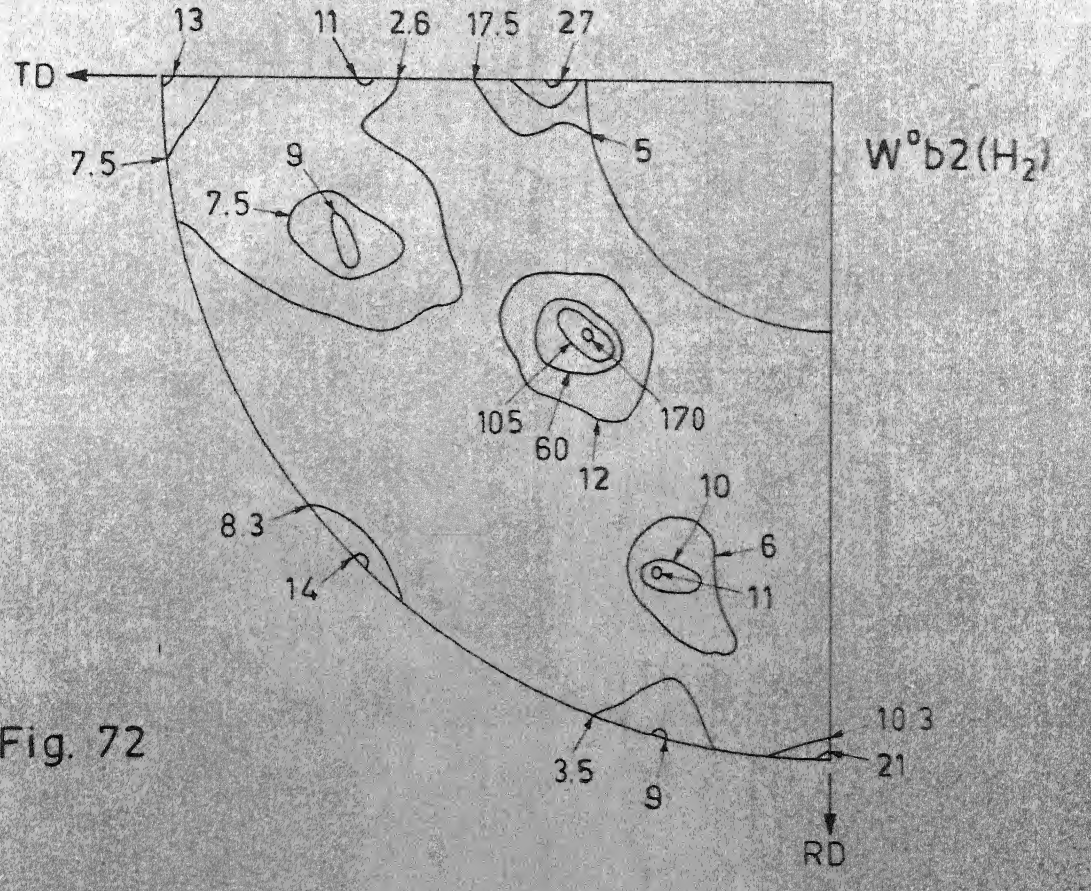
TD
13
11
2.6
17.5
27
7.5
9
7.5
5
105
60
12
170
10
6
11
8.3
14
3.5
9
10.3
21
RD
W°b2(H2)

Fig. 72

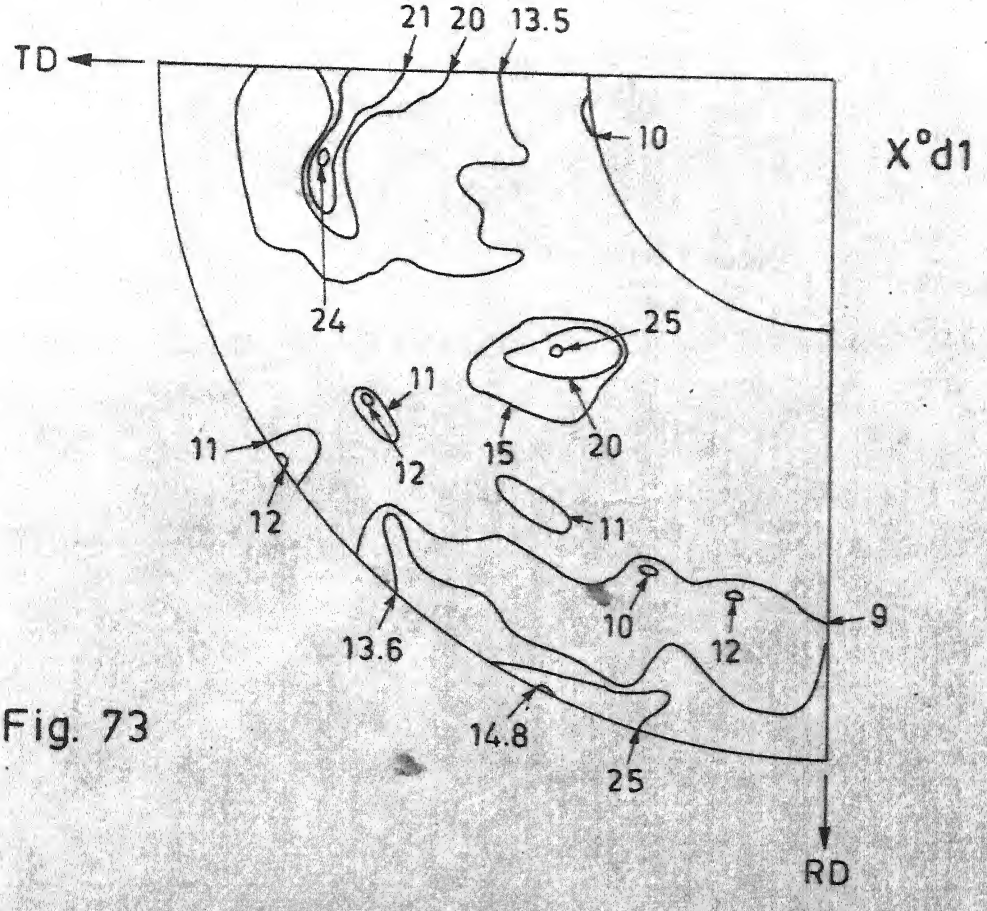

Fig. 73

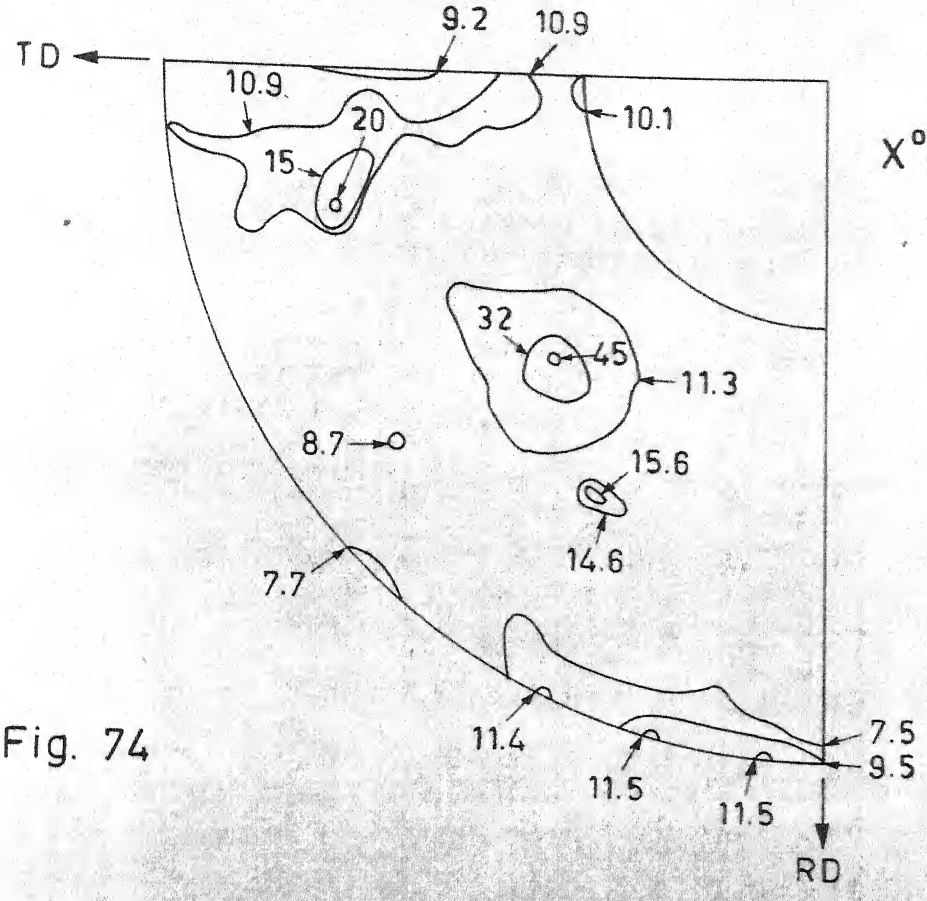
TD
9.2
10.9
10.9
20
15
10.1
X°d2
32
45
11.3
8.7
15.6
14.6
7.7
11.4
11.5
11.5
7.5
9.5
RD

Fig. 74

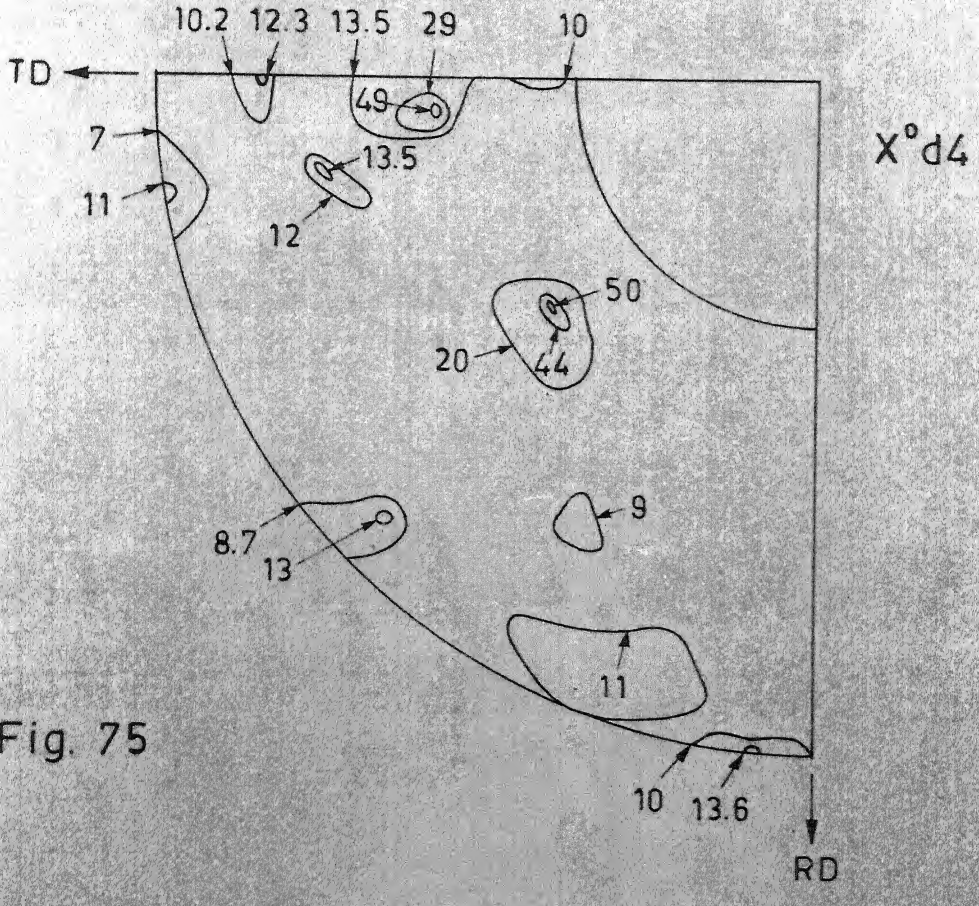
10.2
12.3
13.5
29
10
TD
49
7
13.5
11
12
X°d4
50
20
44
9
8.7
13
11
10
13.6
RD

Fig. 75

Table IX : Effect of composition and process variables on annealed texture of 5 pct. Cu bearing permalloys.

Alloy designation	Intensity of (111) reflection at different locations relative to 7 or 8								Fig. No.
	1	2	3	4	5	6	7	8	
1	2	3	4	5	6	7	8	9	10
$P^{o}b4$	6.3	3.8	6.1	9.4	3.1	12.7	1.0	1.1	40
$T^{o}b2$	5.5	2.7	-	5.9	1.6	14.6	1.0	1.2	42
$T^{o}b4$	5.2	3.9	-	6.6	2.5	11.6	1.0	1.2	43
$T^{o}c2$	1.7	3.1	-	1.9	1.8	16.6	1.0	1.6	44
$T^{o}c4$	4.5	2.8	-	6.3	1.6	11.3	1.0	1.2	46
$T^{o}c2(H_2)$	1.3	2.6	-	2.0	1.5	13.3	1.0	1.0	45
$U^{o}b2$	1.3	1.0	-	2.3	1.0	8.0	1.8	1.0	47
$U^{o}b4$	4.5	2.8	-	7.6	2.2	19.0	1.0	1.6	48
$U^{o}c2$	3.0	1.6	-	3.5	1.0	8.0	1.0	1.0	49
$U^{o}c4$	3.3	1.8	-	4.0	1.3	18.3	1.1	1.0	50
$U^{o}c6$	2.6	1.1	-	4.3	1.1	5.2	1.0	1.0	51
$U^{o}c2(H_2)$	1.2	2.2	-	2.9	1.4	14.7	1.0	1.6	52
$V^{o}b2$	5.4	2.3	-	3.1	1.9	16.5	1.0	1.0	53
$V^{o}b4$	5.0	1.9	-	6.1	1.8	17.9	1.0	1.1	54
$V^{o}b6$	5.0	2.2	-	1.4	1.4	9.2	1.0	1.0	55
$V^{o}c1$	2.4	3.3	-	3.3	1.6	26.4	1.0	1.1	57

Table IX (Contd.)

1	2	3	4	5	6	7	8	9	10
$V^{o}c2$	7.0	2.0	-	3.5	2.0	14.7	1.0	1.0	58
$V^{o}c4$	3.7	2.4	-	2.3	1.5	9.8	1.0	1.1	59
$V^{o}c2(H_2)$	1.8	3.8	-	2.8	2.1	17.9	1.0	1.6	56
$V^{1}d1$	3.1	4.3	-	2.9	2.1	24.9	1.0	1.1	60
$V^{1}d2$	5.6	3.3	-	7.5	2.3	65.0	1.0	1.0	61
$V^{1}d4$	3.0	4.0	-	4.5	2.1	33.1	1.0	1.3	62
$X^{o}d1^{+}$	2.2	1.0	-	2.3	1.0	2.3	1.0	1.0	73
$X^{o}d2^{+}$	2.0	1.0	-	1.2	1.0	4.5	1.0	1.5	74
$X^{o}d4^{+}$	1.4	1.1	-	1.4	1.4	5.6	1.5	1.0	75

+ These alloys contain 10 pct. Cu.

Table X: Effect of composition and process variables on annealed texture of 14 pct. Cu bearing permalloys.

Alloy designation	Intensity of (111) reflection at different locations relative to 7 or 8								Fig. No.
	1	2	3	4	5	6	7	8	
$R^{o}c4$	2.5	3.0	5.0	5.0	1.7	8.0	1.0	1.0	41
$W^{o}b2$	3.3	3.0	θ	3.0	1.5	33.0	1.1	1.0	63
$W^{o}b4$	5.1	4.3	-	4.6	2.6	45.7	1.4	1 0	64
$W^{o}b2(H_2)$	1.4	3.0	-	2.3	1.6	18.9	1.0	1.2	72
$W^{o}c2$	1.8	3.1	-	2.4	1.8	19.6	1.1	1.0	65
$W^{o}c4$	3.2	3.7	-	2.6	1.4	15.0	1.0	1.5	66
$Y^{o}b2$	2.9	2.4	-	2.0	1.2	17.9	1.0	1.0	67
$Y^{o}b4$	2.1	2.7	-	2.9	1.9	24.7	1.0	1.0	68
$Y^{o}b2(H_2)$	1.8	2.2	-	2.2	1.7	13.8	1.0	1.0	71
$Y^{o}c2$	1.5	2.2	-	3.1	1.2	8.2	1.0	1.2	69
$Y^{o}c4$	1.5	2.6	-	2.7	1.5	9.1	1.7	1.0	70

method has been employed to present the texture data for the annealed sheets. Tables IX and X show the intensity of (111) reflection at locations 1 through 8 relative to the intensity at location 7 or 8.

III.3 Magnetic measurements

Using PAR model 150A vibrating sample magnetometer, some magnetic properties were measured for alloys with different heat treatments: (1) annealed and (2) annealed just above T_c and quenched in hot water. The results obtained using magnetometer are shown in Figs. 76-77 and 79-80 as plots of M vs H. For alloys V^1d2 and Y^0b4, complete B-H loops were obtained using the magnetometer (Fig. 78). Mr, iH_c, $M_{H=500\theta e}$ and μ_m of the alloys obtained with the help of M vs H plots are tabulated in Table XI. The Figs. 76 to 80 show that all the alloys are essentially magnetically saturated in magnetic fields ranging from $\sim 80\ \theta_e$ to $150\ \theta_e$.

The permeameter magnetisation values could not be calibrated. Hence the measurements made using the permeameter can be used only for qualitative analysis of B-H curves. A very approximate calibration of B values obtained using permeameter was done with the help of data obtained with the magnetometer. The magnetisation curves obtained for the specimen V^1d2 was used for this purpose. The B value

corresponding to a magnetic field of $\sim$25 θ_e was compared with the B value of the same specimen measured with the permeameter. The B value obtained through the magnetometer was found to be about 4 times higher. Hence, a scale factor of 4 was used to convert the permeameter B values. In the Fig. 81 the modified B scale has been shown. Table XI gives the H_c values for different specimens before and after magnetic cooling.

FIGURE CAPTION

Figure 76 : Magnetisation vs field strength curves for $T^{o}c2$, $T^{o}c2$ (440, HW85) and $U^{o}c4$ (Magnetometer data).

Figure 77 : Magnetisation vs field strength curves for $U^{o}c4$ (450, HW85), $V^{1}d2$ and $V^{1}d2$ (enlarged scale) (Magnetometer data).

Figure 78 : B-H loops for $V^{1}d2$ and $Y^{o}b4$ (Magnetometer data).

Figure 79 : Magnetisation vs field strength curves for $V^{1}d4$, $V^{1}d4$ (460, HW85) and $W^{o}b4$ (Magnetometer data).

Figure 80 : Magnetisation vs field strength curves for ($W^{o}b4$ (220, HW85), $Y^{o}b4$, and $Y^{o}b4$ (260, HW85) (Magnetometer data).

Figure 81 : Magnetic induction vs field strength curves for $T^{o}c2$, $U^{o}c4$, $V^{1}d2$ and $W^{o}b4$ (Permeameter data).

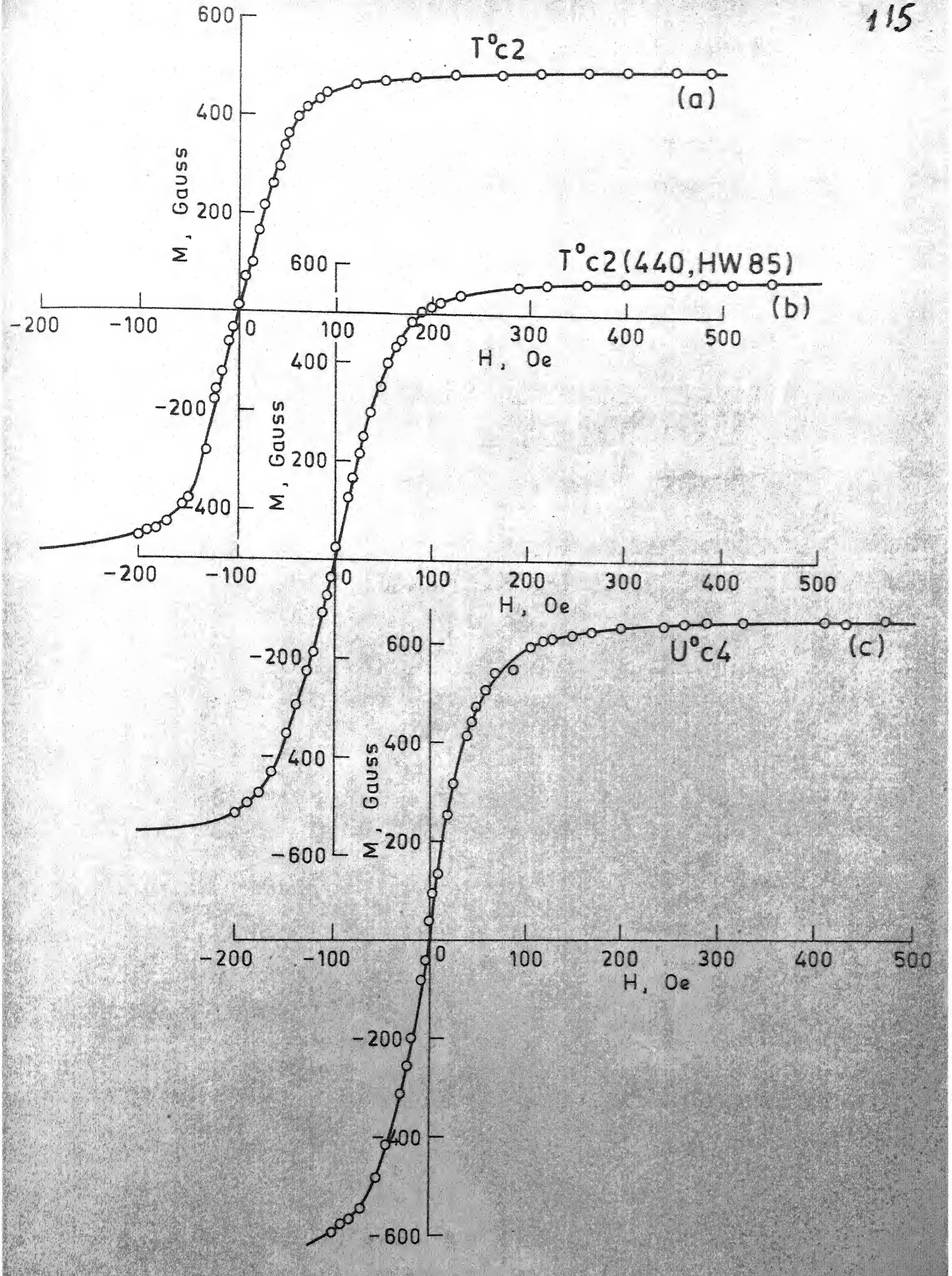

Fig. 76

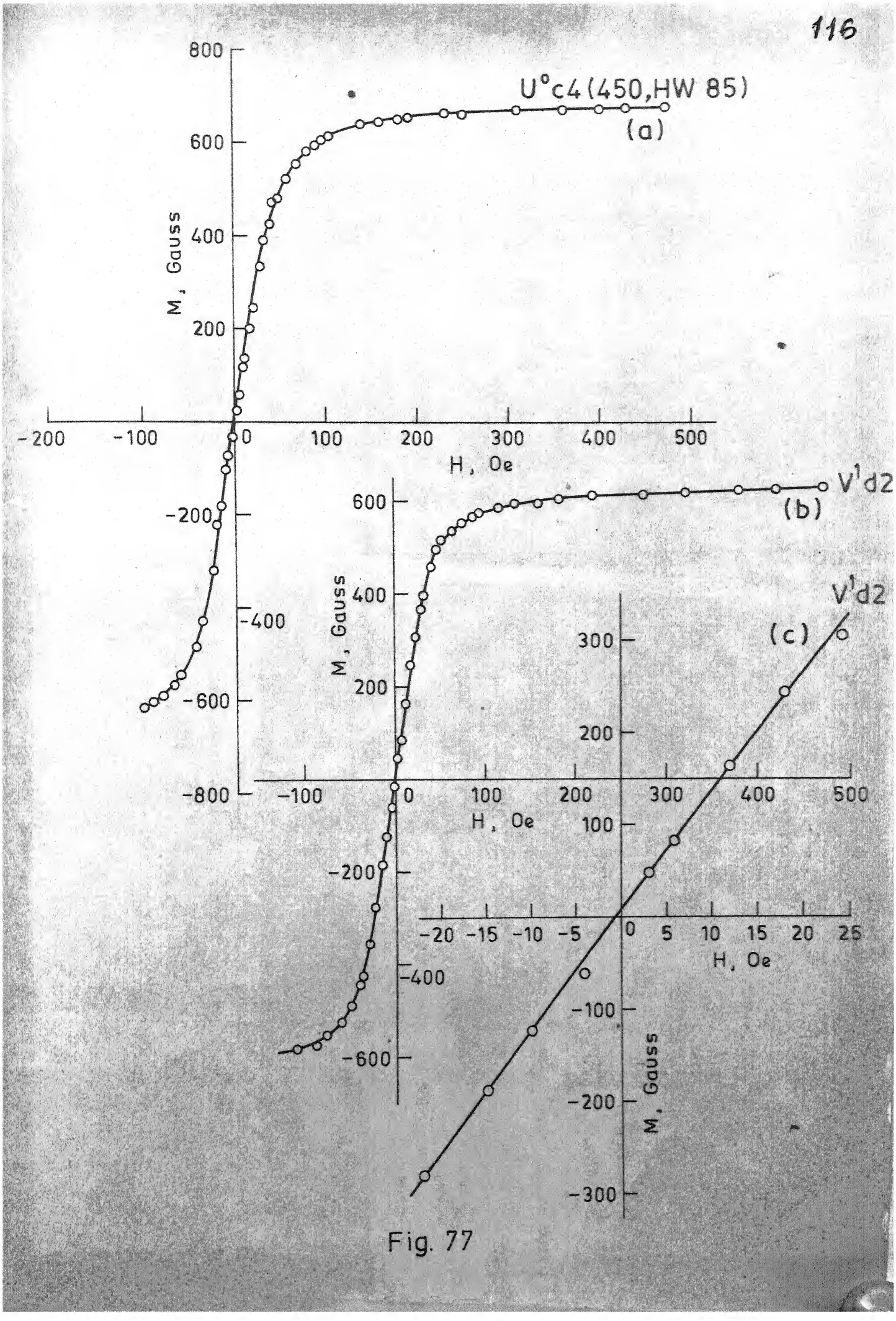

Fig. 77

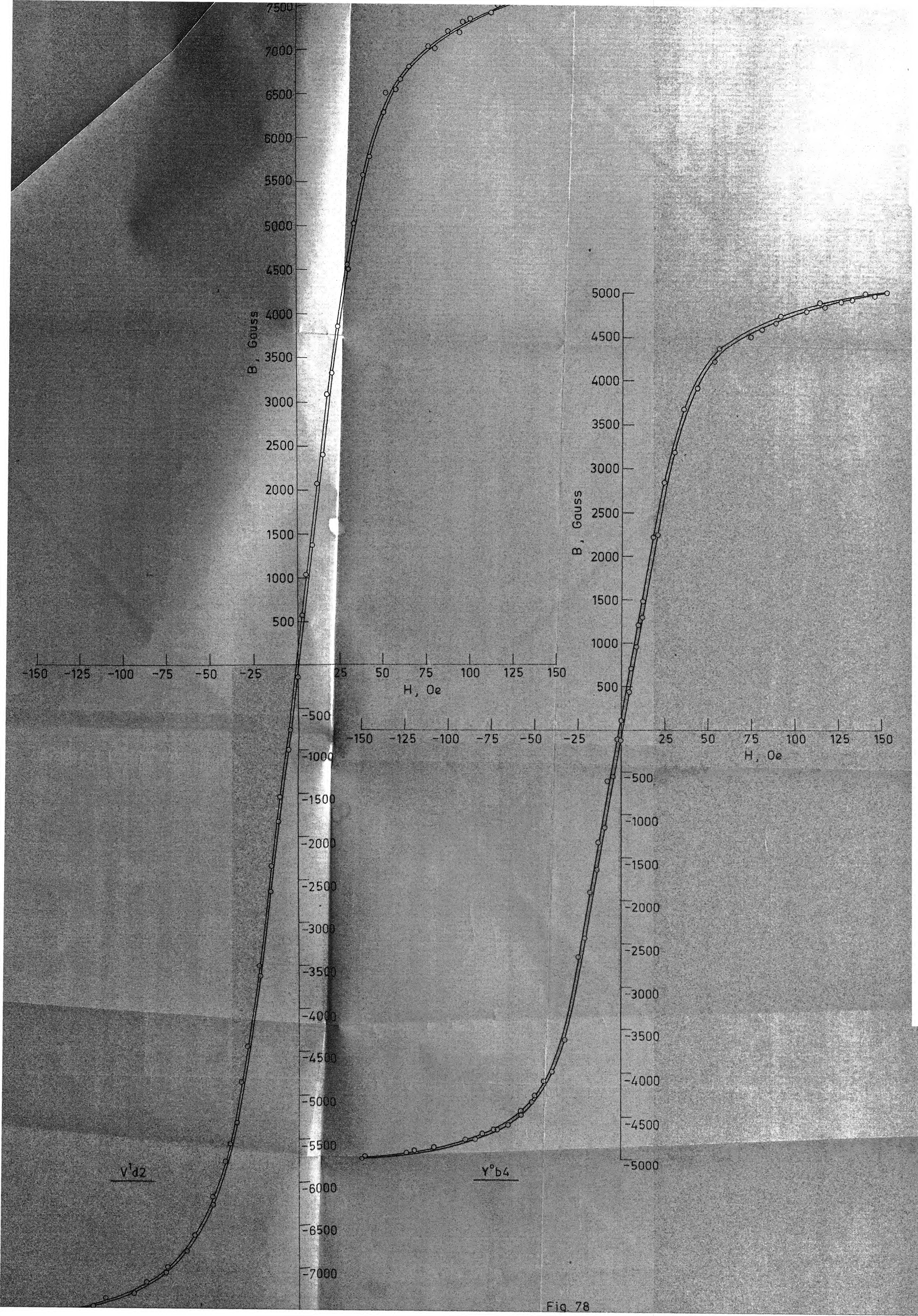

Fig. 78

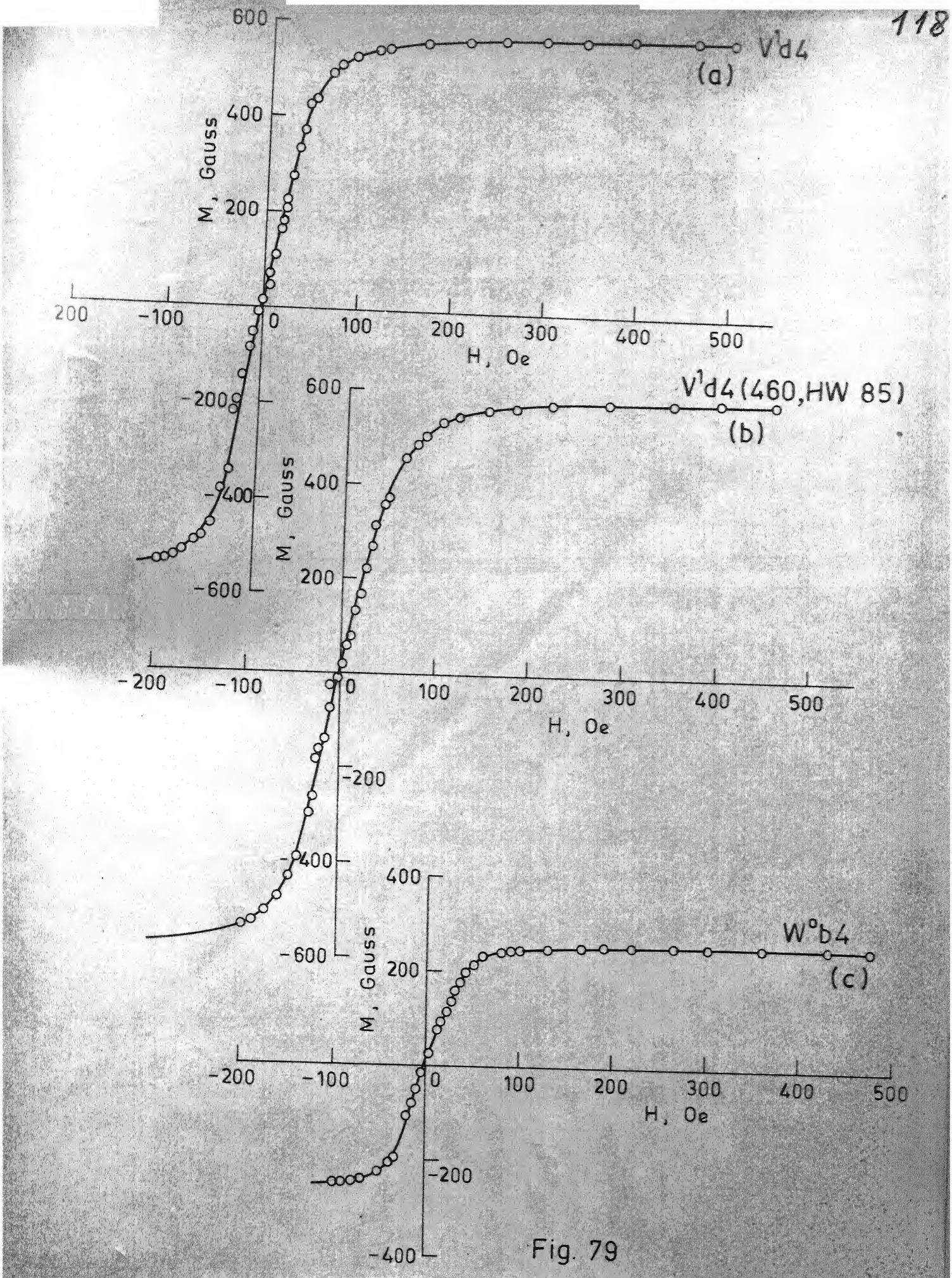

Fig. 79

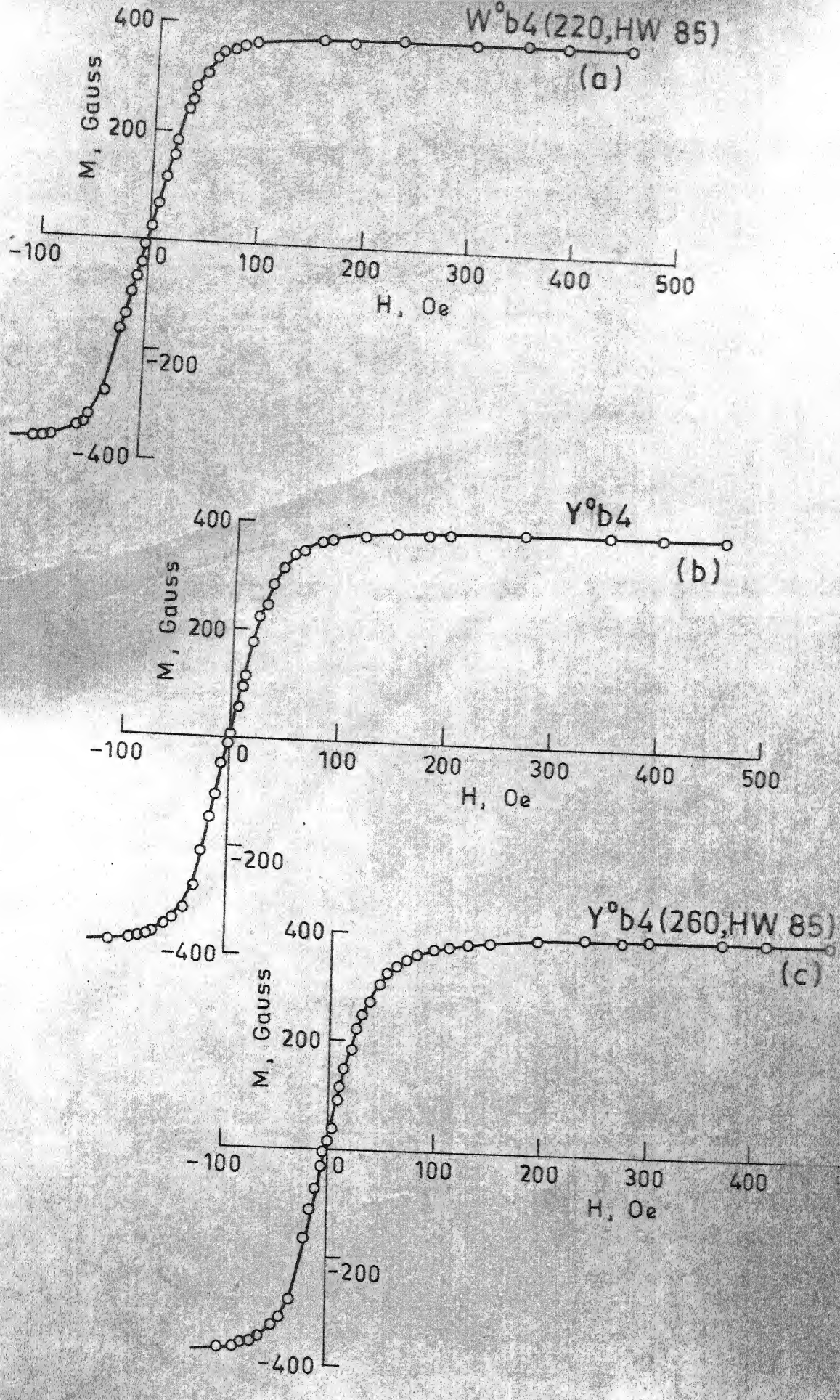
W°b4(220,HW 85)
(a)
M, Gauss
H, Oe
400
200
-200
-400
-100
0
100
200
300
400
500
Y°b4
(b)
M, Gauss
H, Oe
Y°b4(260,HW 85)
(c)
M, Gauss
H, Oe

Fig. 80

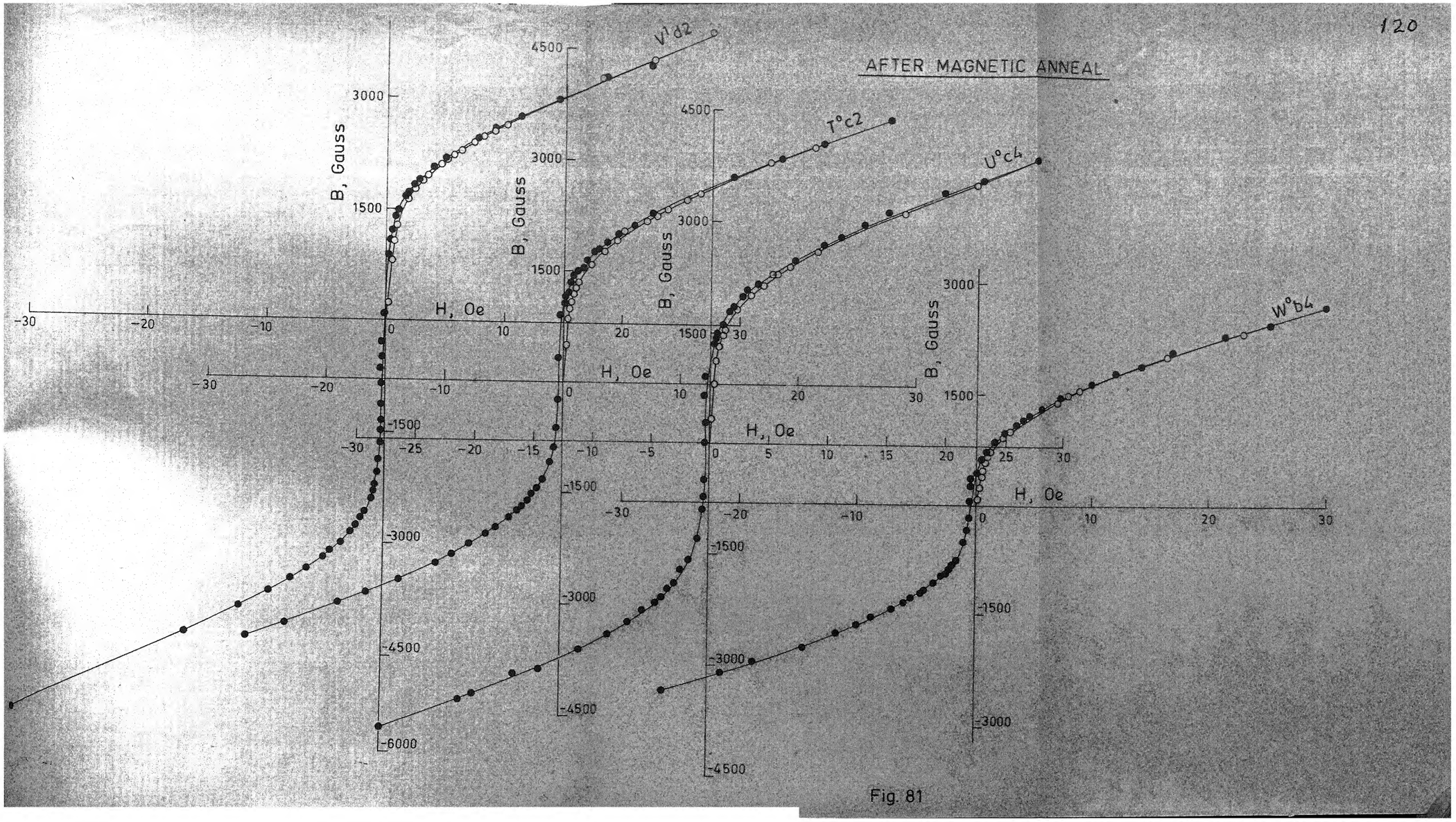

Fig. 81

Table XI : Magnetic properties of Cu bearing permalloys.

Alloy designation φ	Magnetometer data iHc (Θe)	Mr (Gauss)	$M_{H=500Θe}$ (Gauss)	μm	Permeameter data Before magnetic cooling Hc (Θe)	After mag. cooling Hc (Θe)
$T^{o}c\ 2$	0.5	5	500	94	0.2	0.4
$T^{o}c2$(440, HW 85)	0.7	5	575	96	-	-
$U^{o}c4$	0.8	14	650	142	∽ 0.25	0.3
$U^{o}c4$(450, HW 85)	0.5	4	685	137	-	-
$V^{1}d2$	0.5	7	630	161	< 0.1	<0.1
$V^{1}d4$	0.6	8	590	112	-	-
$V^{1}d4$(460, HW 85)	0.8	7	585	99	-	-
$W^{o}b4$	1.2	5	260	63	0.2	0.3
$W^{o}b4$(220, HW 85)	0.8	5	390	90	-	-
$Y^{o}b4$	1.0	9	400	114	-	-
$Y^{o}b4$(260, HW 85)	1.0	9	350	97	-	-

φ Alloy designation followed by (T, HW 85) indicates quenching of the alloy from T^{o} C in hot water at 85°C.

CHAPTER IV

DISCUSSIONS

CHAPTER IV

DISCUSSIONS

In the present study an attempt has been made to develop cube texture in Cu bearing permalloys. Physical and mechanical properties of the material also plays an important role in developing proper texture and magnetic properties. Since the physical and mechanical properties of some of the alloys are not known, some important properties of these alloys have been measured.

IV.1 Physical and mechanical properties of Cu bearing permalloys

IV.1.1 Mechanical properties of Cr and Ti containing alloys

The mechanical test data presented in Table VI indicate that addition of Ti and Cr to 5 pct. and 14 pct. Cu bearing alloys has slightly increased the pct. elongation of the alloys compared to the corresponding Fe-Ni alloys. The Cr and Ti containing alloys have been found to behave in a more ductile manner and the alloys could be cold rolled to very small thickness without developing cracks. Thus addition of Ti and Cr to Cu bearing permalloys makes it easy to prepare cold rolled sheets of suitable thickness for texture development.

IV.1.2 Electrical resistivity of Cr and Ti containing alloys

Addition of Cr to 5 pct. and 14 pct. Cu containing alloys has been found to cause a larger increase in electrical resistivity than the addition of Ti (Table VII). Electrical resistivity of 78 permalloy is only ~16 μ cm (Table I) whereas the electrical resistivity of 5Cu alloy containing Cr and Ti (V^1) has been measured to be ~ 50 μΩcm (Table VII). Because of the increase in electrical resistivity of 75 Ni permalloy due to the additions of Ti and Cr, the new alloys are expected to reduce eddy current loss.

IV.1.3 Chemical order in Cr and Ti containing alloys

After a step anneal in the temperature range of 450°C to 250°C, no ordering could be detected in the Cr and Ti containing alloys. Order-disorder reaction in these alloys appears to have become sluggish due to presence of Ti and Cr. These results thus show that no chemical ordering is to be expected in the alloys under the normal cooling conditions employed after hot rolling. Better ductility of the Cr and Ti containing alloys, showing only a slight improvement in pct. elongation over those alloys having no Cr and Ti, is possibly because the ordering reaction in the alloys is suppressed by the alloying element addition.

IV.1.4. Curie temperature of Cr and Ti containing alloys

Addition of Cr to 5Cu and 14Cu alloys has been found to lower T_c to a much larger extent than the addition of Ti (Table VII). Addition of 1Ti and 1Cr to 5Cu alloy has decreased T_c from 530°C (for alloy containing 5Cu without Ti and Cr) to 458°C. Even larger decrease in T_c has been observed for 14Cu alloys containing 1Ti and 1Cr ($\sim$217°C) which is due to the presence of large amount of Cu in the 14Cu alloys.

IV.2 Texture development

The textures developed after cold rolling and annealing have been studied through X-ray diffraction technique employing a transmission texture goniometer. The limitation of this type of goniometer is that the maximum angle of rotation of specimen around the diffractometer axis (α) is 50°. Because of this it was not possible to determine the central portion of the (111) pole figure. For both cold rolled and annealed sheets (111) pole figures were determined. The results are discussed below.

IV.2.1 Cold rolled textures of Cu bearing permalloys

In the development of cube texture, it has been found that the production of cube texture and its perfection depends

on whether cold rolling produces in the material a sharp Cu type texture (Fig. 4). Hence it was considered necessary to study the cold rolled textures of the Cr and Ti containing alloys. The partial pole figures determined were compared with the features of well developed Cu type texture (Fig. 4) to find out the nature of cold rolled texture developed.

If the intensity measurement is carried out in the angular range of $\alpha = 0$ to 90°, the (111) pole figure for cold rolled Cu (Fig. 4(a)) indicates essentially peak intensities at three locations in the pole figure namely A, C' and E (see Fig. 4(a) for pole locations) with a peculair intensity distribution around location C'. In the present study the (111) reflection intensity could be measured only in the angular range of $\alpha = 0$ to 50°. Hence it may be possible to observe only the tip of car like intensity distribution around C'. Such intensity distribution at location C, was observed by Sarkar[28] in his study of 48 permalloy. Since it is known that with increase in pct. reduction not only the intensity at the locations A, C and E increases but the spread in intensity gets reduced, an indication of stronger cold rolled texture. It may be possible that if strong cold rolled texture is produced, the intensity distribution at location C' may become so limited that the tip of the ear like distribution may go out of the angular range of investigation of the pole figures.

IV.2.1.1 Cold rolled textures of 5Cu alloys

IV.2.1.1.1 Texture of 2Cr alloy

The (111) pole figures of cold rolled texture of 2Cr alloys shown in Figs. 29 to 30. Cold rolled textures of these alloys are somewhat different from Cu type texture because in addition to intensity peaks at locations A, C, and E there are other peaks occuring at locations B, D, F, G and H (See Appendix I for location of poles in (111) pole figure). Unlike a copper type texture, the intensity at location G was found to be considerable even at 96 pct. cold rolling (CR). On further cold rolling to 97 pct. reduction, the intensity at location A, E and G increased but the other intensity peaks at locations B, C D and F vanished. As has been discussed above the disappearance of peak intensity at location C is possibly due to the development of strong cold rolled texture.

IV.2.1.1.2 Texture of 2Ti alloy

The 96 pct. cold rolled 2Ti alloy ($U^{o}bO$) produced a cold rolled texture (Fig. 31) which in appearance was found very similar to Cu type texture because intensity peaks at locations G and F were not present. The intensity at location C was found to be high. Weak intensity were also found at locations B, D and H. With increase in pct.reduction

to 97 pct., however, the intensity peak at location C disappeared and a strong intensity peak appeared at location G. Several other intensity peaks found for 96 pct. CR 2Cr alloy also appeared in the pole figure after the 97 pct. cold rolling of 2Ti alloy.

IV.2.1.1.3 Texture of 1Ti and 1Cr alloy

96 pct. CR 1Ti and 1Cr alloy developed a texture similar to that produced in 2Cr alloy (Fig. 33). With increase in pct. reduction to 97 pct., the intensity at location G was found to increase (Fig. 34). Compared to the 96 pct. CR 97 pct. CR was found to reduce the intensity at locations C and F. With further increase in pct. reduction to 98 pct., the intensity at locations C, D, F and H disappeared whereas the intensity at locations A, E and G were found to increase (Fig. 35).

IV.2.1.2 Cold rolled textures of 14 Cu alloys

IV.2.1.2.1 Texture of 2Ti alloy

In 96 pct. CR alloy, a strong peak around location G is present in addition to intensity peaks at A and E. The peaks around C, D, F and H were absent (Fig. 38). With increase in pct. reduction to 97 pct., the intensity at locations A and G was found to increase without the appearance of peak intensities at C, D, F and H (Fig. 39).

at location G. In all cases increase in pct. reduction produced strong cold rolled textures with increase in intensity at locations A, E, and G and decrease at locations B, C, D, F and H.

IV.2.2 Annealed textures of Cu bearing permalloys

The (111) pole figure for well developed cube texture in annealed Cu is shown in Fig. 5(a). The (111) pole figure of annealed Cu indicates cube texture intensity at location 6 and two more low intensity peaks which are due to grains having twin orientation relationship with respect to the cube oriented grains, (See Appendix I for pole locations in (111) pole figure for annealed texture). These textures can be described as $\{122\}\langle 21\bar{2}\rangle$ and for a well developed cube texture these secondary textures should be less prominent. For Cu the intensity ratio between locations 6 and 7 or 8 is 40:1. No secondary textures other than the $\{122\}\langle 21\bar{2}\rangle$ texture is reported for annealed Cu having strong cube texture.

In the present investigation annealed textures of all Cr and Ti containing alloys were determined and the (111) pole figures are shown in Figs. 40 to 75. Along with these figure the annealed textures of similar alloys having no Cr and Ti are also shown in Figures 40 and 41. Unlike the annealed texture of Cu (Fig. 5(a)), the annealing textures of the Cu

bearing permalloys show that several secondary textures are always present along with the cube texture. The annealing textures of Cu bearing permalloys were found to be essentially similar to the textures of 48 permalloy studied by Sarkar[28]. The identification of the secondary textures formed was done by Sarkar. Since the secondary textures were always found to be present the process variables were adjusted so as to maximise the cube orientation intensity. Texture is bad or good is determined by (1) higher (111) reflection intensity at location 6, (2) low intensity at all other (111) pole locations, and (3) spread of intensity around each locations. The texture data for the different alloys are discussed in the following sections.

IV.2.2.1 Annealed textures of 5Cu alloys

Addition of alloying elements to 5Cu alloys appears to have developed better texture compared to the 5Cu alloys containing no other alloying element. Addition of alloying elements appears to have eliminated the (111) reflection intensity from location 3 of the pole figures. Sarkar[28] during his study of 48 permalloy, could not remove the intensity peak at location 3 even after several adjustments of process variables. Ti or Cr containing alloys, however, still show intensity peaks at the other locations 1 through 8.

IV.2.2.1.1 Texture of 2Cr alloy

96 pct. CR 5Cu alloy containing no Ti and Cr ($P^{o}b4$) shows weak cube texture after annealing at 1058°C for 4 hrs (Fig. 40). Intensity at locations 1 and 4 are relatively high and all secondary textures appear strong relative to the cube texture. In comparision to the $P^{o}b4$ alloy the 96 pct. CR 2Cr alloy ($T^{o}b2$) after 2 hrs. annealing developed somewhat stronger cube texture, but the intensity values at locations 1, 4, 7 and 8 are also high (Fig. 42). The same alloy annealing for 4 hrs. ($T^{o}b4$) has increased the cube texture intensity but it still shows very high intensity at locations 1 and 4 (Fig. 43). In the 97 pct. CR alloy 2 hrs. annealing ($T^{o}c2$) produced better texture compared to 4 hrs. annealing ($T^{o}c4$) (Figs. 44 and 46). In $T^{o}c2$, the secondary textures are less prominent compared to the $T^{o}b2$ alloy. 97 pct. CR alloy after annealing for 2 hrs. in hydrogen ($T^{o}c2$ (H_2)) appears to develop improved cube texture because intensity values at 1, 4 and 5 are reasonably low (Fig. 45). The intensity values at 7 or 8 are also somewhat high. It is possible that better cube texture may be produced by longer annealing of the ($T^{o}c$) alloy in hydrogen atmosphere.

IV.2.2.1.2 Texture of 2Ti alloy

In 96 pct. CR alloy ($U^{o}b4$) 4 hrs. annealing developed somewhat better texture compared to the 2 hrs. annealing ($U^{o}b2$)

case but the intensity values at locations 1 and 4 are very high relative to the intensity at location 6 (Figs. 47-48). In 97 pct. CR alloy 4 hrs. annealing developed better textures compared to the 2 hrs. annealing (Figs. 49-50). But on further increase in annealing time to 6 hrs. the texture developed was not good because intensity values at 1 and 4 became too high (Fig. 51). The increase in annealing time appears to improve cube texture but some of the secondary textures also become too prominent. The texture developed after 2 hrs annealing of 97 pct. CR alloy in hydrogen ($U^{o}c2$ (H_2)) is comparatively better because the secondary textures are less prominent (Fig. 52). Longer annealing in hydrogen atmosphere may show still better results.

IV.2.2.1.3 Texture of 1Ti and 1Cr alloy

96 pct. CR alloy after 2 hrs annealing ($V^{o}b2$) and 4 hrs. annealing ($V^{o}b4$) has been found to have developed very similar texture because intensity at different locations are practically the same (Figs. 53-54). With further increase in annealing time to 6 hrs., the texture developed is not good because intensity values at locations 1, 2, 4, 7 and 8 are rather high (Fig. 55). In the 97 pct. CR alloy, 1 hr. annealing has developed reasonably strong cube texture with less prominent secondary textures (i.e. low intensities at

locations 1, 2, 4 and 5) (Fig. 57). With increase in annealing time to 2 hrs. and 4 hrs., however, the secondary textures corresponding to locations 1, 2, 4 and 5 have become rather strong (Figs. 58-59). The hydrogen annealed alloy ($V^{o}c2$ (H_2)) has shown slight improvement in texture compared to $V^{o}c2$ as the intensity values at locations 1 and 4 have reduced compared to $V^{o}c2$ (Fig. 56). The 96 pct. CR alloy has developed much improved texture compared to 2Cr and 2Ti alloys. 1 hr. annealing ($V^{1}d1$) appears to develop strong cube texture (Fig. 60). The intensity values at 1, 4 and 5 are very low compared to cube orientation intensity. Higher annealing time developed very strong cube texture. Both 2 hrs. and 4 hrs. annealing (Figs. 61-62) have developed strong cube texture with very little change in intensity at 1, 4 and 5. For 4 hrs. annealing the (111) reflection intensity at locations 2, 7 and 8 has increased compared to the 2 hrs. annealing case. Since in Table IX the tabular data indicate as if the 4 hrs. annealing has not produced as good a texture as was obtained through 2 hrs. annealing. If the small increase in the twin oriented grains is tolerated the 4 hrs annealed alloy may give still better magnetic properties.

IV.2.2.2 Annealed textures of 14Cu alloys

The pole figures (Figs. 63 to 72) and the texture data in Table X show that the addition of Ti and Cr to 14Cu alloys have developed better texture compared to the corresponding alloys containing no Ti and Cr. Like the 5Cu alloys addition of Ti and Cr to 14Cu alloys appears to have removed the (111) reflection intensity from location 3 in the pole figures. Ti or Cr added alloys however, still show the other secondary textures at locations 1 through 8.

IV.2.2.2.1 Texture of 2Ti alloy

4 hrs. annealing of 96 pct. CR sheets ($Y^{o}b4$) developed better texture compared to the 2 hrs. annealing ($Y^{o}b2$) case (Figs. 67-68). The texture data indicate that the intensity at location 6 has increased without any appreciable change in the intensities at locations 1, 2, 4 and 5. This may suggest that slightly longer annealing of the sheets will produce still better cube texture in the Y^{o} series alloys. For 97 pct. CR alloy, the textures developed after 2 hrs. annealing ($Y^{o}c2$) and 4 hrs. annealing ($Y^{o}c4$) are similar to each other (Figs. 69-70). Textures developed in 97 pct. CR alloys are not good compared to $Y^{o}b$ alloys. The 96 pct. CR alloy after annealing in hydrogen for 2 hrs. ($Y^{o}b2$ (H_2)) appears to show

remanence of CR texture and cube texture in this case is very weak (Fig. 71). Texture may possibly improve after longer annealing time.

IV.2.2.2.2 Texture of 1Ti and 1Cr alloy

The 96 pct. CR alloy after 2 hrs. annealing and 4 hrs. annealing developed good textures with less prominent secondary textures. $W^{o}b2$ texture is somewhat better than the $W^{o}b4$ texture because secondary textures are of somewhat low intensity in the former case (Figs. 63-64). 97 pct. CR alloys did not produce good texture compared to 96 pct. CR alloys. The 96 pct. CR alloy after annaling in hydrogen for 2 hrs. ($W^{o}b2$ (H_2)) developed reasonably strong cube texture with very low intensity secondary textures (Fig. 72). Larger annealing time may produce better texture. The texture developed in these alloys are better than the texture developed in 2Ti alloys.

IV.2.2.3 Annealed textures of 10Cu alloy

Since the amount of U^{o} alloy was not sufficient for giving it 98 pct. cold reduction, a new alloy of the same composition was melted and given 98 pct. CR. On chemical analysis the alloy was however, found to contain 11 pct. Cu. Hence, the alloy was designated as X^{o} alloy. No systematic work was done with this alloy. The 98 pct. CR alloy sheets

were annealed at 1050°C for 1 hr., 2 hrs. and 4 hrs. and the textures were determined. The texture data shown in Table IX and the pole figures (Figs. 73 to 75) indicate that the cube texture is not prominent in this alloy.

IV.3 Magnetic measurements

Since a considerable amount of time was spent in developing strong cube texture in the Cu bearing permalloys and that proper magnetic measurement equipments for sheet material were not available, only limited amount of work was done to improve magnetic properties through heat treatment. The results of the magnetic measurements are discussed in the following sections.

IV.3.1 Magnetic measurements using vibrating sample magnetometer

Since the magnetometer makes use of very small size specimens, it is not suited for the determination of the magnetic properties of textured sheet material. In the absence of a suitable sheet samples tester, one set of measurements were carried out using the magnetometer to determine some of the basic magnetic characteristics of the new set of alloys investigated. For magnetic measurements using magnetometer, specimen of size $\frac{1}{8}$" x $\frac{1}{8}$" were cut from the specimens used for texture determination. The magnetic

properties obtained through these small specimens are presented in Table XI and Figs. 76 to 80. The M vs H plots indicate that these alloys get magnetically saturated in the magnetic field ranging between ~ 100-150 Oe. The saturation induction for 78 permalloy is 10.8 kgauss (Table I). Addition of Cu is expected to reduce B_s. Addition of other alloying elements Cr and Ti is expected to reduce B_s still further. Available literature data for μ-metal containing 77Ni, 5Cu and 2Cr (nominal composition) shows (Table I) $B_s \simeq 6.5$ kgauss. The T^o alloy containing 75Ni, 5Cu and 2Cr shows B_s = 6050 gauss which is comparable with the literature value. The small difference in the B_s values is possibly due to small variation in the Cr and Cu contents. Both 2Ti and 1Ti + 1Cr alloys have higher B_s values than the 2Cr alloy, the highest value of B_s (8.3 kgauss) was observed for the 2Ti alloy. Since the W^o and Y^o alloys have much higher Cu contents than the T^o, U^o and V^o alloys, the expected B_s for the W^o and Y^o alloys is small. Results indicate that the B_s values for the W^o and Y^o alloys are 5.05 kgauss and 3.25 kgauss respectively. In this case also the higher B_s was observed for the Ti containing alloys. Thus the rate of decrease of B_s appears to be small when Ti is added.

Unlike B_s the other magnetic properties derived through magnetisation curves such as Br, H_c, μm, μ_o and hysteresis

loss are dependent on the processing parameters. Most of the literature data give only the final magnetisation curve which is obtained after suitable heat treatment given to the material following the preliminary treatment which develops the texture. Hence most of the present results, which were obtained after the preliminary heat treatment, cannot be compared with the literature data.

The $_iH_c$ values of the copper bearing alloys are $\lesssim$ 1 Oe. M_r values have been found in the range of 5 to 14 Gauss. Among the three 5Cu alloys, the (1Ti + 1Cr) alloy has the highest μ_m and the 2Cr the lowest. For the 14Cu alloys, however, the alloy containing 2Ti has higher μ_m than the (1Ti + 1Cr) alloy.

After quenching the specimens in hot water (85°C) $_iH_c$ appears to have increased slightly for the alloy specimens $T^{o}c2$ and $V^{1}d4$ whereas it has decreased somewhat for the alloy specimens $U^{o}c4$ and $W^{o}b4$. The $_iH_c$ remains practically the same for alloy specimen $Y^{o}b4$. M_r does not show any appreciable change after quenching treatment for most of the cases except for a small decrease of $\sim$10 Gauss observed for the $U^{o}c4$ specimen. M_s also shows some small change on hot water quenching. The observed changes in magnetic properties after hot water quenching of specimens are rather too small and

possibly are within the experimental errors. It appears that quenching in hot water is not effective.

IV.3.2 Magnetic measurements using permeameter

The specimens used for magnetometer were too thin and very small in size ($\frac{1}{8}$" x $\frac{1}{8}$"). Hence they do not give representative magnetic properties of larger sheet specimens. This is because in a small specimen number of grains will be very small compared to the larger specimens. Therefore in order to study the magnetic properties of larger sheet specimens, a locally fabricated permeameter was used which could measure the properties of a 4" long x 0.354" wide specimen. The permeameter field strength (H) values were calibrated using a gaussmeter and fluxmeter. Calibration of B values was not possible since the magnitude of the B values obtained through permeameter appeared to show a nonlinear dependance on the mass of the specimen. For nearly the same mass of specimens the B values seemed to show normal expected behaviour. Because of this difficulty the B scale of the fluxmeter could not be calibrated to get absolute B values. Since all the specimens used for the test were having similar weights, a rough calibration of the B scale was done using the B value of one specimen (V^1) obtained through the magnetometer data. The scale factor (4.04) thus obtained has been used to multiply

the B values measured through the fluxmeter. Fig. 81 shows these modified B scales. Since the B scale could not be calibrated, the magneticproperty value obtained through the permeameter can be used only for comparative study.

The $_{B}H_{c}$ values for most of the investigated alloys are found to be $\leq$ 0.2 Oe and it is $<$ 0.1 Oe for the V^{1} specimen. The later $_{B}H_{c}$ value is comparable with 0.05 Oe for μ-metal (Table I). The B_{r} values of most of the large specimens used in the permeameter are comparatively higher than the B_{r} values of small specimens obtained through the magnetometer. The B_{r} values of $T^{o}c2$, $U^{o}c4$ and $W^{o}b4$ were found to 170, 390 and 64 gauss respectively. The B_{r} for $V^{1}d2$ specimen was, however, practically zero. Since in the permeameter small adjustment of magnetising currents was possible and that the specimens could be easily demagnetised before performing magnetic measurement, it was possible to study the initial part of the magnetisation curve. The magnetisation curves of Fig. 81 indicate that the initial magnetisation rate of the specimens is quite high. A rough estimate of the low field permeability (μ') was made for a small magnetising field of 0.37 Oe. The permeability values for the specimens are as follows: $\mu'(V^{1}d2) = 3290$, $\mu'(U^{o}c4) = 3120$, $\mu'(T^{o}c2) = 2278$ and $\mu'(W^{o}b4) = 674$.

Magnetic cooling of the textured specimens (4" long x 0.354" wide) was performed by raising the material to 700°C and allowing to cool in the furnace. The initial cooling rate was 5°C/min. After magnetic cooling except for the specimen V^1 the $_BH_c$ was found to increase slightly for all the cases. $_BH_c$ for the specimen V^1 was still $<$ 0.1 Oe. A small improvement in the B_r value was also noticed after magnetic cooling. The B_r values of T^o, U^o, V^1 and W^o specimens after magnetic cooling was 1068, 1140, 68 and 425 respectively.

Magnetic cooling is expected to bring about a very large change in the magnetisation and demagnetisation curve of permalloys. The present results suggest that the magnetic cooling was not effective for these alloys. Possibly reason why the magnetic cooling did not show good results in the present study could be the following:

Magnetic cooling data is available for 65 permalloy. In this case the magnetic cooling follows the preliminary annealing. In the present case a two step process has been used, i.e., a textured material had to be heated up again to higher temperature for magnetic cooling. This may have disturbed the texture formed because it has been found that longer annealing decreases the cube texture intensity. The cooling rate used for the 65 permalloy was slightly less (at 700°C) than what has been used in the present case. The curie

temperature of 65 permalloy is $\sim$600°C and in the present alloys it is $<$ 500°C. Since magnetic cooling through T_c essentially produces diffusion of atoms under a magnetic field so that magnetic anisotropy is produced in the material, lower T_c of the alloys will mean the diffusion rate is slow. Hence it is possible that the cooling rate employed is too high to produce enough diffusion of atoms during the cooling process. A slower cooling rate or magnetic annealing near T_c may produce better magnetic property.

CHAPTER V

CONCLUSIONS

CHAPTER V

CONCLUSIONS

From the present study on the development of cube texture in copper bearing permalloys, the following conclusions can be drawn:

1. The Cu bearing alloys containing Ti and Cr were found to behave in a more ductile manner compared to the corresponding alloys containing no Ti and Cr. The 2Ti containing alloy was found to be more ductile compared to 1Ti + 1Cr or 2Cr alloys. These alloys could be cold rolled down to 0.003" thickness without cracking of the rolled sheets.
2. Addition of Ti and Cr to 5Cu and 14Cu alloys increased the electrical resistivity compared to the alloys containing no Ti and Cr. There was a larger increase in the electrical resistivity due to addition of Cr compared to the addition of Ti.
3. No order-disorder reaction could be detected in the Cr and Ti containing alloys.
4. Curie temperature of 5Cu and 14Cu alloys decreased due to addition of Ti and Cr. The 14Cu alloys showed larger decrease than the 5Cu alloys. The decrease in the curie temperature due to addition of Cr is more compared to the addition of Ti.

5. The 5Cu, 2Ti alloy ($U^{o}b0$) developed a cold rolled texture very similar to the Cu type texture after 96 pct. cold reduction. For all other alloys, the texture developed after cold reduction of 96 pct. or above seems to be somewhat different from the Cu type texture as new peak intensities appear in the (111) pole figure. With increase in pct. reduction, the Cu type texture developed in U^{o} alloy changes to the texture found for other alloys.
6. Annealed textures developed in all the alloys show several secondary textures along with strong cube texture.

7. With increase in annealing time, the cube texture intensity increases in the beginning and then shows a decreasing trend. The secondary textures, especially the one for which [111] $\parallel$ RD increases with increase in annealing time.

8. The alloy containing 75 Ni, 5 Cu, 1Ti, 1Cr appears to develop very strong cube texture after 98 pct. cold reduction followed by 2 hrs. annealing.

9. Hydrogen annealing of the alloys appears to cause slow development of cube texture compared to argon annealing and the secondary textures appear to be less prominent.

10. Magnetic properties indicate that 2Ti alloy has higher B_s than (1Cr + 1Ti) and 2Cr alloys. The alloys have very low coercivity, ${}_{B}H_{c} < 0.2$ Oe and low B_r values.

REFERENCES

REFERENCES

1. M. Hansen and K. Anderko, 'Constitution of Binary Alloys' McGraw Hill, 1958.
2. A.E. Berkowtiz and E. Kneller, 'Magnetism and Metallurgy', Academic Press, New York, 2, 1969, 549.
3. J. Wakelin and E.L. Yates, Proc. Physical Society, Section-B, 66, 1953, 221.
4. H.D. Arnold and G.W. Elmen, J. Franklin Inst. 195, 1923, 621.
5. J.H. Crede and J.P. Martin, J. Appl. Phy., 20, 1949, 966.
6. H. Hu and S.R. Goodman, Trans. AIME, 227, 1963, 627.
7. C.S. Barrett and T.B. Massaslski, 'Structure of Metals' McGraw Hill, 1966.
8. P.A. Beck, Trans. AIME, 191, 1951, 475.
9. J.G. Benford, J. Appl. Phys., 4, 1963, 1307.
10. G. Wasserman and J. Grewen, 'Texturen Metallischer Werk steff', Springer-Verlag, Berlin, 1962 705.
11. N.F. Littman, E.S. Harris and C.E. Ward, J. Appl. Phys., 33, 1962, 1229.
12. M.J. Savitski, J. Appl. Phys., 29, 1958, 353.
13. D.A. Colling and R.G. Aspden, J. Appl. Phys., 40, 1969, 1571.

14. G.A. Kelsall, Physics, 5, 1934, 169.

15. I.K. Kang and A.P. Martin, J.Appl. Phys., 38, 1967, 1178.

16. R.M. Bozorth, J.F. Dillinger and G.A. Kelsall Phy. Rev., 45, 1934, 742.

17. A.J. Bradely, W.F. Cox and H.J. Goldschmidt J. Inst. Metals, 67, 1941, 189.

18. W. Köster and W. Dannöhol, Z. Metallkunde, 27, 1935, 154.

19. H.G. Muller, Z. Metallkunde, 31, 1939, 322.

20. O. Auwers and H. Neumann, Wiss. Veroffentl. Siemens-Werken, 14, 1935, 52, 155.

21. R.M. Bozorth, ibid, 120.

22. I.Z. Svestka and I.Z. Tischer, Trans. IEEE, Mag-10, 1974, 139.

23. D.J. Snee, J. Appl. Phys., 38, 1967, 1172,

24. A. Kussman and B. Scharnow, Z. Physik, 54, 1929, 1.

25. G.Y. Chin, Trans. IEEE, Mag-7, 1971, 102.

26. H.H. Scholefield, R.V. Major, B. Gibson and A. Martin, Brit. J. Appl. Phys., 18, 1967, 41.

27. R.V. Major and M.C. Martin, Trans. IEEE Mag-6 1970, 101.

28. P. Sarkar, M.Tech. Thesis, I.I.T., Kanpur 1979.

29. R.M. Bozorth, 'Ferromagnetism', Van Nostrand, New York, 1951.

30. A.E. Berkowitz and E. Kneller, 'Magnetism and Metallurgy', Academic Press, New York, 1, 1969.

31. D.F. Decker, D. Harter and E.T. Asp, J. Appl. Phys., 19, 1948, 388.

32. ASTM Standards Part-8, ASTM Philadelphia, 1965, 29.

33. F.A. Underwood, 'Textures in Metal sheets' Macdonald, London, 1961.

34. I.L. Dillamore, R.E. Smallman and W.T. Roberts, Phil. Mag., 9, 1964, 517.

Appendix I

Figure Caption

(111) pole locations in (111) pole figure of Cu bearing permalloys. ● pole locations in cold rolled texture, ■ pole locations in annealed texture.

(111) pole locations in stereogram

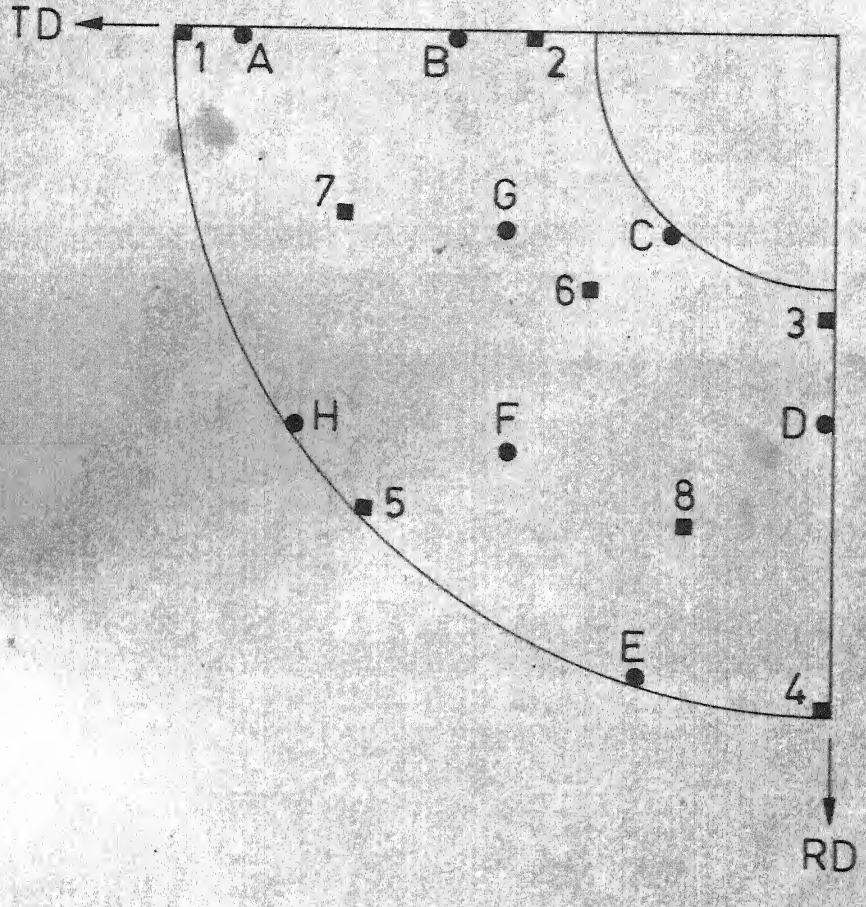

- Cold rolled texture [(111) pole figure]
- Annealed texture [(111) pole figure]

Appendix I

ME-1981-M-VER-STU